AD-A164 931 THE ATCHAFALAYA RIVER DELTA REPORT 7 ANALYTICAL ANALYSIS OF THE DEVELOPME..(U) LOUISIANA STATE UNIV BATON ROUGE COASTAL ECOLOGY LAB F C WANG SEP 85 1/3

UNCLASSIFIED WES/TR/HL-82-15 DAC339-81-C-0004 F/G 8/8 NL

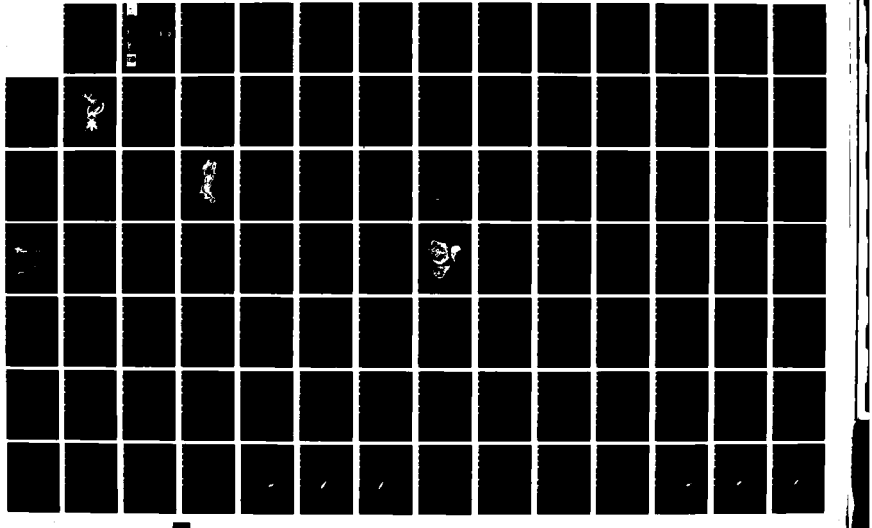

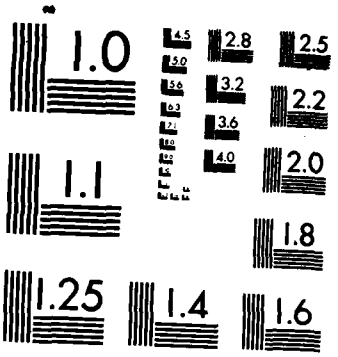

MICROCOPY RESOLUTION TEST CHART
NATIONAL BUREAU OF STANDARDS-1963-A

US Army Corps of Engineers

TECHNICAL REPORT HL-82-15

(12)

THE ATCHAFALAYA RIVER DELTA

Report 7

ANALYTICAL ANALYSIS OF THE DEVELOPMENT OF THE ATCHAFALAYA RIVER DELTA

by

Flora C. Wang

Coastal Ecology Laboratory
Center for Wetland Resources
Louisiana State University
Baton Rouge, Louisiana 70803

September 1985
Report 7 of a Series

Prepared for US Army Engineer District, New Orleans
PO Box 60267, New Orleans, Louisiana 70160
Under Contract No. DACW39-81-C-0004
Monitored by Hydraulics Laboratory
US Army Engineer Waterways Experiment Station
PO Box 631, Vicksburg, Mississippi 39180-0631

HYDRAULICS LABORATORY

Destroy this report when no longer needed. Do not return it to the originator.

The findings in this report are not to be construed as an official Department of the Army position unless so designated by other authorized documents.

The contents of this report are not to be used for advertising, publication, or promotional purposes. Citation of trade names does not constitute an official endorsement or approval of the use of such commercial products.

Unclassified

SECURITY CLASSIFICATION OF THIS PAGE *(When Data Entered)*

REPORT DOCUMENTATION PAGE	READ INSTRUCTIONS BEFORE COMPLETING FORM
1. REPORT NUMBER Technical Report HL-82-15 2. GOVT ACCESSION NO. AD-A164 931	3. RECIPIENT'S CATALOG NUMBER
4. TITLE *(and Subtitle)* THE ATCHAFALAYA RIVER DELTA; Report 7, ANALYTICAL ANALYSIS OF THE DEVELOPMENT OF THE ATCHAFALAYA RIVER DELTA	5. TYPE OF REPORT & PERIOD COVERED Report 7 of a series 6. PERFORMING ORG. REPORT NUMBER
7. AUTHOR(s) Flora C. Wang	8. CONTRACT OR GRANT NUMBER(s) Contract No. DACW39-81-C-0004
9. PERFORMING ORGANIZATION NAME AND ADDRESS Coastal Ecology Laboratory, Center for Wetland Resources, Louisiana State University Baton Rouge, Louisiana 70803	10. PROGRAM ELEMENT, PROJECT, TASK AREA & WORK UNIT NUMBERS
11. CONTROLLING OFFICE NAME AND ADDRESS US Army Engineer District, New Orleans PO Box 60267 New Orleans, Louisiana 70160	12. REPORT DATE September 1985 13. NUMBER OF PAGES 199
14. MONITORING AGENCY NAME & ADDRESS *(if different from Controlling Office)* US Army Engineer Waterways Experiment Station Hydraulics Laboratory PO Box 631 Vicksburg, Mississippi 39180-0631	15. SECURITY CLASS. *(of this report)* Unclassified 15a. DECLASSIFICATION/DOWNGRADING SCHEDULE

16. DISTRIBUTION STATEMENT *(of this Report)*

Approved for public release; distribution unlimited.

17. DISTRIBUTION STATEMENT *(of the abstract entered in Block 20, if different from Report)*

18. SUPPLEMENTARY NOTES

Available from National Technical Information Service, 5285 Port Royal Road, Springfield, Virginia 22161.

19. KEY WORDS *(Continue on reverse side if necessary and identify by block number)*

Atchafalaya River--delta (LC)
Deltas (LC)
Hydrological forecasting (LC)
Hydrodynamics--mathematics (LC)
Sedimentation and deposition (LC)

20. ABSTRACT *(Continue on reverse side if necessary and identify by block number)*

The diversion of fresh water and sediments from the Mississippi River to the Atchafalaya River is developing a new delta on the south-central Louisiana coast. The building of this new wetland area has prompted scientific interest in predicting delta evolution.

This study reports the analytical prediction of future delta growth based on the theory of turbulent jets that issue from river outlets and discharge into

(Continued)

DD FORM 1 JAN 73 1473 EDITION OF 1 NOV 65 IS OBSOLETE

Unclassified

SECURITY CLASSIFICATION OF THIS PAGE *(When Data Entered)*

20. ABSTRACT (Continued).

quiescent bays. An integrated form of the hydrodynamics equations of flow continuity and momentum balance, coupled with the advection-diffusion mass transport equation, have been formulated into a two-dimensional spatial domain. Closed-form analytical solutions are obtained with the aid of similarity functions for the velocity and sediment concentration profiles. A numerical procedure for estimating the area and volume of deposition of the delta sediments is presented.

The results show that the deposited sediment forms a saddle-shaped bottom. Rapid accumulation of suspended sediment near the river outlet and an abrupt decline of sediment deposition away from the outlet are observed. It is concluded that the riverine inflow has a significant influence of sediment deposition within a short longitudinal distance, and that beyond that distance the riverine inflow is insignificant.

The analytical predictions are compared with the predictions made by other statistical and generic approaches; an agreement is found. A sensitivity analysis is performed to assess the relative importance of various parameters in the river-bay-delta system.

PREFACE

This study presents the results of an analytical prediction of delta development in Atchafalaya Bay, Louisiana. The research was supported as a negotiable project with the Estuaries Division, Hydraulics Laboratory, US Army Engineer Waterways Experiment Station (WES), Vicksburg, Mississippi, for the US Army Engineer District, New Orleans (LMN), Louisiana. Work was performed under Contract No. DACW39-81-C-0084 between WES and the Center for Wetland Resources, Louisiana State University, Baton Rouge, Louisiana.

This study was performed under the direction of Messrs. H. B. Simmons, Chief of the Hydraulics Laboratory; F. A. Herrmann, Jr., Assistant Chief of the Hydraulics Laboratory; and R. A. Sager, Chief of the Estuaries Division. The work was performed under the supervision of Mr. W. H. McAnally, Jr., Project Manager and Program Officer. Gratitude is extended to Messrs. J. V. Letter, A. Teeter, and T. Thomas for consultation and review.

The principal investigator gratefully acknowledges her research associates Dr. W. Y. Kuu, Dr. J. S. Wei, and Mr. P. D. Scarlatos for their contributions to the project; also, her colleagues Dr. S. P. Murray and Dr. S. A. Hsu for reviewing earlier versions of the manuscript.

Thanks are also extended to Ms. C. A. Moncreiff for her excellent assistance in editing and proofreading the entire report; to Mr. J. R. Brown for his skillful drafting of the figures, and to Mrs. B. S. Grayson and Mrs. C. K. Lemon for their patience in typing the numerous equations and in revising the manuscript.

COL Tilford C. Creel, CE, and COL Robert C. Lee, CE, were Commanders and Directors of WES during the conduct of the study. COL Allen F. Grum, USA, was Director of WES during the preparation and publication of this report. Mr. Fred R. Brown and Dr. Robert W. Whalin were Technical Directors.

CONTENTS

CONTENTS (Continued)

CONTENTS (Continued)

LIST OF SYMBOLS

English letters:

a	Bottom slope
A	Normalized entrainment coefficient
b	Half-width of the jet
b_i	Body force components
b_o	Half-width of the jet at the outlet
B	Normalized width of the jet
c	Sediment concentration
c_a	Sediment concentration in the receiving waters
c_c	Center-line sediment concentration
c_d	Deposited sediment
c_o	Sediment concentration at the outlet
C	Normalized sediment concentration
C_z	Chezy's coefficient of friction
d	Deposited sediment layer thickness
D	Normalized friction variable
D_i	Molecular diffusion coefficient
e	Entrainment coefficient
E	Entrainment function
E_i	Molecular and eddy diffusion coefficient
f	Friction factor
F	Normalized friction factor
g	Acceleration of gravity
G	Similarity function of the velocities
h	Depth of the water
h_o	Depth of the water at the outlet
H	Normalized depth of the water
i	Counter
I	Integrals
k	Counter
m	Counter
p	Pressure
P_o	Atmospheric pressure

LIST OF SYMBOLS (continued)

r	Normalized longitudinal coordinate
R	Similarity function of the sediment concentration profiles
s	Normalized lateral coordinate
S	Source or sink function
t	Time
u	Velocity
u_c	Center-line velocity
u_{cr}	Critical velocity for deposition to occur
u_i	Velocity components
u_o	Velocity at the outlet
U	Normalized velocity
U_{cr}	Normalized critical velocity
w	Wind velocity
w_i	Wind velocity components
w_o	Sediment settling velocity
W_o	Normalized sediment settling velocity
x_i	*Cartesian coordinates in space*
Y	Integration constant

Greek letters:

γ	Coefficient of air friction
ε_h	Horizontal eddy viscosity coefficient
ε_v	Vertical eddy viscosity coefficient
ε_i	Eddy diffusion coefficient
η	Wave height
μ	Molecular viscosity
ρ	Density of the water
ρ_a	Density of the air
τ_b	Bottom shear stresses
τ_s	Surface shear stresses
τ_{ik}	Stress components
Φ	Geographical latitude
Ω	Angular velocity of the earth

Superscripts:

$(-)$	Mean values
$(')$	Perturbated values

CONVERSION FACTORS, NON-SI TO SI (METRIC) UNITS OF MEASUREMENT

Non-SI units of measurement used in this report can be converted to SI (metric) units as follows:

Multiply	By	To Obtain
cubic feet	0.02831685	cubic metres
cubic feet per second	0.02831685	cubic metres per second
feet	0.3048	metres
feet per second	0.3048	metres per second
miles (US statute)	1.609344	kilometres
square feet	0.09290304	square metres
square miles (US statute)	2.589988	square kilometres
tons (2,000 lb, mass)	907.1847	kilograms

THE ATCHAFALAYA RIVER DELTA
ANALYTICAL ANALYSIS OF THE DEVELOPMENT OF THE ATCHAFALAYA RIVER DELTA

PART I: INTRODUCTION

Objectives

1. The objective of this research is to quantify the dynamic interaction of the resources of the Atchafalaya River, namely, the sediments forming the delta and the riverflow that carries the sediment. Our study is focused on fresh water discharging into a quiescent bay and its dynamic response to the forcing function. Our results are developed for short-term predictions of the delta growth in early stages.

2. The specific objectives of this research are:

   a. To apply the theory of turbulent jets in predicting the short-term process of delta growth at the river mouth.

   b. To formulate the problem of river outlet freshwater discharge into a quiescent bay as a two-dimensional plane jet.

   c. To develop an analytical approach that quantifies the areal and mass extent of delta growth as influenced by the river discharge.

   d. To test the adequacy of the analytical technique based on presently mapped bathymetry and to verify the result with the independently measured bathmetry changes in the bay.

   f. To perform a sensitivity analysis on various hydrodynamic parameters, and to assess the relative importance of river stage and discharge, channel configuration, and bottom resistance as they relate to the river outlet sediment deposition.

Background of Deltaic Processes

3. Coleman and Wright (1975) discussed the various aspects of interacting coastal processes and their effects on delta formation.

The most important factors are climate, water and sediment discharge, vegetation and soil, geometry of river mouth, winds and nearshore currents, wave power and tidal regime, and bathymetry of the receiving bay. Figure 1 shows the major components of a river basin, bay, and delta system (Coleman and Wright 1975).

4. The river mouth is the point at which the fresh water leaves the confined channel and spreads and mixes with ambient bay water, causing a decrease in flow velocity and total momentum, and consequently, the deposition of sediment. The river discharge depends on the climatic and hydrologic regime within the drainage basin. The pattern of delta growth depends upon the rate of sediment supply by the river discharge and reworking of sediment by wave and current forces in the receiving bay.

5. The pattern of sediment deposition depends upon the properties of the sediment and the relative roles of three primary forces (Coleman 1976):

a. The inertial force of river effluent and associated turbulent diffusion.

b. The frictional force between the river effluent and the bed immediately seaward of the mouth.

c. The buoyant force resulting from density differences between river effluent and ambient fluids.

6. Extensive observations and representative data collected at the mouth of the Mississippi River by Wright and Coleman (1974) have indicated that the relative roles of these forces vary in space and time, causing corresponding changes in the modes and patterns of sediment transport and deposition. Figure 2 illustrates the river mouth mechanisms and the resulting effluent plume and subaqueous bar (Coleman 1976). Conditions for the four cases illustrated and their results are as follows:

a. Inertial forces dominant. When riverflow velocities are high, depths immediately seaward of the mouth are large, density differences are negligible, inertial forces are dominant, and the river effluent spreads and diffuses as a turbulent jet. Narrow and linear sandbars are formed (Figure 2a).

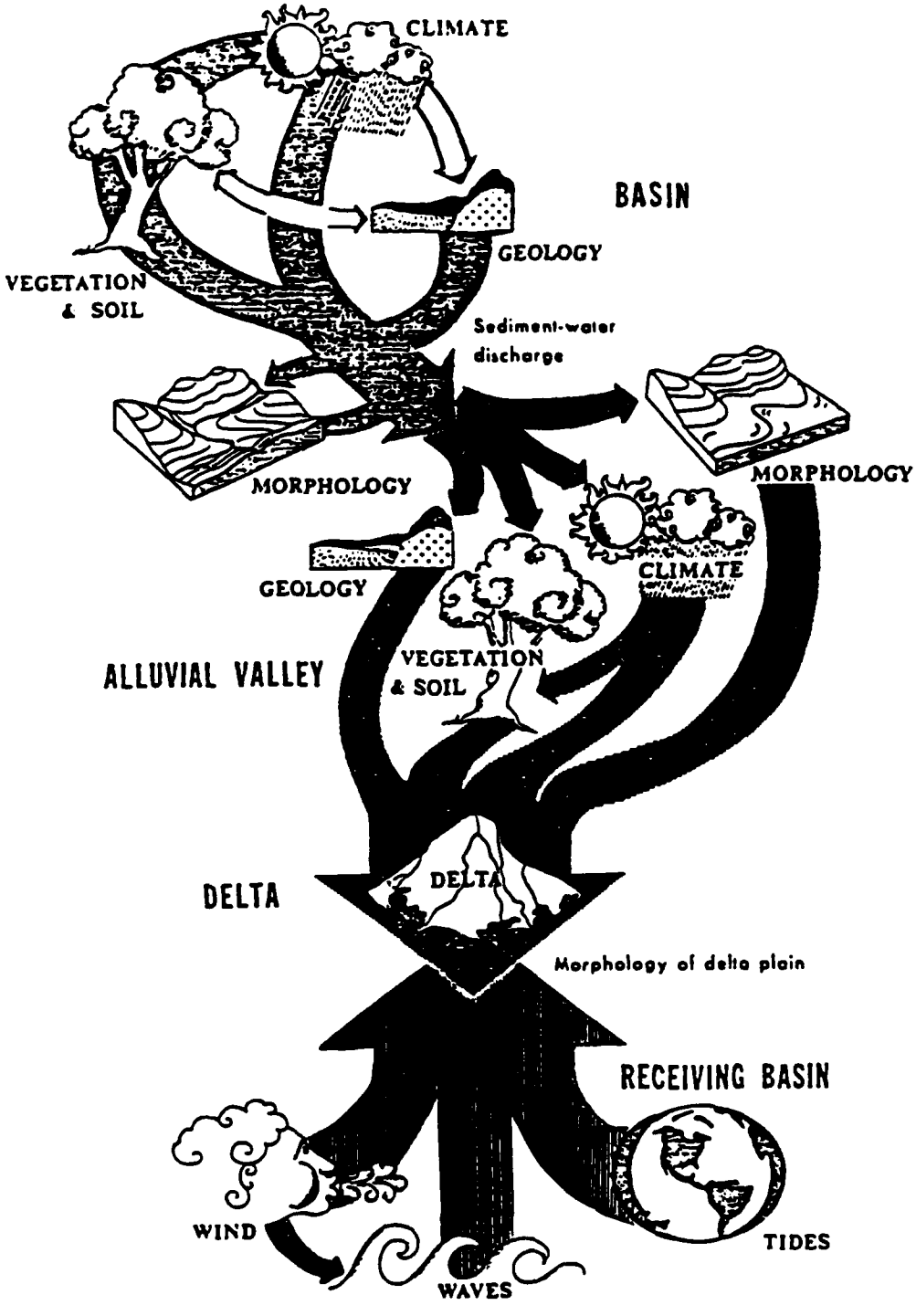

Figure 1. Major process controls on a river system (Coleman and Wright 1975)

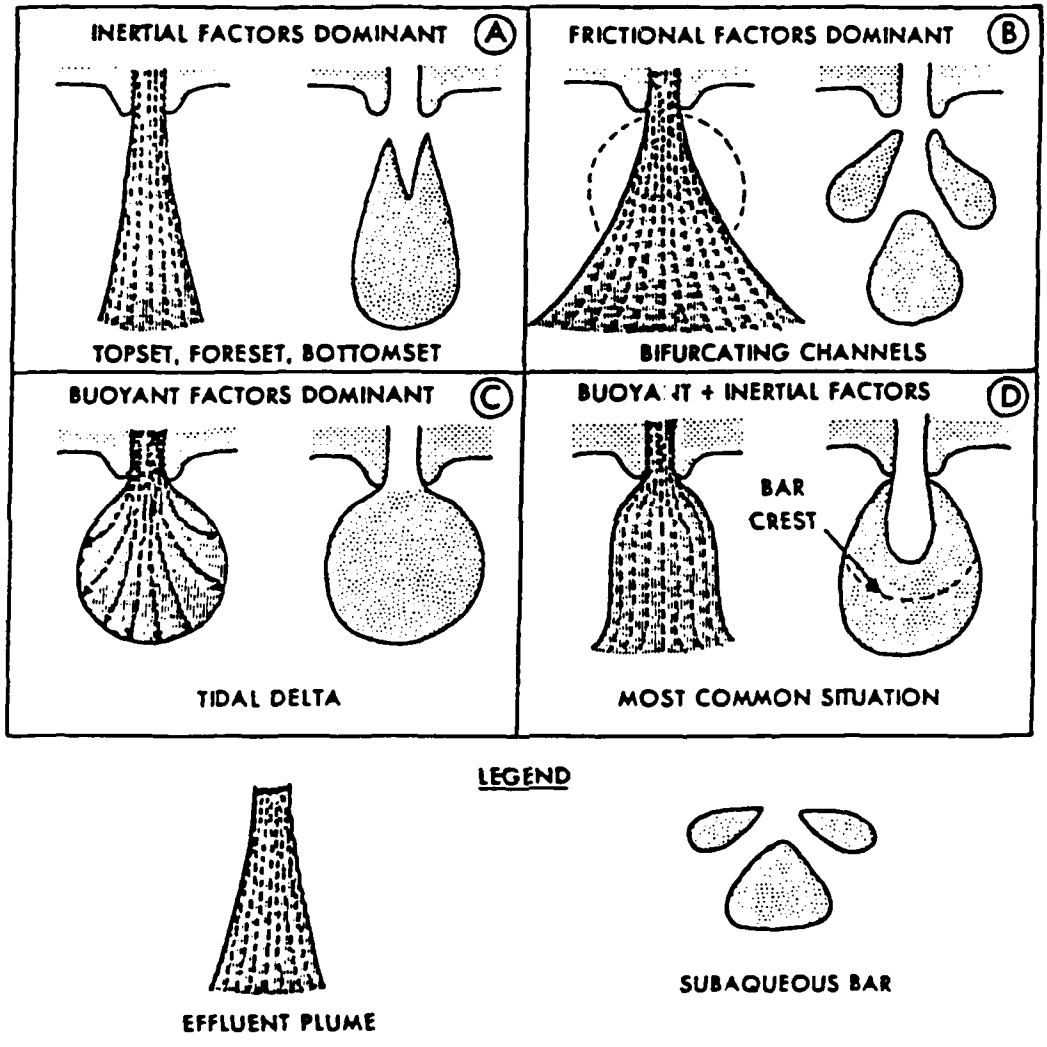

Figure 2. River mouth mechanisms (Coleman 1976)

b. Frictional forces dominant. When riverflow velocities are high, but the depths seaward of the mouth are shallow, turbulent flux penetrates to the entire water column and bottom friction plays a major role in causing the river effluent to be decelerated and expanded as a fan shape plume. Bifurcating sandbars are established (Figure 2b).

c. Buoyant forces dominant. When the density of ambient bay water is much higher than the density of river effluent, then strong vertical density gradient exists at the river mouth and buoyancy becomes of paramount importance in spreading both the river effluent and sand bars radially away from the mouth (Figure 2c).

d. Interaction of forces. Various combinations of these three forces exist in modern deltas. Interactions between buoyant and inertial forces are common in many modern rivers (Figure 2d).

Approach in Analyzing the Atchafalaya River Delta

7. The environmental settings of a river, bay, and delta system provide some idealization to analyze the influencing factors. In our study, four main features are apparent:

a. The large input of fresh water and sediments from the Lower Atchafalaya River is undoubtedly the dominant forcing function in shaping the Atchafalaya River Delta.

b. The Atchafalaya Delta is building into a shallow bay, in contrast to the continential shelf location of the Mississippi Modern Balize Delta (modern birdfoot delta).

c. The Atchafalaya Bay domain is constrained within an area of 233 square miles* (33 miles wide, and 8 miles long). The average depth in the bay is about 5 ft, and the water volume is about 3.25×10^{10} ft^3 (McAnally and Heltzel 1978).

d. The average salinity of the waters in Atchafalaya Bay is 0.37 ppt (US Fisheries and Wildlife Service 1976).

8. From above information, we infer that the main forces that affect the behavior of Atchafalaya River discharge and subsequent

*A table of factors for converting non-SI units of measurement to SI (metric) units is presented on page 7.

delta formation in the bay are primarily inertial force and bottom friction. Therefore our analytical approach, based upon the turbulent plane jet theory, to quantify the delta development in early stages is logical. Our scheme for characterization of fresh river water discharging into a quiescent bay is defined in Figure 3.

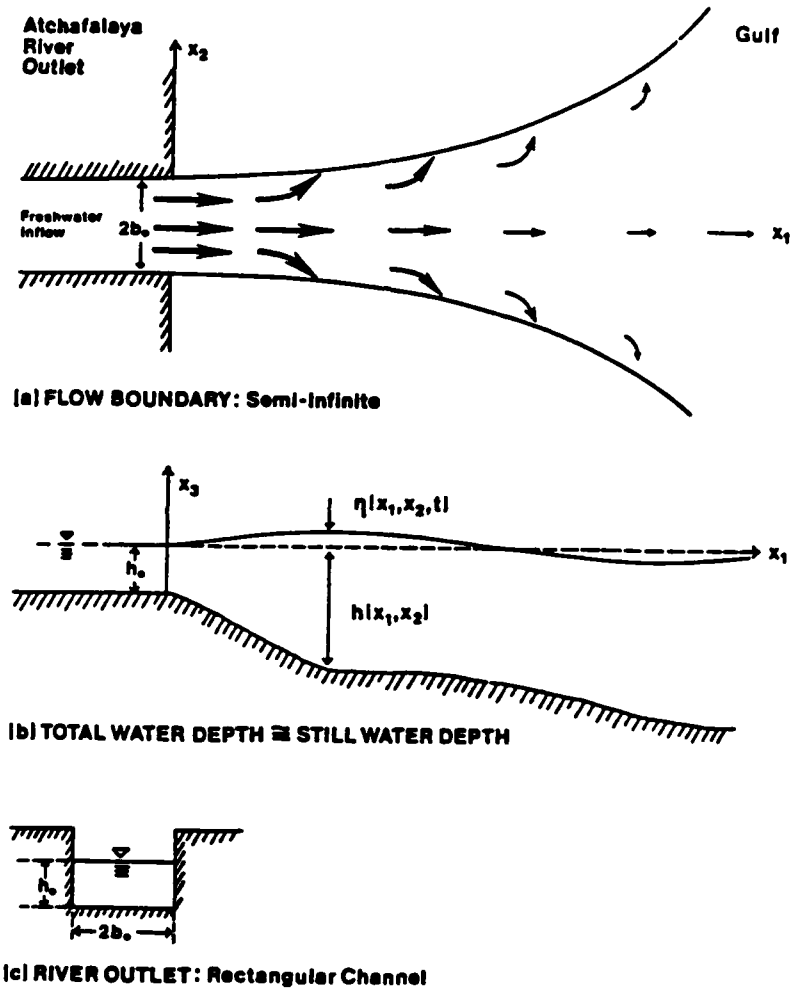

Figure 3. Schematization of fresh river water discharging into a quiescent bay

PART II: LITERATURE REVIEW OF TURBULENT JETS

Review of General Basics of Turbulent Jets

9. Fresh water discharging from a river into coastal waters forms a turbulent jet. River discharge at the mouth transports sediments into the bay. Mass transport of these materials determines the ultimate distribution of sediments and the bathymetric changes near river mouths. Essential features of river effluents have been summarized briefly in Part I and have been documented thoroughly by Coleman (1976).

10. There are many articles and technical papers on turbulent jets. The literature reviewed in this chapter is limited primarily to surface jets and plumes with bottom friction and lateral entrainment.

Types of turbulent jets

11. A general view of the basics of turbulent jets is given by Pai (1954), Townsend (1956), and Schlichting (1968). Much more detailed analysis is presented in the classical work of Abramovich (1964) and in the relatively recent book by Rajaratnam (1976).

12. Turbulent jets are a special category of turbulent shear flows. Depending on their dominant driving force, they are distinguished as momentum jets or as plumes. For the former momentum is the predominant factor, while for the latter buoyancy is the governing force. Jets are also classified according to their geometrical shape as plane or axisymmetrical.

13. There is usually not a distinct separation line between the two categories; a jet is then of the mixed-type. In this case, at the area close to the outlet the jet is influenced by the initial momentum of the fluid and is treated as a momentum jet, while at some distance from the outlet the buoyant effects become more important so that the jet is treated like a plume.

Surface heated jets

14. Considerable research in dealing with surface heated jets has been done. Hayashi and Shuto (1967) were among the first who

presented an approximate theory for the solution of thermal jets discharged horizontally at the water surface. Many assumptions were incorporated in the analysis. Their solution is valid where the Richardson's number is close to unity.

15. Another model for surface thermal jets was developed by Hoopes, Zeller, and Rohlich (1967), in which the wind shear stresses on the jet surface and the entrainment due to the wind were included. Their model is two-dimensional with constant jet depth and no vertical entrainment. They assumed that the jet spreads linearly; buoyant effects and current drag forces are neglected.

16. Motz and Benedict (1970) studied the problem of heated surface jet discharges into rivers. Their model is also two-dimensional with constant jet thickness, but considers both vertical entrainment and drag forces. Although buoyancy was assumed to induce vertical entrainment, it was neglected with respect to jet spreading.

17. In the study of the discharge of heated water into deep receiving waters, Koh and Fan (1970) were first to introduce interfacial shear stress in the formulation of turbulent jet problems. Internal hydraulic jump due to the transition of the supercritical issuing jet in the near-field zone into a subcritical flow in the far-field zone was discussed in their study.

18. Shirazi and Davis (1974) have developed a model for buoyant surface jets, which in essence is similar to the one given by Stolzenbach and Harleman (1971), but differs in the fact that they used Gaussian similarity profiles. Shirazi and Davis estimated the coefficients of entrainment, turbulent exchange, drag,and shear through calibration of field and experimental data. This approach seems less desirable since many errors might be lumped into the coefficients (Jirka, Abraham, and Harleman 1975).

Ebb tidal jets

19. Tidal inlets act as an interface between estuarine and coastal waters. Tidal currents near inlets and estuary mouths play important roles in transporting pollutants and sediments. Patterns of tidal flow change with time during a tidal period. During ebb, the

flow on the ocean side separates from boundaries, as opposed to the nonseparated flow during flood (Ozsoy 1977). Therefore a turbulent jet is often formed during ebb flows.

20. An attempt was made by French (1960) to model the ocean flow patterns during a tidal period. In his study, constant depth and negligible bottom friction were assumed. The results thus obtained did not simulate the actual conditions. In reality, the bottom slope and bottom friction may become important, especially during ebbing tide when a jet flow is found.

21. Ozsoy (1977) incorporated variable bottom topography, bed resistance, and lateral entrainment into the jet flow phenomenon. He described simulated turbulent jet characteristics extensively. His results of the flow patterns at the vicinity of tidal inlets have been compared with a small physical model and good agreement was found.

22. Sill, Fisher, and Whiteside (1981) investigated deposition in an inlet where the hydrodynamics were simulated by a one-dimensional jet, considering only ebbing tide. Their conclusions were that the dimensions of the equilibrium horseshoe-shaped shoal were proportional to the inlet velocity and that the two-dimensional theoretical isopachs do not adequately predict the shape of the shoal.

Freshwater effluent plumes

23. Bates (1953) suggested that at most natural river mouths freshwater effluent diffusion can be based upon the theory of turbulent jets. A jet boundary occurs near the river mouth as fresh water discharges into a quiescent bay. Due to the discontinuity in the velocity of flow, a zone of turbulent mixing is established.

24. Wright and Coleman (1971) suggested that freshwater flow from a river mouth, its deceleration, and consequent sediment deposition reflect varying conditions of outflow inertia and associated turbulence, bottom fricition, buoyancy induced by density differences, and the winds, tides, and currents of the receiving basin.

25. Based on extensive observations and representative field data, Wright and Coleman (1971) found that the jet expansion rate in

deep receiving water can be expressed by an explicit function of the density ratio between river water and seawater and the densimetric Froude number. They concluded that the flow deceleration is due mainly to vertical rather than lateral mixing.

26. A further investigation of river effluent dynamics for the Mississippi River was conducted by Wright and Coleman in 1974. In their study, they divided the mouth of the river into four semi-discrete regions with specific morphologic and sedimentary characteristics. The relative contributions of outflow inertia, buoyancy, bottom friction,and marine hydrodynamics to the evolution of the delta of a stratified river were documented.

27. A dual treatment of the effluent plume, both theoretical and experimental, was presented by Bowman and Iverson (1978). They concluded that the plume is independent of the bathymetry of the region and its driving mechanism is the horizontal pressure gradient due to the sloping interface between the plume and the ambient water. Also, they differentiate plumes from saline wedges on the basis that the former tends to entrain and mix downward, while the saline wedge tends to entrain and mix upward.

Review of Previous Efforts in Analyzing Turbulent Jets

28. The governing equations of fluid hydrodynamics and substance conservation constitute the basis for the mathematical model for turbulent jets. The formulation is a system of partial differential equations of three to five equations, that is, one for fluid mass continuity; one to three, depending on the nature of the problem, for the momentum components; and one for the conservation of the substance under consideration.

29. Because of the nonlinear nature of the mathematical problem formulated, no analytical solution for the complete system has yet been found. The approximate solution to this mathematical model can be found by means of a numerical technique (finite difference and finite element numerical methods) using a digital computer. However,

by making certain simplifying assumptions the system of partial differential equations can be reduced into a system of ordinary differential equations which can then be solved analytically or numerically. This kind of approach is called "integral methods." In essence, the integral equations of mass, momentum, and energy are utilized.

Assumption of self-similarity

30. To obtain a closed-form solution of a set of ordinary differential equations, the self-similarity of velocity profiles along the longitudinal distance is assumed. The similarity hypothesis has a firm basis for the classical turbulent jets as demonstrated by theory (Abramovich 1964; Schlichting 1968).

31. Various functional forms of velocity profiles and sediment concentration, such as Gaussian probability distribution (Shirazi and Davis 1974), have been developed based on different sets of hypotheses. Experimentally, the similarity is well established for the case of free jets. However, in cases of attached jets with interface friction, the similarity is under question. Another approach is the split of the spatial solution field into a near-field model (close to the outlet) and a far-field model (far from the outlet).

32. Recent experiments by Safaie (1979) suggest that the similarity function depends not only on the width of the outlet but also on the bed slope and the aspect ratio (the ratio of the width and depth of an outlet). Such a dependence should be expected, but could increase the complexity of the problem for reaching an analytical solution.

Assumption of entrainment velocity

33. A positive step toward the mathematical modeling of turbulent jets is found in the pioneering work of Ellison and Turner (1959) in which they assumed that the entrainment is proportional to the velocity multiplied by an empirical entrainment parameter which is a function of the Richardson number. Their work was justified by their laboratory experiments for surface jets and inclined plumes.

34. Hirst (1971) introduced an entrainment function which was related to the buoyancy and the jet orientation. His analysis was based on the integral forms of the conservation of mass, energy, and two-component momentum equations. Gaussian similarity profiles were used. The results of his predictions compared with experimental data were proven to coincide satisfactorily. The receiving water was taken as quiescent and stratified.

35. A further analysis of the entrainment mechanism was conducted by Price (1979). Using the experimental data of Kato and Phillips (1969) and of Kantha, Phillips, and Azad (1979) for stratified and nonstratified receiving water, Price computed the entrainment function from the mean buoyancy and momentum equations. In the momentum equation, a sidewall friction term was included in order to incorporate the effects of the experimental tank walls. This investigation covered a wide range of Richardson's numbers.

Presence of crosscurrents

36. Keffer and Baines (1963) experimentally investigated the case of an axisymmetrical turbulent jet subjected to a crosswind. Their results concluded that the position of the jet in space can be described by a single function of the entrainment parameter and the momentum of both the jet and the wind. They also showed that the similarity assumption is still valid for the case of a crosswind.

37. A comprehensive turbulent jet integral model was developed by Stolzenbach and Harleman (1971). The model considered the cases of both nonbuoyant and buoyant jets as well as buoyant jets in crossflows. The main characteristic of their analysis was the separation of the jet hydrodynamic field into four separate regions depending on the shear pattern of the flow. Thus for the near-field zone, the governing equations were written for each individual region separately and were then linked together through transfer equations. For the far-field zone, there was only one region. By scale analysis the original system was reduced into a simpler one, which was then transformed into an ordinary differential system by utilizing the similarity profiles

in a polynomial form. The final system was solved numerically by a fourth-order Runge-Kutta integration algorithm.

38. Jirka, Adams, and Stolzenbach (1981) gave a general presentation of the buoyant surface jets theory. Based on dimensional analysis and some physical arguments, they defined the flow using a set of independent variables, including the kinematic buoyant flux, the volume flux, and a characteristic source length. Their analysis covers the near field of buoyant jets for deep or shallow receiving waters. The case of crossflow was included also.

39. The diffusion of axisymmetric jets into inflowing streams was recently investigated by Rajaratnam and Stalker (1982). In their experiment, the velocity of the jet ranged from 2 to 30 times the stream current; experimental results showed the similarity of the velocity profiles except within the boundary layer portion. The various jet characteristics were correlated to the excess momentum thickness.

Closed-form analytical solutions

40. Hayashi and Shuto (1967) were the first to present an analytical solution for the surface heated discharge problem. In their formulation, the following assumptions were used:

a. In the momemtum equation the horizontal diffusion terms balanced the pressure gradient.

b. Similarity existed for the velocity profiles in horizontal and vertical planes.

c. The entrainment rate was proportional to a characteristic velocity.

d. The turbulent diffusion coefficients were constant.

Furthermore, they neglected the advective terms, the vertical velocities, and the shearing forces at the surface and the bottom. A closed form solution was obtained for the velocities by a biharmonic stream function equation where the entrainment was taken as zero. Their solution holds true where the Richardson number is close to unity.

41. An analysis of the surface heated jets at small Richardson's numbers has been done by Engelund and Pederson (1973). Their main assumptions were:

a. Similarity profiles for velocities and densities.

b. Linear density variation along the depth.

c. Hydrostatic pressure.

d. Shear stresses existing only in the horizontal planes.

By considering that the longitudinal momentum dominates the pressure forces, they derived a system of ordinary equations from which a closed-form solution was obtained.

42. In 1976 Engelund improved this earlier model. Based on their original system of equations, he gave a second order closed-form solution for the near field and moderate Richardson's numbers, using a perturbation technique. His solution is the only analytical one which does not give similar profiles.

43. Abraham (1976) presented an analytical form of the axisymmetric momentum jets and plumes in stagnant and flowing receiving waters. He described the limits of the jet diffusion theory based on the similarity assumption and the entrainment concept. A comprehensive study was done by Policastro and Dunn (1976) on the integral models of surface thermal plumes. Their investigation is thorough and outlines the advantages and disadvantages of the various models.

44. A model for nonbuoyant jets in shallow receiving waters for the case of sediment transport was developed by Ozsoy (1977). He integrated the shallow-water wave equations along the jet width, including the lateral entrainment and bottom friction. Using the similarity functions for near- and far-field zones as given by Stolzenbach and Harleman (1971), Ozsoy obtained analytical solutions to the jet equations.

45. The articles discussed briefly in this chapter suffice only for a general review of turbulent jets. It is not an exhaustive list. Our attempt is to cover the evolving theory of turbulent jets and the developing stage of analysis in jet phenomenon.

46. Our main task is to formulate the freshwater discharge into a quiescent bay as a two-dimensional plane jet, to derive an analytical solution for the governing equations of fluid dynamics and

mass transport, and to predict the areal and mass extent of delta growth in early stages.

PART III: DEVELOPMENT OF THE ATCHAFALAYA RIVER DELTA

General Description

47. The development of the river delta in Atchafalaya Bay since 1950 has provided the opportunity to document the evolution of two new Mississippi delta lobes, the Lower Atchafalaya River Delta and the Wax Lake Delta. Numerous descriptive studies (Garrett, Hawxhurst, and Miller 1969; Shlemon 1972; Cratsley 1975; Roberts, Adams, and Cunningham 1980; Adams and Baumann 1980; Van Heerden 1980; and Van Heerden, Wells, and Roberts 1981) have been conducted in the bay, which form the basic foundation for this research.

48. Delta development is primarily the product of an interplay between river sediment input and reworking by physical processes in the receiving basin (Wright and Coleman 1974). However, the Atchafalaya Delta is fundamentally different from the Mississippi Balize Delta (modern bird-foot delta). The Atchafalaya Delta is building into a nonstratified shallow bay protected by a series of discontinuous oyster shell reefs, as shown in Figure 4 (Shlemon 1972). This reef chain, known as the Point Au Fer Reef, forms the Atchafalaya Delta's seaward margin, in contrast to the continental shelf location of the Mississippi modern bird-foot delta (Van Heerden 1980). The Point Au Fer Reef, including its submarine extension, was about 10 miles long before it died out in the late 1960's, due to the increasing influx of fresh water and sediment into Atchafalaya Bay (Shlemon 1972).

49. Cratsley (1975) showed that the quantity and size distribution of sediment available to the Atchafalaya Delta are directly related to the modern history of the Atchafalaya Basin and River. The Atchafalaya system is presently river-dominated; average salinity of the waters in Atchafalaya Bay is 0.37 ppt (US Fisheries and Wildlife Services 1976). Salt-wedge intrusion does not appear to significantly affect the system.

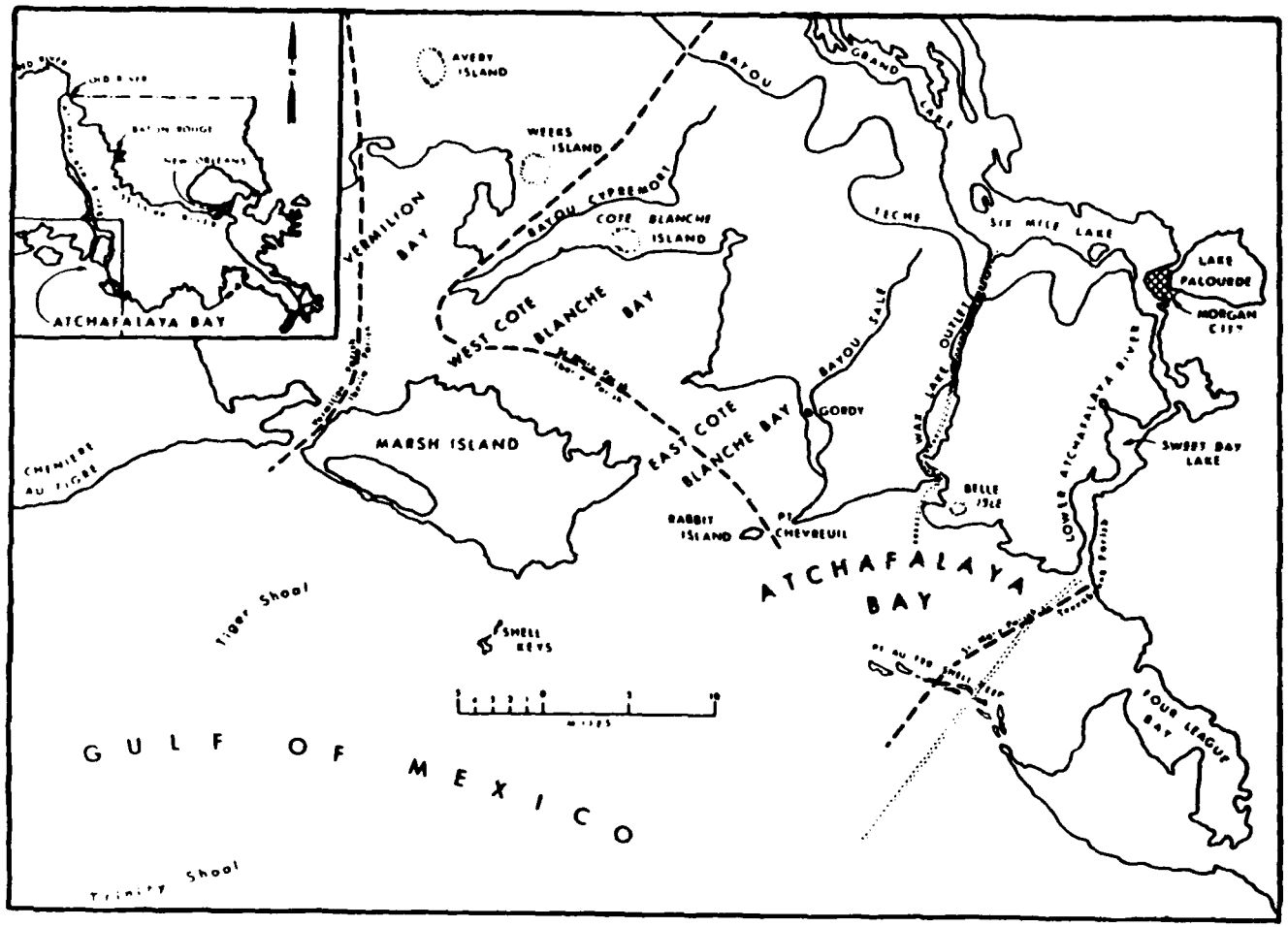

Figure 4. Location map of the Lower Atchafalaya area (Shlemon 1972)

50. This study, as outlined in PART I, is focused on use of a freshwater discharge into a quiescent bay for the prediction of the extent of area and mass of delta growth in early stages. The evolutionary history of the Atchafalaya Delta, gathered from literature, serves as the basis of our evaluation of the phenomena to be analyzed. The pertinent information on river discharge, sediment characteristics, and bay bathymetry are reviewed and arranged in chronological order in the following sections.

Historical Development

Prior to 1950's

51. The Atchafalaya River system flowed through a broad basin characterized by extensive freshwater swamps and numerous small lakes. Prior to the early 1950's, most of the sediments were trapped in the catchment basin before they reached Atchafalaya Bay. The bottom configuration of the bay virtually remained unchanged. The bay depth was maintained at a constant depth of 6 ft (Shlemon 1972). Very little sediment was deposited in the bay. Prodelta clays and silty clays were accreted on the continental shelf off the Atchafalaya Bay (Cratsley 1975).

1952 to 1962

52. From 1952 to 1962, as the diversion of Mississippi River flow through the Atchafalaya River system increased steadily and as the catchment basins were filled, accelerated sedimentation in Atchafalaya Bay marked the beginning of a subaqueous delta (Cratsley 1975). As displayed in Figure 5, Grand Lake and Six Mile Lake, which had been natural settling basins for coarse-grained sediments (silt and sand), were rapidly filled by deltaic deposits. These catchment basins are now directly routing sediment through the natural Lower Atchafalaya River Outlet and the man-made Wax Lake Outlet.

53. Shlemon (1972) indicated that about 47 square miles of the bay bottom had been covered by at least a 1-ft thickness of sediment by 1962; over 6 ft of fill occurred just south of Shell

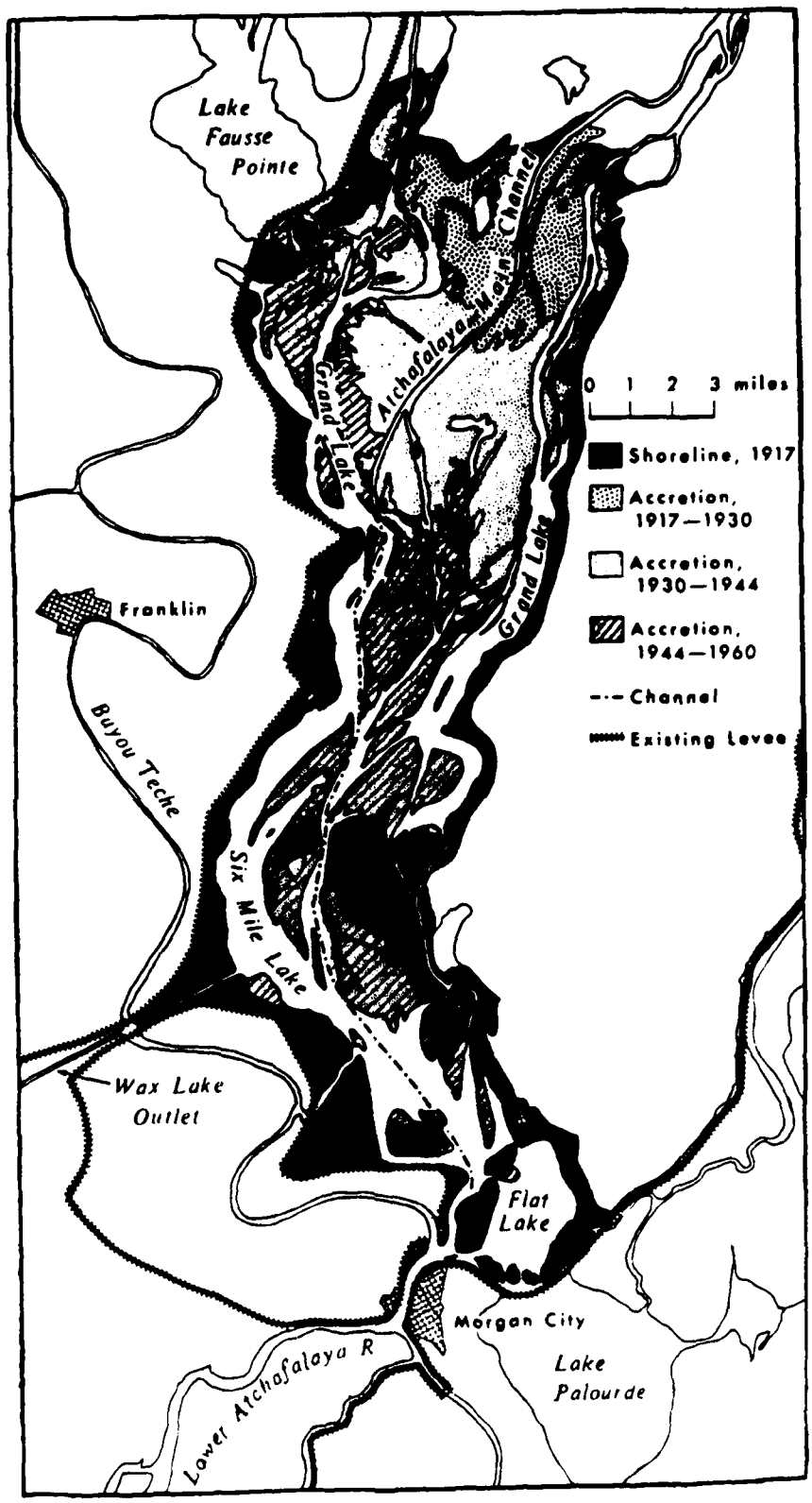

Figure 5. Lacustrine delta accretion in the Lower Atchafalaya Basin, 1917-1960 (Shlemon 1972)

Island, as shown in Figure 6 and Table 1. In Figure 6, the delta front environment in the Wax Lake Outlet mouth area is much less extensive than that of the Lower Atchafalaya River mouth area, reflecting the relative discharges from the two outlets during the period of 1952 to 1962 (Cratsley 1975).

1965 to 1967

54. In the late 1960's, the increasing discharge of the Atchafalaya River and the increasing rate of suspended sediment transport were responsible for the formation of the distributary bars at the mouths of the Wax Lake Outlet and the Lower Atchafalaya River (Cratsley 1975). The average monthly discharge at the latitude of the outlets during the period 1965-1967 and the corresponding suspended load transported through the outlets were summarized by Garrett, Hawxhurst, and Miller (1969), and Cratsley (1975) as reproduced in Figure 7. The combined average annual freshwater flow through the outlets was about 165,000 cfs. High riverflows occurred from January through June, reaching a maximum of 325,000 cfs in May and a minimum of 73,000 cfs in September. The textural composition of the suspended load was 25 percent sand and 75 percent silt and clay (Garrett, Hawxhurst, and Miller 1969).

1967 to 1972

55. The period 1967 to 1972 was characterized by the expansion of the delta front environment throughout Atchafalaya Bay, the establishment of distributary mouth bars in the bay, and the rapid progradation of the distal bar (Cratsley 1975). Very definite subaerial delta lobes appeared in 1972. These initial subaerial exposures were shoals, composed largely of sediment, extending from the Atchafalaya River Outlet to Point Au Fer Shell Reef.

56. The rapid expansion of the delta front environment in the Wax Lake Outlet channel mouth area is shown in Figure 8, the 1972 bathymetric map prepared by the US Army Engineer District, New Orleans (Adams and Baumann 1980). A more detailed evaluation of the progradation of the delta front environment was made by Cratsley (1975) by

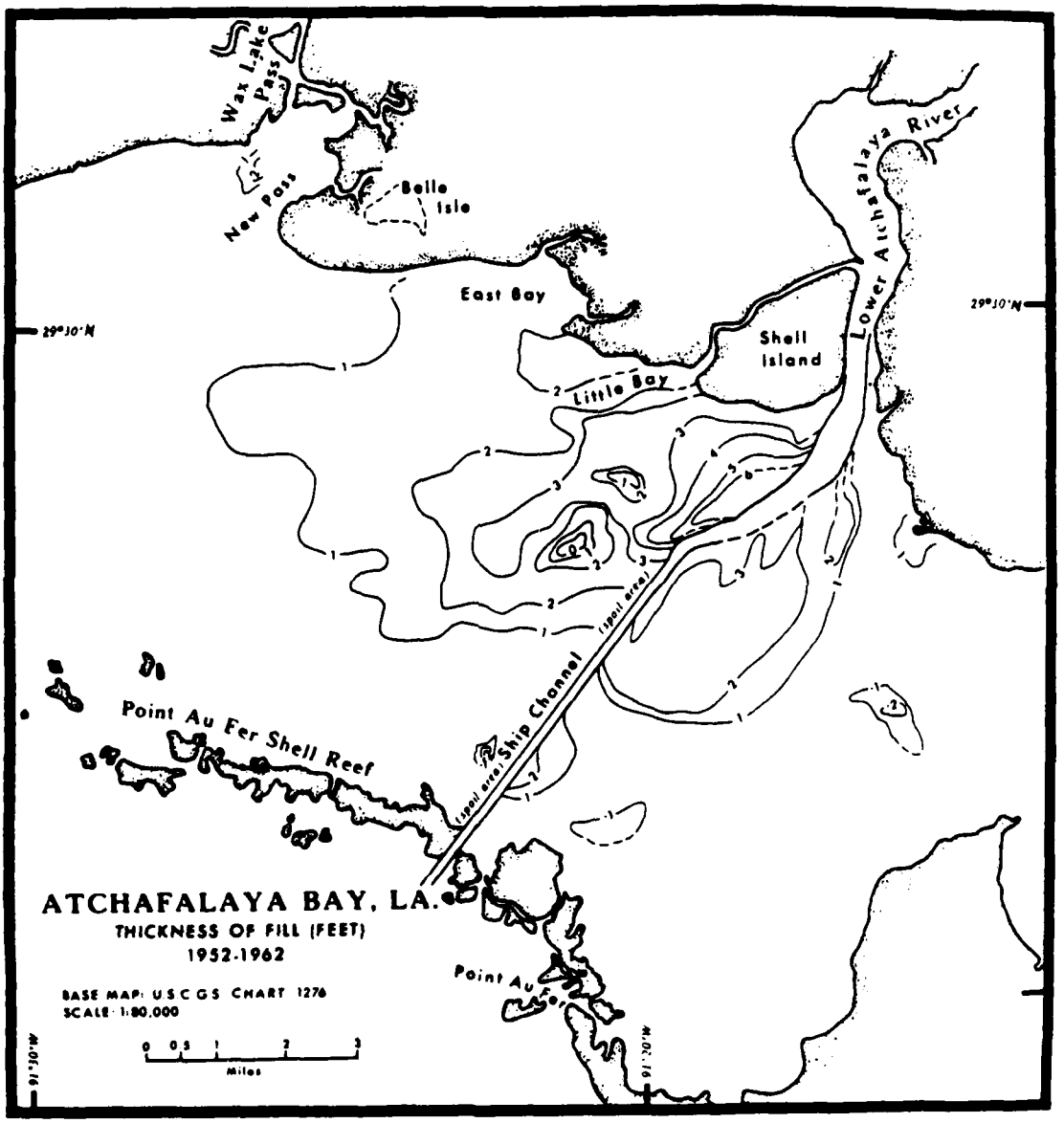

Figure 6. Isopach map showing area and thickness of deltaic fill in Atchafalaya Bay, 1952-1962 (Shlemon 1972)

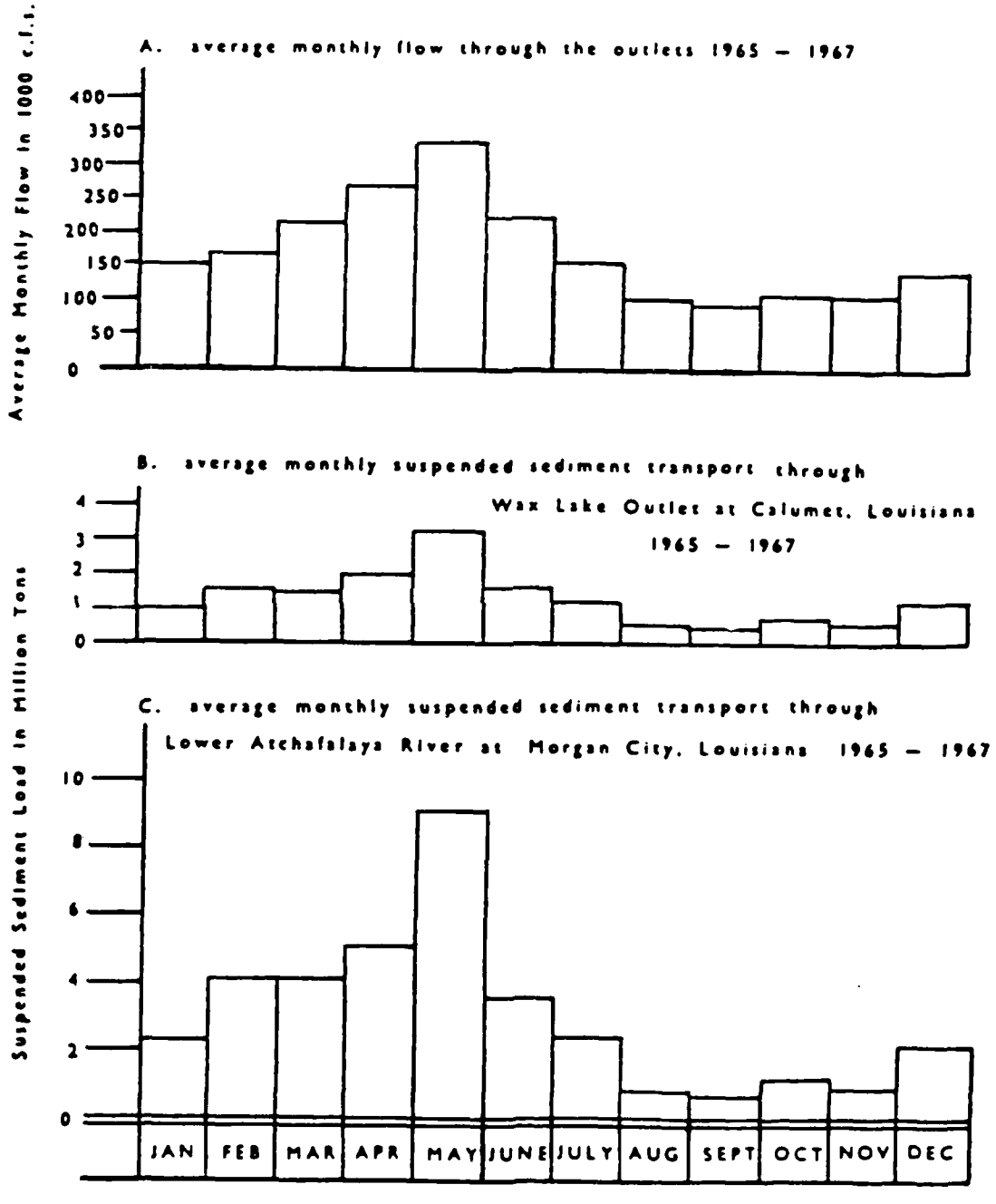

Figure 7. Average monthly flow and suspended sediments transported through the outlets during the period 1965-1967 (Cratsley 1975)

Figure 8. Bathymetric map of Atchafalaya Bay, 1972 (Adams and Baumann 1980)

measuring the changes in bottom topography along the six profile lines as delineated in Figure 9 and plotted in Figure 10.

57. The annual flow in the Atchafalaya River at Simmesport, Louisiana (near the diversion point in the upper basin), from 1967 to 1972, was 208,000 cfs, and the average annual peak flow was 303,000 cfs (Adams and Baumann 1980). Adams and Baumann (1980) indicated that the increase in discharge during the period of 1967 to 1972 occurred predominantly during traditionally low flow months; the peak discharges during the spring months were not great enough to increase sediment load entering the bay. The average annual sediment load delivered to Atchafalaya Bay was about 63 x 10^6 tons for the period 1965-1971 (USACOE 1974).

1973 to 1975

58. The 1973-1975 years were abnormally high-water years compared with the past 20 years of flow records at Simmesport, Louisiana, as displayed in Figure 11 (Van Heerden 1980). During 1973-1975, flows averaged 315,000 cfs at Simmesport; peak flows of over 700,000 cfs occurred in April 1973 and over 600,000 cfs in April 1975.

59. Similar high-flow averages and peak flow were recorded at Morgan City, on the Lower Atchafalaya River, during 1973-1975. Both the discharge and suspended load at Morgan City are displayed in Figure 12 (Roberts, Adams, and Cunningham 1980). Peak flows at Morgan City of over 600,000 cfs occurred in May 1973, and the normal 300,000-cfs peak flows were exceeded during 8 months of 1973-1975.

60. Accompanying these abnormally high discharges were unusually high concentrations of sediment carried as suspended load (25 percent sand, 75 percent silt and clay). The annual suspended sediment load reaching Atchafalaya Bay during the three high-water years was about 123 x 10^6 tons. The sediment budget and size characteristics during the periods of 1965-1971 and 1973-1975 are listed in Table 2 (Roberts, Adams, and Cunningham 1980).

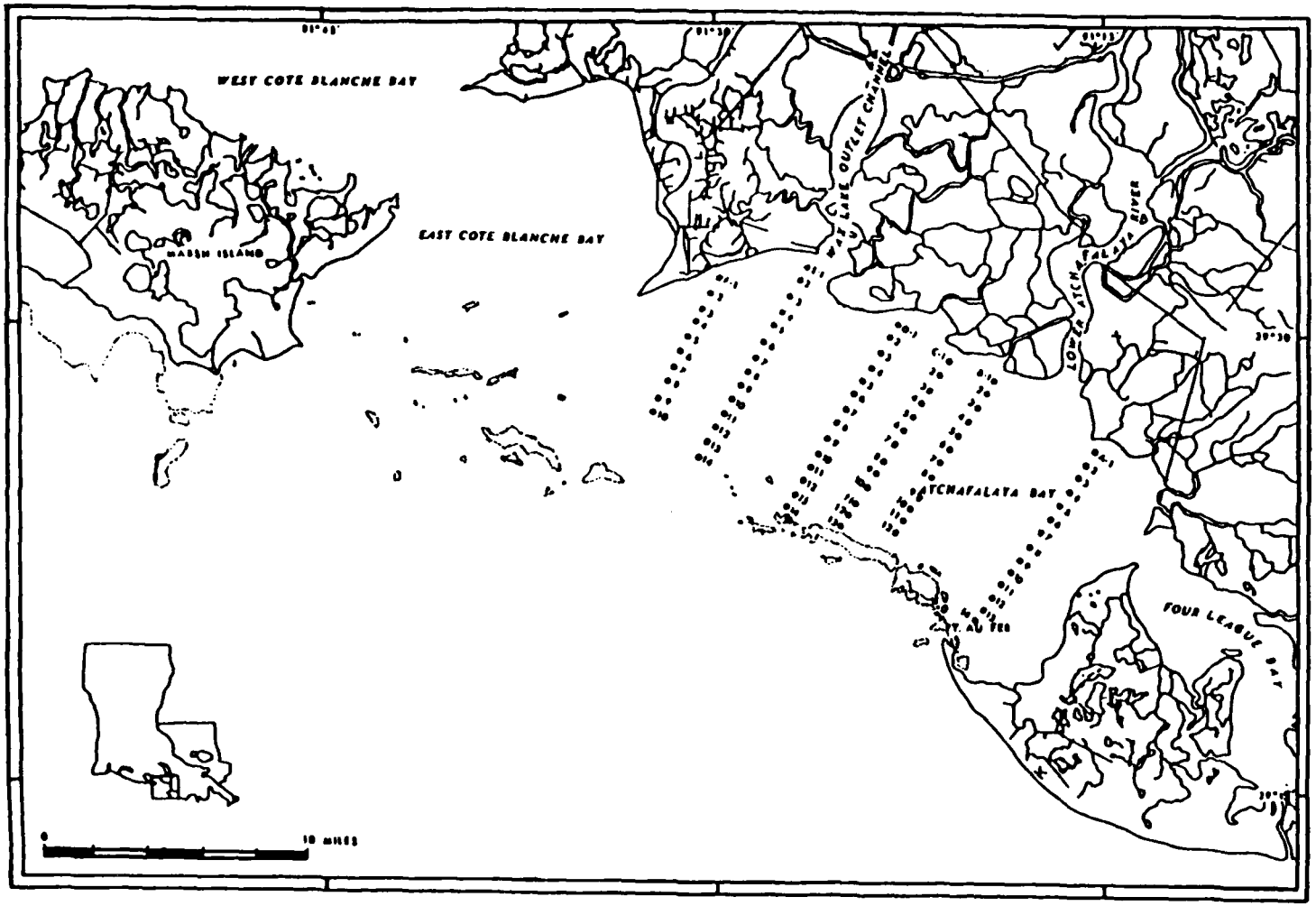

Figure 9. Index map for bottom topography profile lines (Cratsley 1975)

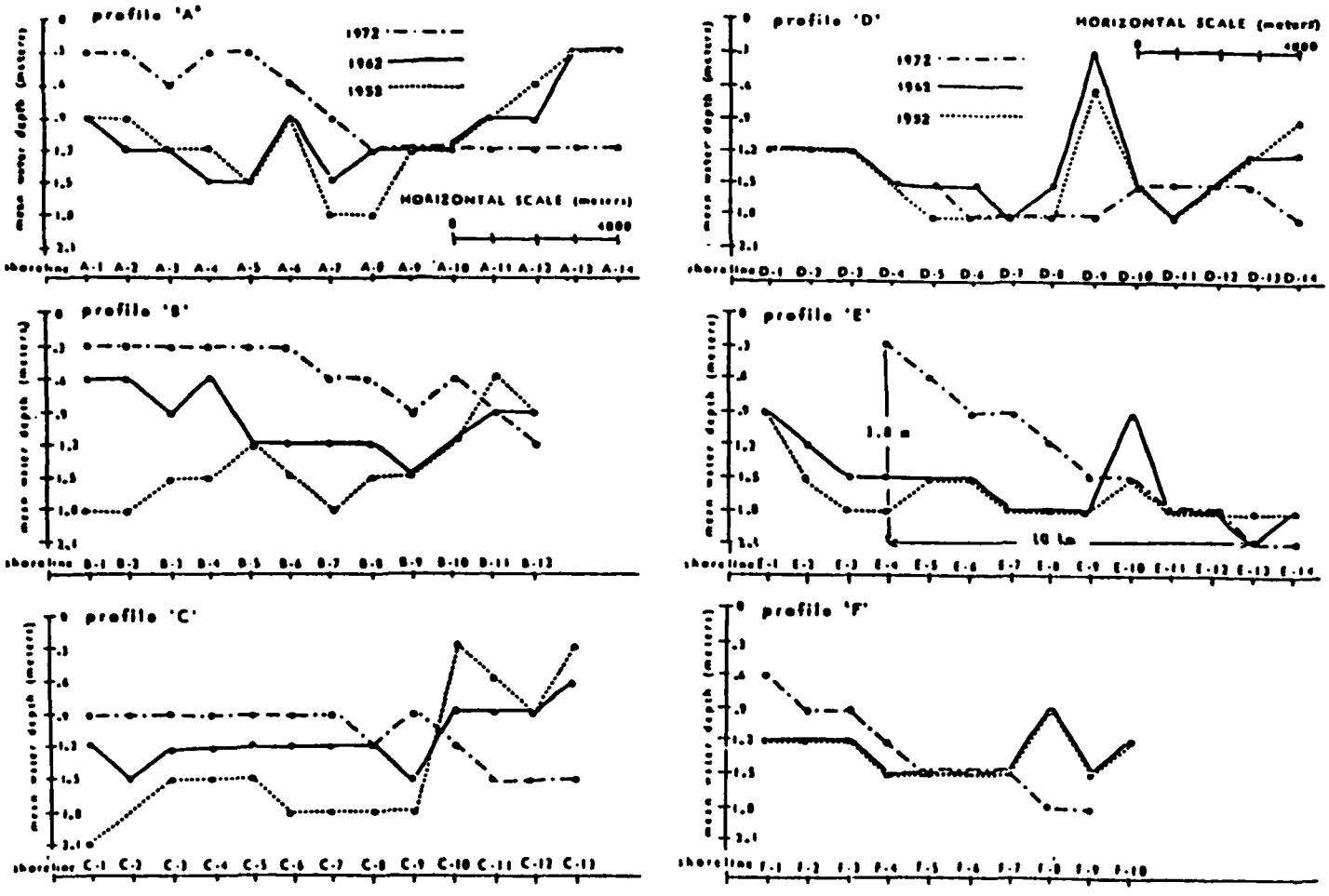

a. Lower Atchafalaya River Outlet

b. Wax Lake Outlet

Figure 10. Atchafalaya Bay bottom topography profiles (Cratsley 1975)

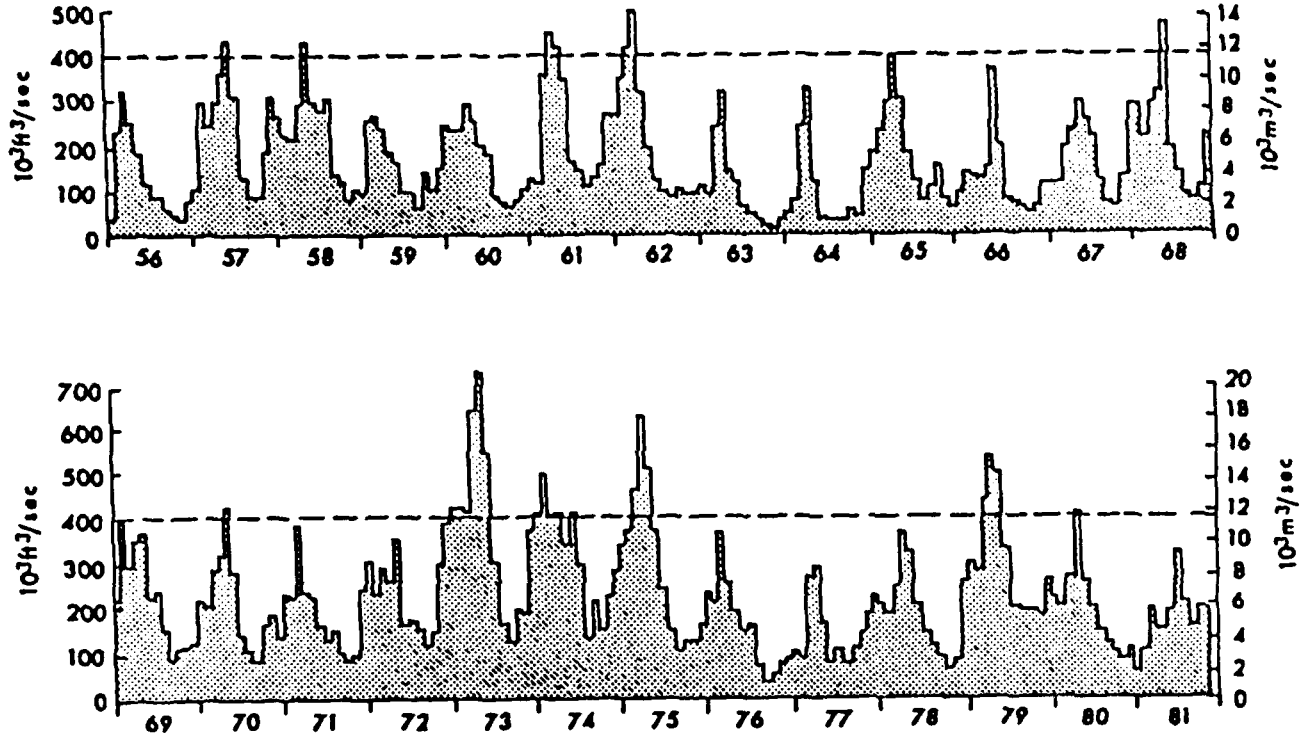

Figure 11. Average monthly discharge of Atchafalaya River at Simmesport, La. (Van Heerden 1980)

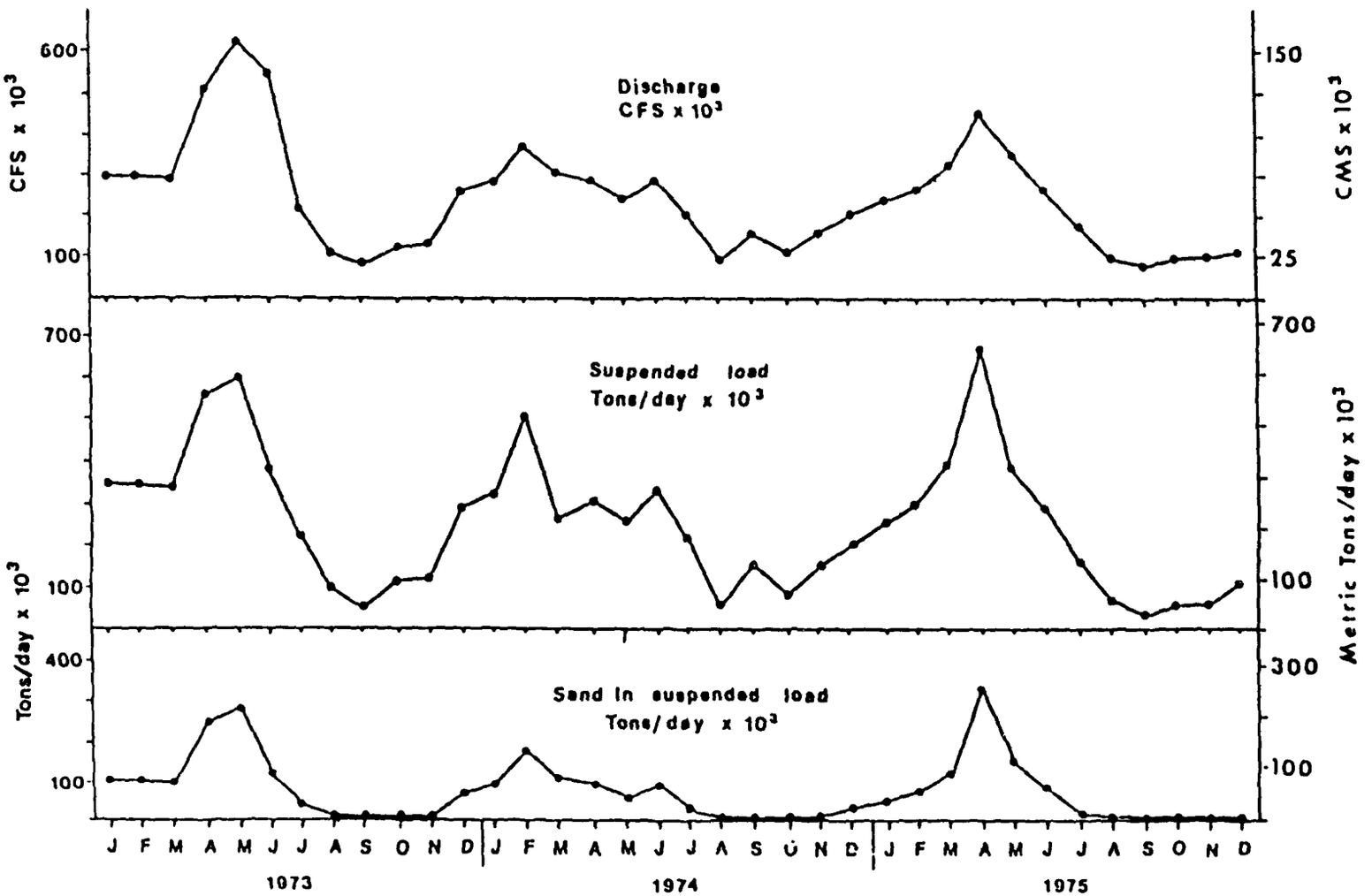

Figure 12. Discharge and suspended load at Morgan City near Lower Atchafalaya River Outlet, 1973-1975 (Roberts, Adams, and Cunningham 1980)

1976 to 1978

61. Although the years 1976 through 1978 were considered as normal flood years (Figure 11), the previous three abnormally high-water years had played an important role in the rapid development of the subaerial delta phase. During 1976-1978, the distributary mouth bar extended seaward and evolved into a complex branching network characteristic of deltas where river mouths are frictionally dominated and are gradually building into low-energy, shallow-water environments (Wright and Coleman 1974).

62. Bathymetric data taken in 1977 by USACOE and adjusted to the 1975 msl datum (Adams and Baumman 1980) indicated that an estimated 6.55 square miles of new land has developed above msl (Figure 13). Above the -1 ft datum, which represents the mean low tide level, a calculated 15.8 square miles of new subaerial land with an approximate width of 6.8 miles had been added to Atchafalaya Bay over the period 1967-1977 (Roberts, Adams, and Cunningham 1980).

1979

63. Another major flood occurred in 1979. A peak flow of over 500,000 cfs was recorded in April 1979 (Figure 11). Roberts, Adams, and Cunningham (1980) concluded that suspended sediment transport during floods was responsible for the abrupt increases in subaerial delta growth.

64. Through using satellite imagery, color infrared photography, and digital current meter data, Wells and Kemp (1981) provided estimates on the suspended sediment concentrations within Atchafalaya Bay. These average about 300 mg/l and range from 250 to 400 mg/l.

Long-Term Future Projection

1970 to 2020

65. Shlemon (1972), using sediment load measurements obtained in the outlets, outlined the probable future configuration of the Atchafalaya Delta by the year 2020 (Figure 14). An average growth rate was inferred and is plotted in Figure 15. A straight line projection of bay filling until the year 2020 will yield an estimated

Figure 13. Bathymetric map of Atchafalaya Bay, 1977 (Adams and Baumann 1980)

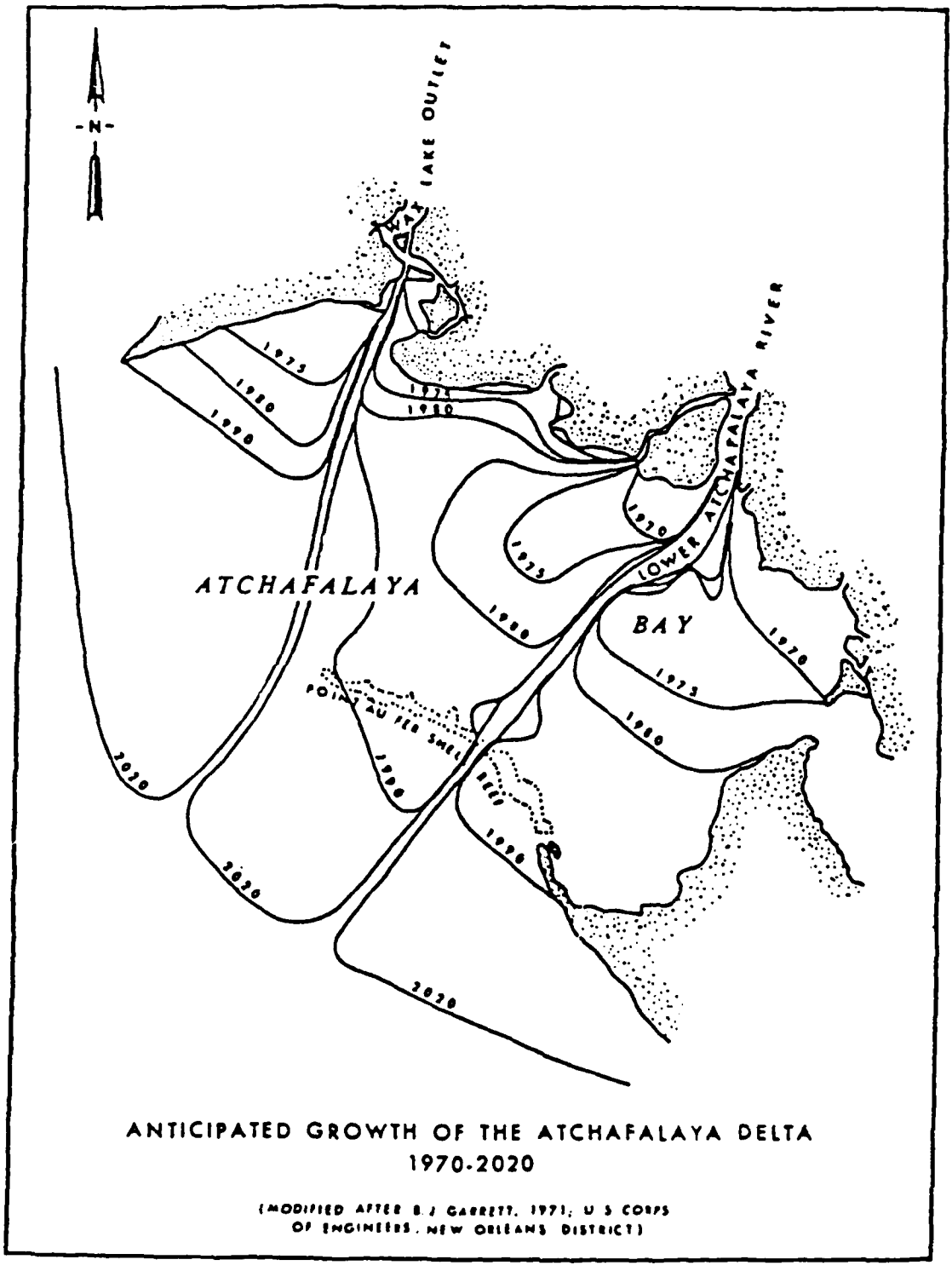

ANTICIPATED GROWTH OF THE ATCHAFALAYA DELTA
1970-2020

(MODIFIED AFTER B. J. GARRETT, 1971; U. S. CORPS OF ENGINEERS, NEW ORLEANS DISTRICT)

Figure 14. Anticipated configuration of the Atchafalaya Delta shoreline by the year 2020 (Shlemon 1972)

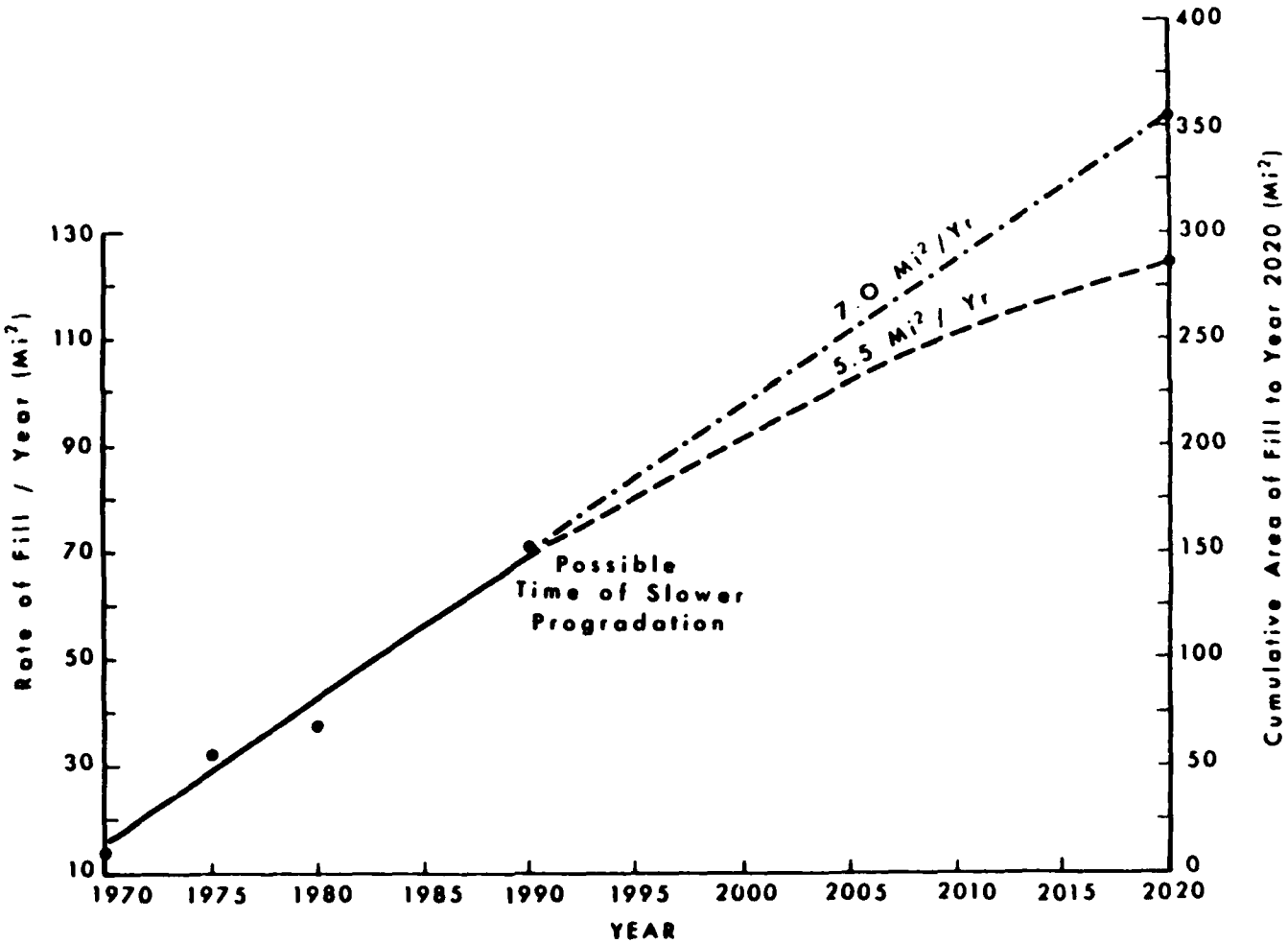

Figure 15. Inferred 50-year (1970-2020) average growth rate of the Atchafalaya River Delta if unmodified by man

filling rate of about 7 square miles per year, covering an area of 350 square miles. Assuming that the peak of subaerial growth will be reached by 1990, a conservative growth rate will be 5.5 square miles per year, with resultant production of nearly 290 square miles of new land by the year 2020.

66. Roberts, Adams, and Cunningham (1980) pointed out that unless an abnormal number of peak floods such as those of the 1973-1975 period occur during the next two decades, Atchafalaya Bay probably will not be filled until after the turn of the century. They further estimated that the sand-dominated phase of the delta will probably cover an area of over 50 square miles before shifting its locus of deposition to the shelf seaward of the Point Au Fer Shell Reef.

67. Van Heerden, Wells, and Roberts (1981) projected that the Atchafalaya Delta should prograde more rapidly, form thin sand bodies, and eventually cover a wider area, much like the Lafourche, St. Bernard, and Teche delta lobes.

1977 to 2027

68. A statistical approach to predict the future growth of the Atchafalaya River delta, based on historical deposition trends in Atchafalaya Bay, has been presented by Letter (1982). He developed a regression model that correlates deposition rates with river discharge, sediment yield, water depth, and the delta mass centroid. Using the 1977 bathymetry as an initial condition, the model is applied to a 50-year hydrograph at 10-year increments of prediction. The results of the regression model showed that within 50 years the delta will evolve gulfward of Eugene Island, the gulfward limit of the bay.

69. Figure 16 shows the predicted condition of the Atchafalaya Bay in the year 2027. The total volume of the deposited sediments is estimated at 58 billion ft^3, and the delta mass volume, based on -3 ft NGVD (National Geodetic Vertical Datum), is about 17.6 billion ft^3 (Letter 1982).

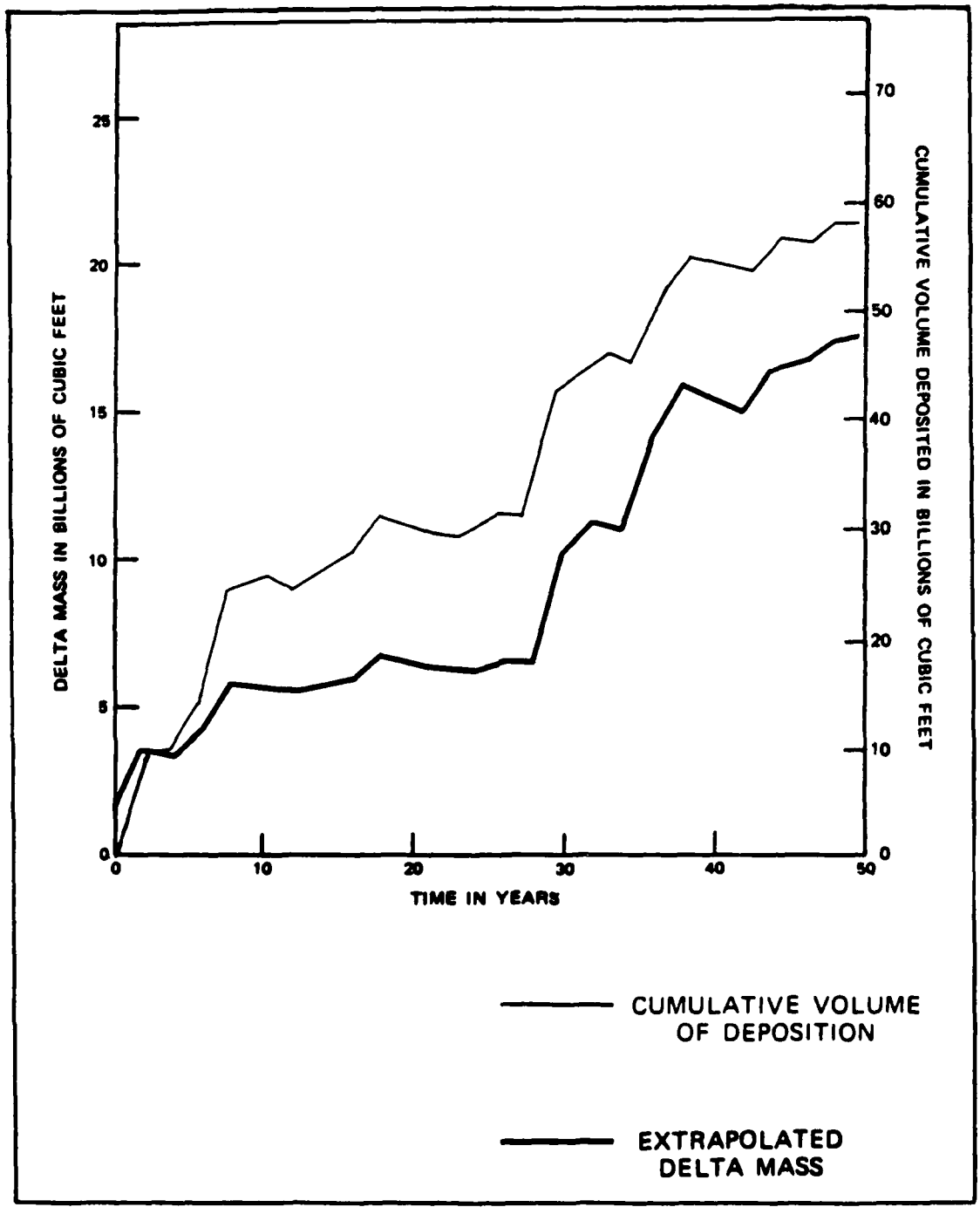

Figure 16. Estimated delta mass and deposited sediment volume for the Atchafalaya Delta, 1970-2020

1980 to 2030

70. Long-term predictions based on the morphologic development of the Atchafalaya River delta and generic analysis of existing deltas have been completed recently by Wells, Chinburg, and Coleman (1984). Utilizing maps, charts, aerial photographs, and LANDSAT imagery, they have examined 10 similar deltas and subdeltas worldwide, and have projected the rate of growth and configuration of subaerial land in Atchafalaya Bay to the year 2030.

71. The requirements for similar deltas that closely resemble the Lower Atchafalaya River delta were defined by Wells, Chinburg, and Coleman (1984) in their generic analysis. The requirements were low wave energy, low tidal energy, a shallow receiving basin, and high suspended sediment load. The results from their study indicate that the subaerial land area in Atchafalaya Bay by the year 2030 will range from 150 km^2 (59 square miles) to 337 km^2 (132 square miles), with 208 km^2 (81 square miles) representing the expected land area in 50 years under average flood conditions.

72. Approximately 14 x 10^6 m^3 (495 x 10^6 ft^3) of sediment per year is retained in Atchafalaya Bay (Wells, Chinburg, and Coleman 1984). Growth prediction curves for subaerial land in the bay were constructed by Wells, Chinburg, and Coleman (1984), as shown in Figure 17. Figure 18 shows the configuration of land in the bay in the year 2030 based on the range of predicted rates of growth.

73. Table 3 summarizes the development of the Atchafalaya River delta in chronological order as gathered from various literature.

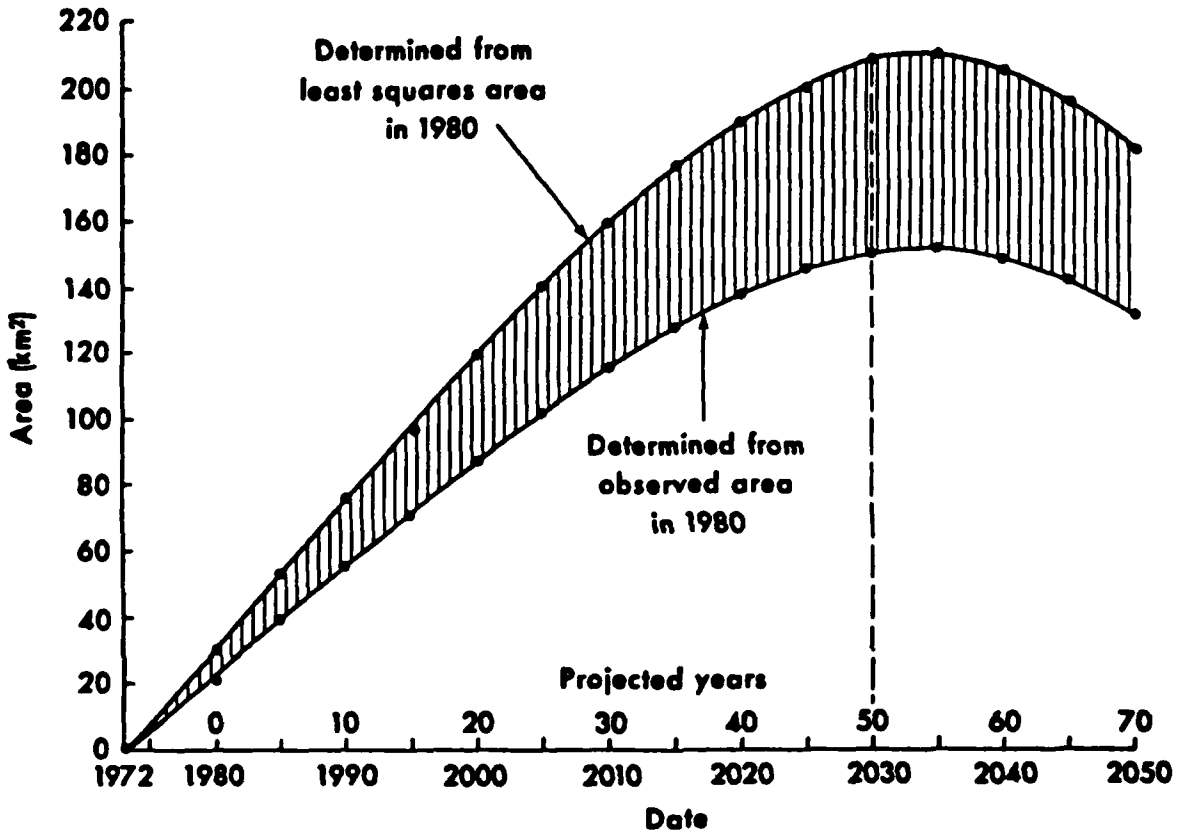

Figure 17. Growth curves predicting subaerial land in Atchafalaya Bay in the year 2030

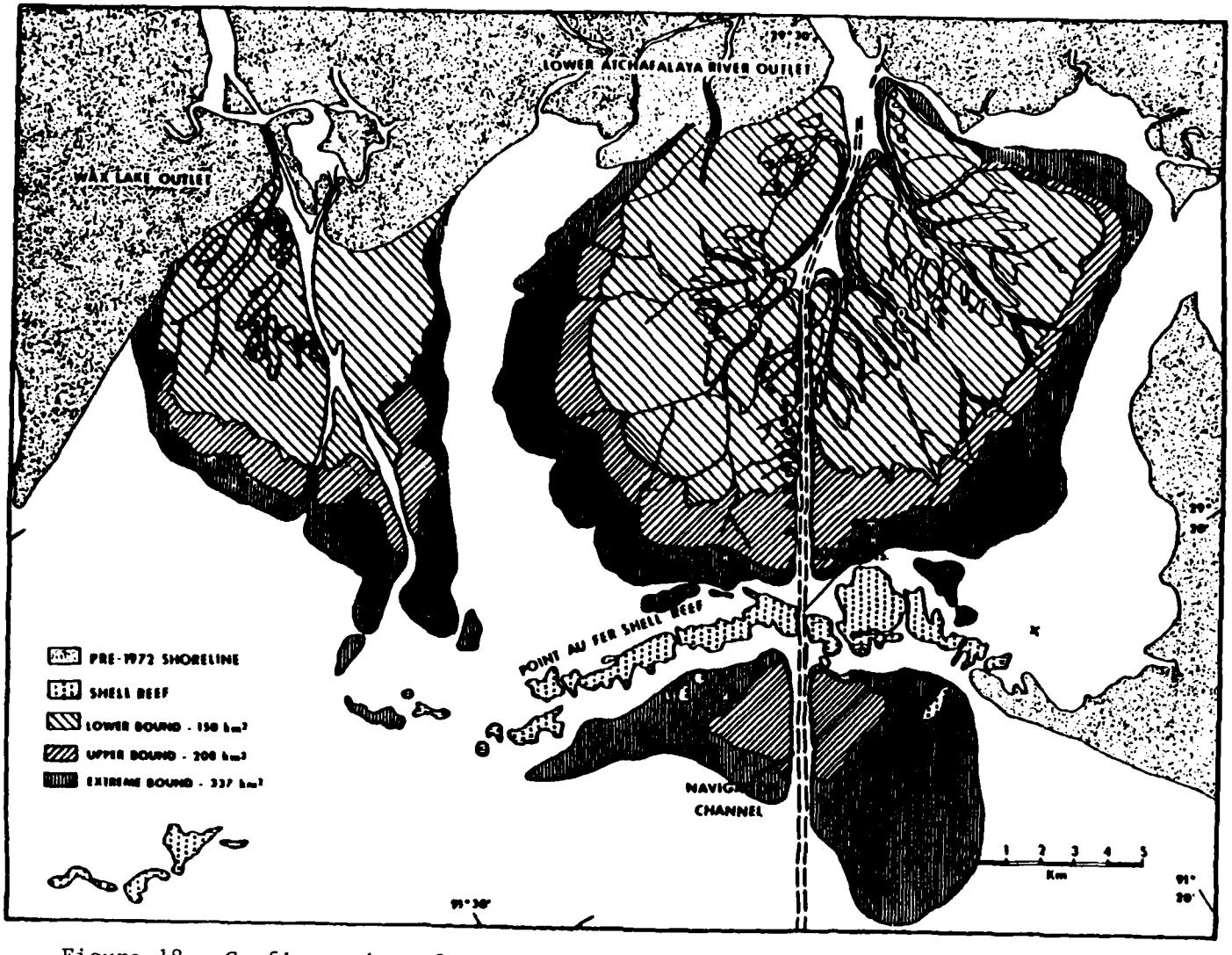

Figure 18. Configuration of subaerial land in Atchafalaya Bay in the year 2030 assuming total areas of 150, 208, and 337 km^2

PART IV: GOVERNING EQUATIONS OF TURBULENT PLANE JETS IN SHALLOW RECEIVING WATERS

General Description of River-Bay Systems

74. River mouths, with their unique features, are very complex physical systems. Because they provide a natural link between inland and sea, most of the world's civilizations and metropolitan cities have been developed close to these areas. Therefore conflicting interests regarding ecologic, economic, recreational, and transportation issues are closely interrelated with these coastal domains, creating a challenge where both human and natural forces are involved.

75. The main factors affecting the processes of river mouth delta formation are river-bay hydrodynamics, geomorphology, climate, and human activities (Coleman 1976). Due to the practical importance of river delta development, many scientific efforts have been placed on the investigation of basic laws and principles that govern the behavior and response of fresh, sediment-laden river water as it issues into the receiving salt waters of the sea.

76. The overall river-bay system is a time-dependent, three-dimensionsal phenomenon, influenced by a vast number of different deterministic and stochastic parameters. To develop a general mathematical model would be a formidable task; thus based on field and laboratory observations of similar phenomena, certain assumptions are made and predominant parameters with deterministic characteristics are used to reduce the problem considerably and to make it suitable for theoretical formulation and analytical approach.

Formulation of River Discharge into a Bay

77. Physically, a river-bay system can be regarded as a plane water jet issuing into a large receiving body of water. Mathematically, the jet hydrodynamics of a river-bay system can be expressed by a system

of time-dependent, nonuniform, incompressible, free-surface, three-dimensional turbulent flow equations (Schlichting 1968). In general, this is a nonlinear, hyperbolic-type partial differential system of four equations, one for mass continuity and three for momentum balance. The independent variables are the three Cartesian axes (x_1, x_2, x_3) and the time (t), as shown in Figure 3, while the dependent variables are the three velocity components parallel to the three axes and the water elevation (η). In many practical cases this system can be reduced into a two- or one-dimensional model and still be able to describe the physical phenomena adequately.

78. The general form of the equation of continuity, or conservation of mass, for an incompressible flow (Schlichting 1968) is written as

$$\frac{\partial u_i}{\partial x_i} = 0 \qquad i = 1, 2, 3 \qquad (1)$$

where u_i = the velocity components, and x_i = the Cartesian coordinates.

79. The equations of momentum are derived from the Navier-Stokes equation (Schlitching 1968) and are expressed as

$$\frac{Du_i}{Dt} = -\frac{1}{\rho}\frac{\partial p}{\partial x_i} + \frac{1}{\rho}\frac{\partial \tau_{ik}}{\partial x_k} + b_i \qquad k = 1, 2, 3 \qquad (2)$$

where the symbol D/Dt denotes the total derivative, that is, the equivalence of an operator,

$$\frac{D}{Dt} = \frac{\partial}{\partial t} + u_1\frac{\partial}{\partial x_1} + u_2\frac{\partial}{\partial x_2} + u_3\frac{\partial}{\partial x_3} \qquad (3)$$

ρ = the density, p = the pressure, τ_{ik} = the stress components, and b_i = the body forces.

Shallow-Water Hydrodynamic Equations

80. The general system can be reduced into a simpler form for the case of shallow waters as pertaining to the Atchafalaya River-Bay system. The basic assumption is the hydrostatic pressure distribution, and by neglecting the vertical stress components and the vertical acceleration, the x_3 momentum balance in Equation 2 reduces to

$$0 = -\frac{1}{\rho}\frac{\partial p}{\partial x_3} - g \tag{4}$$

or

$$p = \rho g(\eta - x_3) + p_0 \tag{5}$$

where η = free surface elevation from the reference datum and p_0 = atmospheric pressure. The reference datum coincides with the mean sea level (Figure 3).

Equation of continuity

81. The free surface can be expressed as $x_3 = \eta(x_1, x_2, t)$. Differentiating this with respect to time yields

$$u_3 = \frac{\partial \eta}{\partial t} + u_1 \frac{\partial \eta}{\partial x_1} + u_2 \frac{\partial \eta}{\partial x_2} \tag{6}$$

Similarly, if $x_3 = -h(x_1, x_2)$ is the distance from the reference datum to the bottom, then

$$u_3 = - u_1 \frac{\partial h}{\partial x_1} - u_2 \frac{\partial h}{\partial x_2} \tag{7}$$

Integration of Equation 1 with respect to the x_3-axis gives

$$\int_{-h}^{\eta} \frac{\partial u_1}{\partial x_1} dx_3 + \int_{-h}^{\eta} \frac{\partial u_2}{\partial x_2} dx_3 + u_3(x_1, x_2, \eta) - u_3(x_1, x_2, -h) = 0 \tag{8}$$

Utilizing Leibnitz's rule of integration (Wylie 1951) together with Equations 6 and 7, Equation 8 yields

$$\frac{\partial}{\partial x_1}\int_{-h}^{\eta} u_1 \, dx_3 + \frac{\partial}{\partial x_2}\int_{-h}^{\eta} u_2 \, dx_3 + \frac{\partial \eta}{\partial t} = 0 \tag{9}$$

Furthermore, due to the shallowness of the bay waters, the velocities are assumed to be uniform along the depth. Then Equation 9 can be written as

$$\frac{\partial (h + \eta) u_1}{\partial x_1} + \frac{\partial (h + \eta) u_2}{\partial x_2} + \frac{\partial \eta}{\partial t} = 0 \tag{10}$$

Equation 10 is the final form of the continuity equation in a two-dimensional, time-dependent shallow-water horizontal domain.

Equation of momentum

82. After introducing the shallow-water approximation and expanding the total derivative, Equation 2 becomes

$$\frac{\partial u_i}{\partial t} + \frac{\partial (u_i u_k)}{\partial x_k} = -\frac{1}{\rho}\frac{\partial p}{\partial x_i} + \frac{1}{\rho}\frac{\partial \tau_{ik}}{\partial x_k} + b_i \qquad (11)$$

$$i = 1, 2$$

$$k = 1, 2, 3$$

Let the time average of the velocity components be represented by

$$u_i = \bar{u}_i(x_1, x_2, t) + u_i'(x_1, x_2, t) \qquad (12)$$

where $\bar{u}_i$ = mean velocities and u_i' = perturbation velocities with zero mean value. Also let the only mass force be the Coriolis force. Thus, for the northern hemisphere,

$$b_1 = 2\,\Omega \sin\phi\, u_2 \qquad (13a)$$

$$b_2 = -2\,\Omega \sin\phi\, u_1 \qquad (13b)$$

where Ω = angular velocity of the earth, and ϕ = geographical latitude of the river mouth of the site. The shearing forces can be approximated as

$$\frac{\partial \tau_{ik}}{\partial x_k} = \mu \frac{\partial}{\partial x_k}\left(\frac{\partial u_i}{\partial x_k}\right) \qquad (14)$$

where μ = molecular viscosity.

83. Substituting Equation 12 for the perturbated velocities, Equations 13a and 13b for the Coriolis forces, and Equation 14 for the approximated shearing forces into Equation 11 and time-averaging it, one arrives at

$$\frac{\partial \bar{u}_1}{\partial t} + \frac{\partial(\bar{u}_1\bar{u}_1)}{\partial x_1} + \frac{\partial(\bar{u}_1\bar{u}_2)}{\partial x_2} + \frac{\partial(\bar{u}_1\bar{u}_3)}{\partial x_3} - 2\,\Omega \sin\phi\ \bar{u}_2$$

$$= -\frac{1}{\rho}\frac{\partial p}{\partial x_1} + \frac{\mu}{\rho}\left(\frac{\partial^2 \bar{u}_1}{\partial x_1^2} + \frac{\partial^2 \bar{u}_1}{\partial x_2^2} + \frac{\partial^2 \bar{u}_1}{\partial x_3^2}\right)$$

$$- \left(\frac{\partial \bar{u}_1'\bar{u}_1'}{\partial x_1} + \frac{\partial \bar{u}_1'\bar{u}_2'}{\partial x_2} + \frac{\partial \bar{u}_1'\bar{u}_3'}{\partial x_3}\right) \qquad (15a)$$

and

$$\frac{\partial \bar{u}_2}{\partial t} + \frac{\partial(\bar{u}_2\bar{u}_1)}{\partial x_1} + \frac{\partial(\bar{u}_2\bar{u}_2)}{\partial x_2} + \frac{\partial(\bar{u}_2\bar{u}_3)}{\partial x_3} + 2\,\Omega \sin\phi\ \bar{u}_1$$

$$= -\frac{1}{\rho}\frac{\partial p}{\partial x_1} + \frac{\mu}{\rho}\left(\frac{\partial^2 \bar{u}_2}{\partial x_1^2} + \frac{\partial^2 \bar{u}_2}{\partial x_2^2} + \frac{\partial^2 \bar{u}_2}{\partial x_3^2}\right)$$

$$- \left(\frac{\partial \bar{u}_2'\bar{u}_1'}{\partial x_1} + \frac{\partial \bar{u}_2'\bar{u}_2'}{\partial x_2} + \frac{\partial \bar{u}_2'\bar{u}_3'}{\partial x_3}\right) \qquad (15b)$$

84. The last two terms of Equation 15a and 15b can be grouped together as total stress terms designated by the eddy viscosity stresses in both horizontal and vertical components. Equations 15a and 15b become

$$\frac{\partial u_1}{\partial t} + \frac{\partial(u_1u_1)}{\partial x_1} + \frac{\partial(u_1u_2)}{\partial x_2} + \frac{\partial(u_1u_3)}{\partial x_3} - 2\,\Omega \sin\phi\ u_2$$

$$= -\frac{1}{\rho}\frac{\partial p}{\partial x_i} + \varepsilon_h\left(\frac{\partial^2 u_1}{\partial x_1^2} + \frac{\partial^2 u_1}{\partial x_2^2}\right) + \varepsilon_v \frac{\partial^2 u_1}{\partial x_3^2} \qquad (16a)$$

and

$$\frac{\partial u_2}{\partial t} + \frac{\partial (u_2 u_1)}{\partial x_1} + \frac{\partial (u_2 u_2)}{\partial x_2} + \frac{\partial (u_2 u_3)}{\partial x_3} + 2\,\Omega \sin\phi\, u_1$$

$$= -\frac{1}{\rho}\frac{\partial p}{\partial x_2} + \varepsilon_h \left(\frac{\partial^2 u_2}{\partial x_1^2} + \frac{\partial^2 u_2}{\partial x_2^2} \right) + \varepsilon_h \frac{\partial^2 u_2}{\partial x_3} \qquad (16b)$$

where ε_h = horizontal eddy viscosity coefficient, and ε_v = vertical eddy viscosity coefficient. The bars (-) were dropped for convenience.

85. Neglecting the vertical velocity component (u_3), substituting the pressure p from Equation 5, integrating Equation 16 from bottom to surface along the x_3-axis, dividing by $h + \eta$, and assuming vertically averaged velocities, Equations 16a and 16b become

$$\frac{\partial u_1}{\partial t} + \frac{\partial (u_1 u_1)}{\partial x_1} + \frac{\partial (u_1 u_2)}{\partial x_2} - 2\,\Omega \sin\phi\, u_2$$

$$= -g \frac{\partial \eta}{\partial x_1} + \varepsilon_h \left(\frac{\partial^2 u_1}{\partial x_1^2} + \frac{\partial^2 u_1}{\partial x_2^2} \right) + \frac{\varepsilon_v}{h+\eta} \left(\frac{\partial u_1}{\partial x_3}\Big|_{\eta} - \frac{\partial u_1}{\partial x_3}\Big|_{-h} \right) \qquad (17a)$$

and

$$\frac{\partial u_2}{\partial t} + \frac{\partial (u_2 u_1)}{\partial x_1} + \frac{\partial (u_2 u_2)}{\partial x_2} + 2\,\Omega \sin\phi\, u_1$$

$$= -g \frac{\partial \eta}{\partial x_2} + \varepsilon_h \left(\frac{\partial^2 u_2}{\partial x_1^2} + \frac{\partial^2 u_2}{\partial x_2^2} \right) + \frac{\varepsilon_v}{h+\eta} \left(\frac{\partial u_2}{\partial x_3}\Big|_{\eta} - \frac{\partial u_2}{\partial x_3}\Big|_{-h} \right) \qquad (17b)$$

where u_1 and u_2 now stand for the average velocities over the depth in the horizontal domain.

86. The last term in Equations 17a and 17b is the expression for the tangential stresses at the surface ($x_3 = \eta$) and at the bottom ($x_3 = -h$). Experimental studies in a one-dimensional rivertlow resulted in an empirical formula for the bottom stresses (τ_b)

$$\tau_b = \rho g \frac{u^2}{C_z^2} \tag{18}$$

where C_z = Chezy's coefficient of friction and u = the mean cross-sectional velocity. The value of C_z depends on various geometrical and flow parameters. It is suggested that this coefficient be evaluated through calibration from actual field data. Experience shows that the coefficient C_z usually varies between 45 $m^{\frac{1}{2}}$/sec and 70 $m^{\frac{1}{2}}$/sec.

87. Similarly, the air-sea interaction stresses (τ_s) can be approximated by a formula like that of Equation 18 and can be written as

$$\tau_s = \rho_a \gamma^2 w^2 \tag{19}$$

where ρ_a = density of the air, γ = constant coefficient and w = wind velocity at some reference height from the water surface. Experimentally it has been found that γ^2 is a function of the wave form, with a value close to 0.0026. Further remarks on the bottom and surface shear stresses can be found in Dronkers (1964) and Nihoul (1975).

88. Neglecting the effects of shear and turbulent mixing, and with the introduction of surface stress (Equation 19) and bottom stress (Equation 18), Equations 17a and 17b can be written as

$$\frac{\partial u_1}{\partial t} + \frac{\partial (u_1 u_1)}{\partial x_1} + \frac{\partial (u_1 u_2)}{\partial x_2} - 2\,\Omega \sin\phi\, u_2$$

$$= - g \frac{\partial \eta}{\partial x_1} - g \frac{u_1 (u_1^2 + u_2^2)^{\frac{1}{2}}}{C_z^2 (h + \eta)} + \frac{\rho_a}{\rho} \gamma^2 \frac{w_1 (w_1^2 + w_2^2)^{\frac{1}{2}}}{h + \eta} \tag{20a}$$

and

$$\frac{\partial u_2}{\partial t} + \frac{\partial (u_2 u_1)}{\partial x_1} + \frac{\partial (u_2 u_2)}{\partial x_2} + 2\,\Omega \sin\phi\, u_1$$

$$= - g \frac{\partial \eta}{\partial x_2} - g \frac{u_2 (u_1^2 + u_2^2)^{\frac{1}{2}}}{C_z^2 (h + \eta)} + \frac{\rho_a}{\rho} \gamma^2 \frac{w_2 (w_1^2 + w_2^2)^{\frac{1}{2}}}{h + \eta} \tag{20b}$$

where w_1 = the wind velocity component along the x_1-axis, and w_2 = the wind velocity component along the x_2-axis. Equations 20a and 20b are the momentum balance equations for a two-dimensional shallow-water wave hydrodynamic model.

89. For the completeness of the mathematical model, the proper conditions must be defined at the spatial domain boundary, and the conditions at the initiation time of the phenomenon must also be provided.

General Description of River-Delta Interaction

90. River delta development is primarily the interaction of river sediment input and the physical processes of the receiving basin (Coleman 1976). The large input of fresh water that carries sediments from the Lower Atchafalaya River is the dominant force in shaping the Atchafalaya River delta.

91. The nature of the sediments plays an important role in the river delta system. The presence of cohesive or noncohesive sediments, and the critical shear stress for erosion, deposition, suspension, or

consolidation are controlling features in delta formation. Cohesive sediments are more complicated to deal with, since they are controlled not only by the hydrodynamic forces but also by the electrochemical forces (Krone 1978).

Sediment Transport and Delta Formation

92. Freshwater effluent from river mouths carries sediments in suspension. The diffusion of these materials and mixing with the ambient bay water determine their ultimate distribution. Based on the hydrodynamic aspects presented in previous sections, the study of turbulent jet diffusion processes in shallow water is formulated in the following sections.

Shallow-water mass transport system

93. When the distribution of a physical property or substance (sediment, salinity, temperature, or chemical wastes) that is carried by the jet needs to be studied, an additional equation is then utilized. This is the convection-diffusion equation with proper source or sink terms. The equation accounts for the mass conservation and is a partial differential equation of the parabolic type, having as a dependent variable the concentration of the substance under consideration.

Equation of mass conservation

94. In general, the conservation of mass of a substance is expressed by the convective-diffusion equation (Ariathurai, MacArthur, and Krone 1977) in the form

$$\frac{\partial c}{\partial t} + \frac{\partial (u_i c)}{\partial x_i} = \frac{\partial}{\partial x_i}\left(D_i \frac{\partial c}{\partial x_i}\right) + S \qquad i = 1, 2 \quad (21)$$

where c = substance concentration, D_i = the molecular diffusion coefficient, and S = the proper source and/or sink term.

95. Assuming again a time mean and a perturbated value for the velocities and concentrations, that is, $u_i = \bar{u}_i + u_i'$, and $c = \bar{c} + c'$,

substituting these terms into Equation 21, and time-averaging it one arrives at

$$\frac{\partial \bar{c}}{\partial t} + \bar{u}_i \frac{\partial \bar{c}}{\partial x_i} + \frac{\partial (\bar{u}_i' \bar{c}')}{\partial x_i} = \frac{\partial}{\partial x_i}\left(D_i \frac{\partial \bar{c}}{\partial x_i}\right) + S \qquad (22)$$

The deviation term can be approximated as

$$\frac{\partial (\bar{u}_i' \bar{c}')}{\partial x_i} = - \frac{\partial}{\partial x_i}\left(\varepsilon_i \frac{\partial \bar{c}}{\partial x_i}\right) \qquad (23)$$

where ε_i = the eddy diffusion coefficient.

96. Combining the expressions for molecular and eddy diffusion, and incorporating their coefficients into a single term (E_i), Equation 22 becomes

$$\frac{\partial c}{\partial t} + u_i \frac{\partial c}{\partial x_i} = \frac{\partial}{\partial x_i}\left(E_i \frac{\partial c}{\partial x_i}\right) + S \qquad (24)$$

where the bars have been dropped for simplicity. Equation 24 is the general equation of the conservation of a substance; when it refers to conservation of sediments, the term S stands for the processes of erosion and/or deposition.

PART V: ANALYTICAL TECHNIQUES AND NUMERICAL SOLUTIONS

Simplifying Assumptions Applying to the Atchafalaya River-Bay System

97. The system of Equations 10, 20, and 24 derived in PART IV is a complicated system of partial differential equations that can be solved by means of a numerical technique through a digital computer. Analytical solutions can be achieved only in the case where the general equations are simplified considerably under certain assumptions. These assumptions can be derived from the specific features of each river-bay system and the characteristic properties of the jet itself. However, misuse of the simplifications may lead to erroneous solutions of little practical value. Thus an extended and detailed knowledge of the physical system under consideration is required so that the limitations of the validity of the solution can be well understood.

98. Regarding the Atchafalaya River-Bay system, on a first approximation basis, the following assumptions were used:

a. Shallow receiving waters and velocities are uniform over depth, where friction is a predominant factor.

b. Well-mixed conditions with no density stratification.

c. Negligible density difference between issuing and receiving waters, that is, a nonbuoyant jet.

d. Very small wave height, η, in comparison to the depth, h, so that $\eta \sim 0$.

e. Negligible Coriolis forces and wind stress effects.

f. Bell-shaped similarity profiles for the velocities and sediment concentration profiles.

e. Entrainment only through the lateral boundaries of the jet.

Entrainment Function and Similarity Profiles

99. The quantitative expression of the entrainment processes was a positive step toward the solution of the turbulent jet problem.

Experimentally, Ellison and Turner (1959) found that the entrainment, E, can be defined as a function of gross properties of the jet,

$$E = eu_c(x_1) \tag{25}$$

where u_c = the axial longitudinal velocity and e = a numerical coefficient.

100. Another property of the jets that simplifies matters and helps the solution is similarity. According to this property, the velocity profile remains similar to itself along the various cross sections of the jet. For cases where bottom friction is important, the similarity assumptions must be used with reservation. Since the exact similarity form is not known, there are a variety of similarity function one can choose from. These can be either of pure exponential form (Fox 1970) or of pure polynomial form (Stolzenbach and Harleman 1971).

101. For this study the similarity expression, G(s), was chose to lie between the two aforementioned cases (see Figure 19), that is,

$$G(s) = (1 - s^2) \exp(-s^2) \tag{26}$$

where s = a nondimensional parameter.

102. The similarity assumption can also be extended to the sediment concentration profiles. Following the suggestion of Stolzenbach and Harleman (1971), this similarity function, R(s), can be taken as

$$R(s) = G(s)^{\frac{1}{2}} = (1 - s^2)^{\frac{1}{2}} \exp(-\tfrac{1}{2}s^2) \tag{27}$$

Nondimensional Form of the Governing Equations

103. Under all the simplifications and assumptions previously mentioned, the governing equations can be drastically reduced into simpler forms. Assuming, furthermore, that the lateral velocity, u_2, is much smaller than the longitudinal, u_1, and also that the velocities are

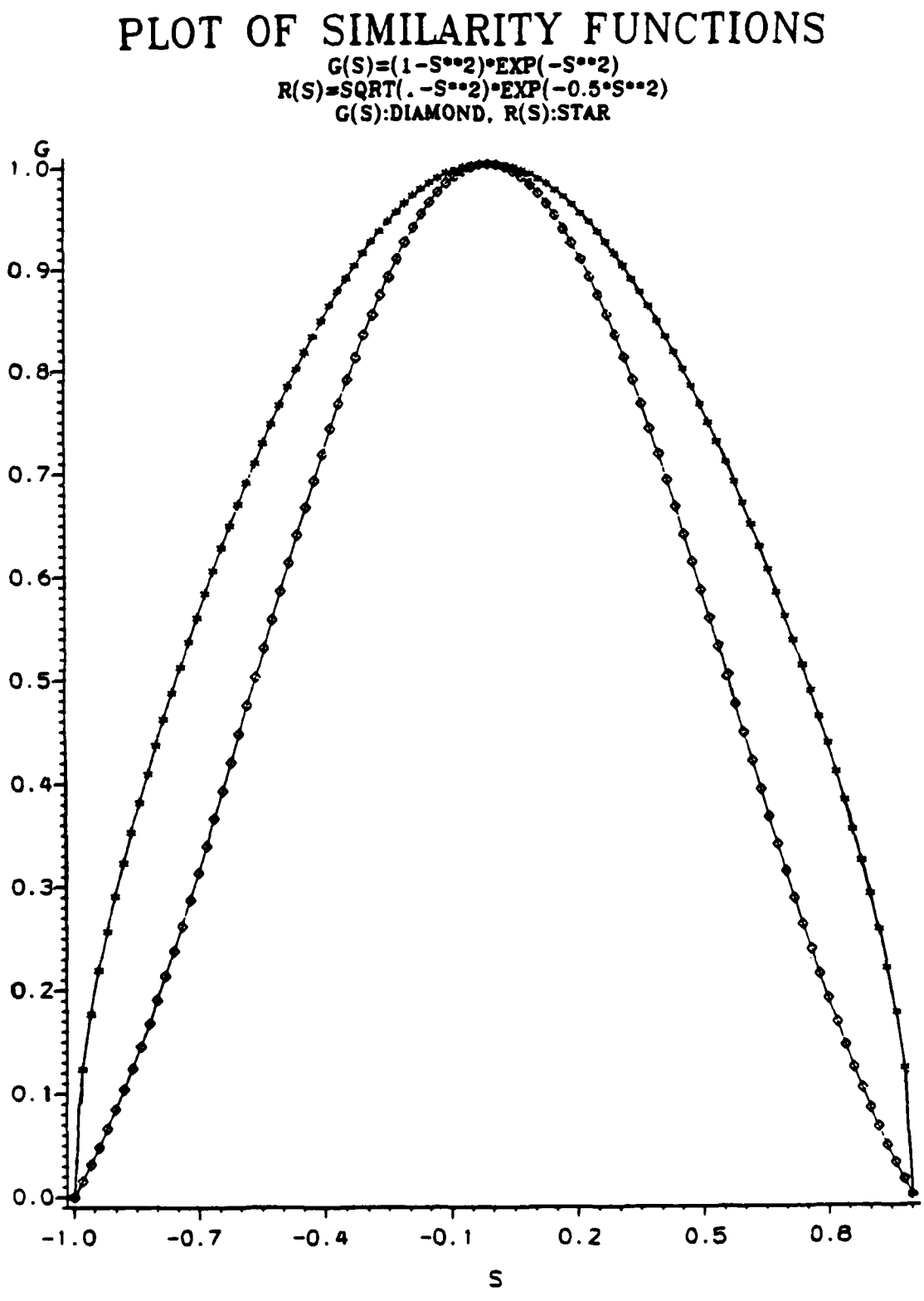

Figure 19. Different types of similarity functions

vanishing at the side boundaries of the jet, the equations can be treated as follows.

Continuity equation

104. Under steady-state conditions Equation 10 can be written as

$$\frac{\partial(hu_1)}{\partial x_1} + \frac{\partial(hu_2)}{\partial x_2} = 0 \tag{28}$$

where h is an one dimensional function of the x_1 coordinate.

105. Integrating Equation 28 along the width of the jet yields

$$\frac{d}{dx_1}\left[h(x_1)\int_{-b(x_1)}^{b(x_1)} u_1(x_1,x_2)dx_2\right] = 2Eh(x_1) \tag{29}$$

where $b(x_1)$ = half width of the jet. A detailed description of the variables involved is given in Figure 20.

106. According to the similarity assumption, the velocity is given as

$$u_1(x_1,x_2) = u_c(x_1)G(s) \tag{30}$$

where $s = \frac{x_2}{b(x_1)}$.

107. Substitution of the velocity Equation 30 and the entrainment Equation 25 into Equation 29 gives

$$\frac{d}{dx_1}\left[h(x_1)u_c(x_1)b(x_1)\int_{-1}^{+1}(1 - s^2)\exp(-s^2)ds\right] = 2eh(x_1)u_c(x_1) \tag{31}$$

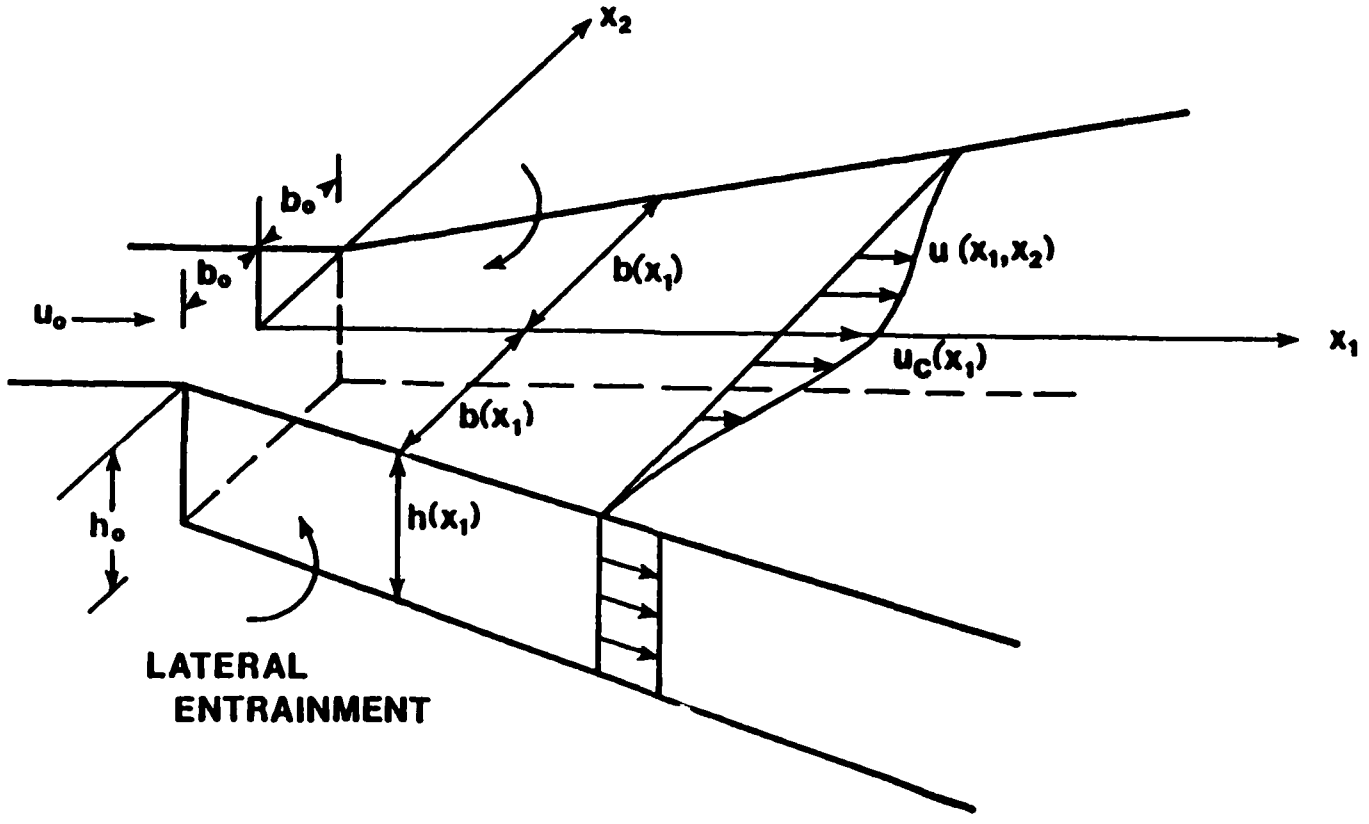

Figure 20. Two-dimensional plane nonbuoyant jet

Using the Gaussian quadrature eight-point numerical integration (see Appendix A), the evaluation of the integral was found to be

$$\int_{-1}^{+1} (1-s^2) \exp(-s^2)\, ds = 1.115 \tag{32}$$

Thus Equation 31 can be written as

$$\frac{d}{dx_1}(hu_c b) = Ahu_c \tag{33}$$

where A = 1.794e. For convenience and generalization the variables are normalized as

$$r = \frac{x_1}{b_0}; \quad B = \frac{b}{b_0}; \quad H = \frac{h}{h_0}; \quad U = \frac{u_c}{u_0} \tag{34}$$

where subscript 0 denotes the value of the variables at the outlet (x_1 = 0). It can be easily shown that

$$\frac{d}{dr}(HUB) = AHU \tag{35}$$

$$\text{with} \quad H = B = U = 1 \quad \text{at} \quad r = 0. \tag{36}$$

Equation 35 is the nondimensional continuity equation that constitutes part of our mathematical model.

Momentum equation

108. Under the same assumptions used for the continuity equation, for steady-state conditions the expression for the momentum balance along the x_1-axis, Equation 20a can be written as

$$\frac{d}{dx_1}\left[\int_{-b(x_1)}^{h(x_1)} \int_{-b(x_1)}^{b(x_1)} u_1^2(x_1,x_2)dx_2\right] = -f \int_{-b(x_1)}^{b(x_1)} u_1^2(x_1,x_2)dx_2 \tag{37}$$

where $f = g/C_z^2$ = Darcy-Weisbach's friction coefficient. Utilizing Equation 30, Equation 37 transforms into

$$\frac{d}{dx_1}\left[h(x_1)u_c^2(x_1)b(x_1)\int_{-1}^{+1}(1 - s^2)^2 \exp(-2s^2)\, ds\right]$$

$$= -fu_c^2(x_1)\int_{-1}^{+1}(1 - s^2)^2 \exp(-2s^2)\, ds \tag{38}$$

or

$$\frac{d}{dx_1}(hu_c^2 b) = -fu_c^2 b \tag{39}$$

Introducing one additional normalized variable for the friction (F) as

$$F = f\frac{b_o}{h_o} \tag{40}$$

and referring to the normalized variables of Equation 34, Equation 39 becomes

$$\frac{d}{dr}(HU^2B) = -FU^2B \tag{41}$$

subjected to the same boundary conditions given by Equation 36. Equation 41 is the nondimensional momentum equation which, along with Equation 35, constitutes the hydrodynamic part of our mathematical model.

Mass conservation equation

109. Following the same previous assumptions and neglecting the diffusion terms as being small in comparison to the advective terms, integrating Equation 24 vertically over depth first and then along the width of the jet results in

$$\frac{d}{dx_1}\left[\int_{-b}^{h} u_1 c\,dx_2\right] = 2Ehc_a - \int_{-b}^{b} w_0 c\left(1 - \frac{u_1^2}{u_{cr}^2}\right)dx_2 \qquad (42)$$

where c = sediment concentration, c_a = sediment concentration in the receiving waters, w_0 = settling velocity of the sediment particles, and u_{cr} = critical velocity under which deposition occurs. The right-hand side of Equation 42 represents the integrated value of S in Equation 24. More specifically, the first term refers to the sediment gains due to lateral entrainment, while the second term is the sediment losses due to deposition. In this model, no erosion processes are taken into account. The expression for the deposition function was first introduced by Krone (1962).

110. According to the similarity assumption, the sediment concentration profiles are expressed as

$$c(x_1,x_2) = c_c(x_1)R(s) \qquad (43)$$

where c_c = the center-line sediment concentration. R(s) is given by Equation 27. Considering the receiving waters as sediment-free (c_a = 0) and the setting velocity as constant (w_0 = constant), and substituting Equation 43 for the concentration in Equation 42, one arrives at

$$\frac{d}{dx_1}\left[hu_c bc_c I\left(\frac{3}{2}\right)\right] = -w_0 bc_c I\left(\frac{1}{2}\right) + w_0 \frac{u_c^2 bc_c}{U_{cr}^2} I\left(\frac{5}{2}\right) \qquad (44)$$

where $$I(m) = \int_{-1}^{+1} (1 - s^2)^m \exp(-ms^2)\, ds \tag{45}$$

Utilizing the Gaussian quadrature numerical integration of Appendix A, the values of the integrals, I(m), are found to be

$$I_1 = I\left(\frac{3}{2}\right) = 0.948;\ I_2 = I\left(\frac{1}{2}\right) = 1.397;$$

$$I_3 = I\left(\frac{5}{2}\right) = 0.760 \tag{45a}$$

111. Introducing the normalized form of new variables in addition to those given by Equation 34,

$$C = \frac{c_c}{c_0};\quad U_{cr} = \frac{u_{cr}}{u_0};\quad W = \frac{b_0 w_0}{h_0 u_0} \tag{46}$$

and substituting them into Equation 44 yields

$$\frac{d}{dr}[I_1 HUBC] = -I_2 WBC + I_3 W \frac{U^2 B}{U_{cr}^2} C \tag{47}$$

Equation 47 can be written as

$$\frac{dC}{C} = \frac{I_3}{I_1} (HUB)^{-1} \left[\left(-\frac{I_2}{I_3} + \frac{U^2}{U_{cr}^2} \right) WB - \frac{I_1}{I_3} \frac{d}{dr}(HUB) \right] dr \tag{48}$$

subjected to the boundary condition

$$C = 1 \quad \text{at} \quad r = 0 \tag{49}$$

Equation 48 is the nondimensional form of the sediment conservation equation which along with the hydrodynamic equations completes our mathematical model.

Analytical Solutions

112. Equations 35, 36, 41, 48, and 49 formulate the mathematical model of a plane, sediment-laden jet issuing into a shallow quiescent bay. In the following, solutions will be given for the cases of constant depth (H = 1) and of linearly varying depth ($H = 1 + arb_0/h_0$, a = slope). The solution will be given in terms of the following dependent variables: velocity $u_1(x_1,x_2)$, width $b(x_1)$, and sediment concentration $c(x_1,x_2)$.

Solution for constant depth (H = 1)

113. For constant depth, H = 1, Equations 35 and 41 become

$$\frac{d}{dr}(UB) = AU \tag{50}$$

and

$$\frac{d}{dr}(U^2B) = -FU^2B \tag{51}$$

From Equation 51 it is easily derived that

$$U^2B = \exp(-Fr) \tag{52}$$

Combining Equations 52 and 50 thus eliminating the variable B, we have

$$\frac{dU}{dr} + FU = -A \exp(Fr)\, U^3 \tag{53}$$

Equation 53 is a Bernoulli-type ordinary differential equation. Following the typical solution procedure of Appendix B, and utilizing the boundary conditions (Equation 36), the nondimensional center-line jet velocity is given as

$$U = \left[- \frac{2A}{F} \exp (Fr) + \left(1 + \frac{2A}{F} \right) \exp (2Fr) \right]^{-\frac{1}{2}} \tag{54}$$

Then the solution for the nondimensionalized jet width, B, can be obtained directly from Equations 52 and 54 as

$$B = - \frac{2A}{F} + \left(1 + \frac{2A}{F} \right) \exp (Fr) \tag{55}$$

In dimensional form the jet velocity, $u_1(r,s)$, and the jet width, $b(r)$, can be written as

$$u_1(r,s) = u_0(1 - s^2) \exp (-s^2) \left[- \frac{2A}{F} \exp (Fr) + \left(1 + \frac{2A}{F} \right) \exp (2Fr) \right]^{-\frac{1}{2}} \tag{56}$$

and

$$b(r) = b_0 \left[- \frac{2A}{F} + \left(1 + \frac{2A}{F} \right) \exp (Fr) \right] \tag{57}$$

114. For constant depth the mass conservation relation, Equation 48, is also reduced to

$$\frac{dC}{C} = \frac{I_3}{I_1} (UB)^{-1} \left[\left(- \frac{I_2}{I_3} + \frac{U^2}{U_{cr}^2} \right) WB - \frac{I_1}{I_3} \frac{d(UB)}{dr} \right] dr \tag{58}$$

or

$$\frac{dC}{C} = - \frac{I_2}{I_1} \frac{W}{U} dr + \frac{I_3}{I_1} \frac{WU}{U_{cr}^2} dr - \frac{d(UB)}{UB} \tag{59}$$

By direct integration it results in

$$\ln C = -\frac{I_2}{I_1} W \int_0^r \frac{1}{U} dr + \frac{I_3}{I_1} \frac{W}{U_{cr}^2} \int_0^r U dr - \ell n\,(UB) \tag{60}$$

or

$$C = \exp\left[-\frac{I_2}{I_1} W \int_0^r \frac{1}{U} dr + \frac{I_3}{I_1} \frac{W}{U_{cr}^2} \int_0^r U dr - \ell n\,(UB) \right] \tag{61}$$

The integrals within the exponential cannot be evaluated analytically. Thus, for the application of Equation 61, a numerical integration technique is required.

115. An essential simplification in the solution can be achieved by making an additional assumption of no entrainment conditions (A = 0) in Equation 54. Then the integrals can be easily evaluated as

$$\int \frac{1}{U} dr = \int \exp\,(Fr)\, dr = \frac{1}{F} \exp\,(Fr) \tag{62}$$

and

$$\int U dr = \int \exp\,(-Fr)\, dr = -\frac{1}{F} \exp\,(-Fr) \tag{63}$$

Therefore Equation 60 can be rewritten as

$$\ln C = -\frac{I_2}{I_1} \frac{W}{F} \exp\,(Fr) - \frac{I_3}{I_1} \frac{W}{U_{cr}^2 F} \exp\,(-Fr) + Y \tag{64}$$

Since $\ell n(UB) = \ell n[\exp(-Fr)\exp(Fr)] = \ell n(1) = 0$, from the boundary condition, Equation 49, the constant of integration, Y, is found to be

$$Y = \frac{I_2}{I_1}\frac{W}{F} + \frac{I_3}{I_1}\frac{W}{FU_{cr}^2} \tag{65}$$

Thus, finally, the solution for the normalized center-line sediment concentration reads

$$C = \exp\left\{\frac{I_2}{I_1}\frac{W}{F}[1 - \exp(Fr)] + \frac{I_3}{I_1}\frac{W}{F}\frac{1}{U_{cr}^2}[1 - \exp(-Fr)]\right\} \tag{66}$$

where $I_2/I_1 = 1.472$ and $I_3/I_1 = 0.801$. In terms of the independent variables, r and s, the sediment concentration within the jet is given as

$$c(r,s) = c_0(1 - s^2)^{\frac{1}{2}} \exp\left(-\frac{1}{2}s^2\right) \exp\left\{\frac{I_2}{I_1}\frac{W}{F}[1 - \exp(Fr)] + \frac{I_3}{I_1}\frac{W}{F}\frac{1}{U_{cr}^2}[1 - \exp(-Fr)]\right\} \tag{67}$$

Solution for linearly varying depth ($H = 1 + arb_0/h_0$)

116. For linearly varying depth Equations 35 and 41 are written as

$$H\frac{d(UB)}{dr} + a\frac{b_0}{h_0}UB = AHU \tag{68}$$

and

$$H\frac{d(U^2B)}{dr} = -\left(a\frac{b_0}{h_0} + F\right)U^2B \tag{69}$$

Solving Equation 69 for U^2B gives

$$U^2B = H^{-(1+D)} \tag{70}$$

where D = f/a. The combination of Equations 70 and 68 yields

$$H\frac{d}{dr}\left[H^{-(1+D)}U^{-1}\right] + a\frac{b_0}{h_0}H^{-(1+D)}U^{-1} = AHU \tag{71}$$

or

$$\frac{d(HU)}{dr} + a\frac{b_0}{h_0}(D - 1)H^{-1}(HU) = -AH^{D-1}(HU)^3 \tag{72}$$

Equation 72 is also a Bernoulli-type ordinary differential equation with respect to the monomial HU. Thus, along with the boundary conditions of Equation 36, the solution for HU (Appendix B) is

$$HU = (2A)^{-\frac{1}{2}}H^{1-D}\left[\frac{h_0}{ab_0}\frac{1}{2 - D}(H^{2-D} - 1) + \frac{1}{2A}\right]^{-\frac{1}{2}} \tag{73}$$

Consequently, the normalized center-line velocity is

$$U = (2A)^{-\frac{1}{2}}H^{-D}\left[\frac{h_0}{ab_0}\frac{1}{2 - D}(H^{2-D} - 1) + \frac{1}{2A}\right]^{-\frac{1}{2}} \tag{74}$$

The normalized jet width can now be derived from Equations 74 and 70 as

$$B = 2AH^{D-1}\left[\frac{h_0}{ab_0}\frac{1}{2 - D}(H^{2-D} - 1) + \frac{1}{2A}\right] \tag{75}$$

Following all these, the velocity and the width of the jet in terms of the variables r and s are given as

$$u_1(r,s) = u_0(2A)^{-\frac{1}{2}}H^{-D}\left[\frac{h_0}{ab_0}\frac{1}{2 - D}(H^{2-D} - 1) + \frac{1}{2A}\right]^{-\frac{1}{2}} \cdot (1 - s^2)\exp(-s^2) \tag{76}$$

and

$$b(r) = b_0 2AH^{D-1}\left[\frac{h_0}{ab_0}\frac{1}{2-D}(H^{2-D}-1) + \frac{1}{2A}\right] \quad (77)$$

117. For linearly varying depth, the sediment conservation relation, Equation 48, after direct integration, reads

$$\ln C = -\frac{I_2}{I_1} W \int_0^r \frac{1}{HU}\,dr + \frac{I_3}{I_1}\frac{W}{U_{cr}^2}\int_0^r \frac{U}{H}\,dr - \ell n\,(HUB) \quad (78)$$

or

$$C = \exp\left[-\frac{I_2}{I_1} W \int_0^r \frac{1}{HU}\,dr + \frac{I_3}{I_1}\frac{W}{U_{cr}^2}\int_0^r \frac{U}{H}\,dr - \ell n(HUB)\right] \quad (79)$$

Again, the integrals within the exponential must be evaluated numerically. In terms of the variables r and s, the sediment concentration is written as

$$c(r,s) = c_0 C(1 - s^2)^{\frac{1}{2}} \exp\left(-\frac{1}{2}s^2\right) \quad (80)$$

where C is given by Equation 79.

Approximation of Sediment Deposition in a Bay

118. The sediments carried by the river waters are the main material for the river delta development. The form of the delta, however, depends on other parameters such as the climate, the hydrodynamic field, the area topography, and the sediment characteristics

themselves. Neglecting erosion and side entrainment of the sediment, under steady-state conditions, material deposition is linear in time and can be computed as

$$c_d(r,s) = \int_0^t w_0 c\left(1 - \frac{u_1^2}{u_{cr}^2}\right)dt = w_0 c\left(1 - \frac{u_1^2}{u_{cr}^2}\right)t \qquad (81)$$

where c_d = deposited sediment and t = time. The values for the velocity, u_1, and the concentration, c, are taken respectively from Equations 56 and 67 or 76 and 80.

119. In the case that the variable c is given in units of mass per volume, the deposited sediment, c_d, is computed in mass per unit area. Therefore, assuming no consolidation processes, the thickness of the deposited sediment layer, d, can be directly computed from Equation 81 as

$$d = \frac{c_d}{\rho_s} \qquad (82)$$

where ρ_s = density of the sediment.

120. For the numerical simulation of river delta evolution, the overall phenomenon is taken as steady for certain time intervals. Then, due to the variation in the bottom topography from deposited sediment buildup, proper adjustments must be made to various parameters and the solution repeated under the new conditions. In such a manner the mathematical model, although being of a steady-state nature itself, predicts the delta development over time.

PART VI: PREDICTION OF THE ATCHAFALAYA RIVER DELTA GROWTH

Basic Data for Analytical Prediction

121. The Atchafalaya River-Bay area is a complicated dynamic physical system. For the purpose of this study, the values of various factors controlling this system must be known. The most essential of these factors are the geometry and topography of the area; the water discharge, and sediment load of the river; and, to a lesser degree, the hydrology and climate of the surrounding environment. Field data pertaining to our analytical analysis of delta development were gathered from various sources and are outlined in the following sections.

Physical dimensions of river outlets

122. Two river outlets, the Lower Atchafalaya River Outlet and Wax Lake Outlet, are forming in Atchafalaya Bay. Each outlet has its own characteristics and these consequently influence the form of the developing delta.

123. Using data from a 1974-76 hydrographic analysis by the Waterways Experiment Station (1981), the cross section of the Lower Atchafalaya River, at river mile 135.8 from Simmesport, La., is plotted in Figure 21a. The river outlet is approximately 3,000 ft wide and reaches a depth of 35 ft. From the same data source, the cross section of Wax Lake Outlet, at river mile 122.3 from Simmesport, is plotted in Figure 21b; the outlet is about 1,000 ft wide and reaches a depth of 56 ft.

124. The Atchafalaya River Outlet is under continuous dredging so that a navigation channel can be maintained throughout the bay. This navigation channel is developing as the future main course of the river through the emerging delta.

Initial bathymetry conditions of the receiving bay

125. Bathmetric maps of the Atchafalaya Bay for the years 1972 and 1977 (Adams and Baumann 1980) give a clear picture of bay bathymetry (Figures 8 and 13). With a depth ranging from 4 to 8 ft (1.2 to 2.4 m), the bay can be classified as shallow and well-mixed,

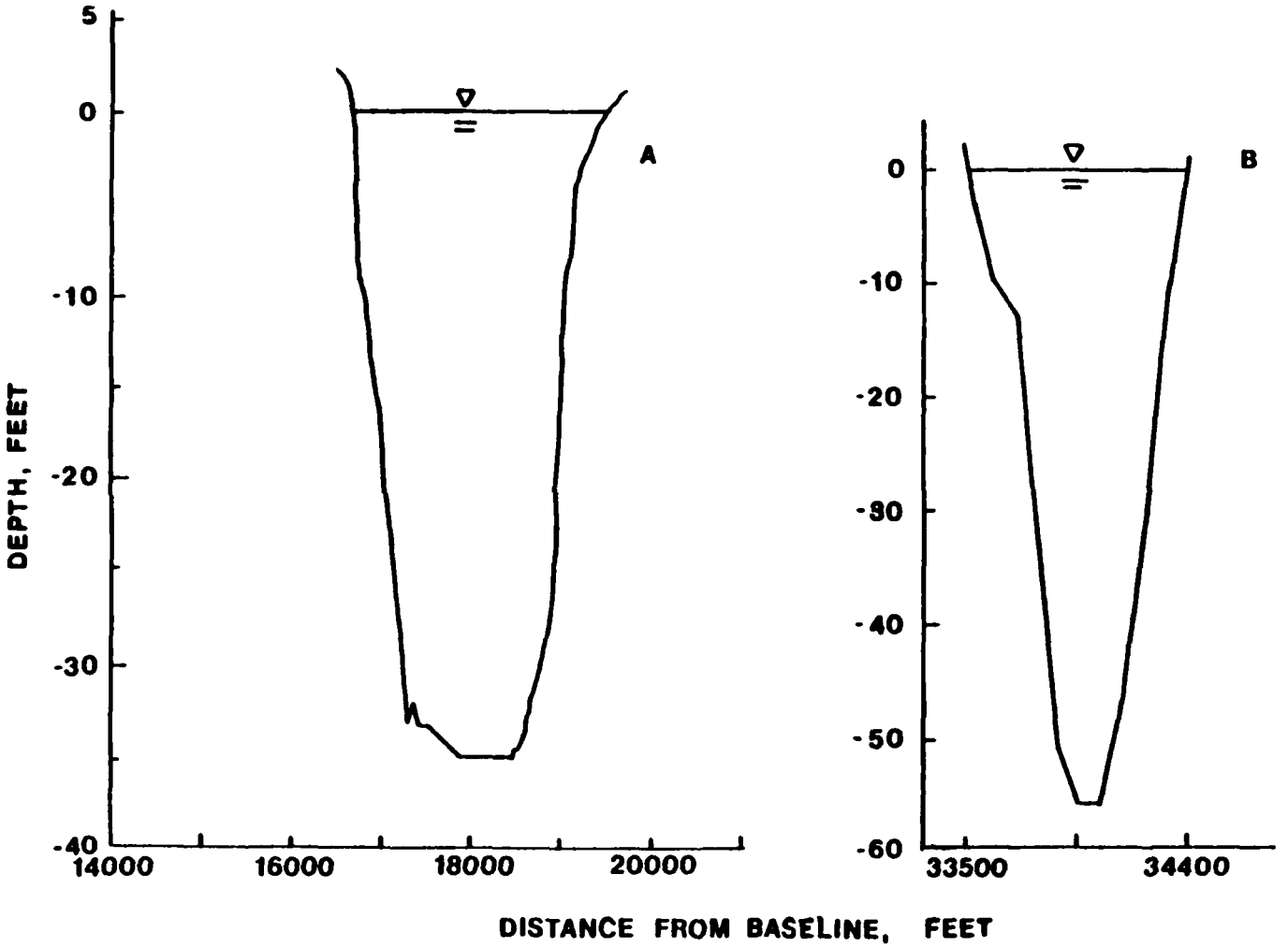

Figure 21. Cross section of the river outlets (Waterways Experiment Station 1981):
(A) Lower Atchafalaya River at river mile 135.8;
(B) Wax Lake Outlet at river mile 122.3

thus bottom friction may play a predominant role. Other indications from these bathymetric maps are that the newly deposited sediment is close to the river mouth, and that the bathymetry of the remaining bay is less affected.

River discharge and suspended sediment load

126. The water discharge of the Atchafalaya River at Simmesport (Figure 11) and at the Lower Atchafalaya River Outlet (Figure 12) is varied. It ranges from 80,000 cfs to 600,000 cfs (2,000 cms to 17,000 cms).

127. The current velocity at the river mouth ranges from 3 fps (1 mps) to 0.2 fps on a diurnal basis due to the tidal action (Figure 22). However, the current always has a southwest direction at the Lower Atchafalaya River Outlet (WES Preliminary Field Data Report 1982).

128. The character of the sediments entering the bay via riverine flows is controlled by the sedimentation processes within the river-bay system. According to Roberts, Adams, and Cunningham (1980), the sediment load is composed mainly of silt and clay (> 75 percent) and a small part of sand (< 25 percent) (Table 2). Thus our study can be simplified by dealing with the fine sediment materials which are transported in suspension only. Whether to treat the sediment as cohesive or noncohesive is a difficult question. Since much of the subaerial sediment is sandy, it is reasonable to use a single equation to predict sedimentation processes without considering various particle sizes.

129. Letter (1982), based on observations of the sediment concentrations in Simmesport, derived a regression equation relating water and sediment discharge obtaining

$$Q_s = 0.0728\ Q_w^{1.444} \tag{83}$$

where Q_s is the suspended sediment load in 1000 tons (2000 lb) per day and Q_w is the water discharge in 1000 cfs. The value of the exponent is close to unity, permitting the assumption of a linear relationship between water and sediment discharge.

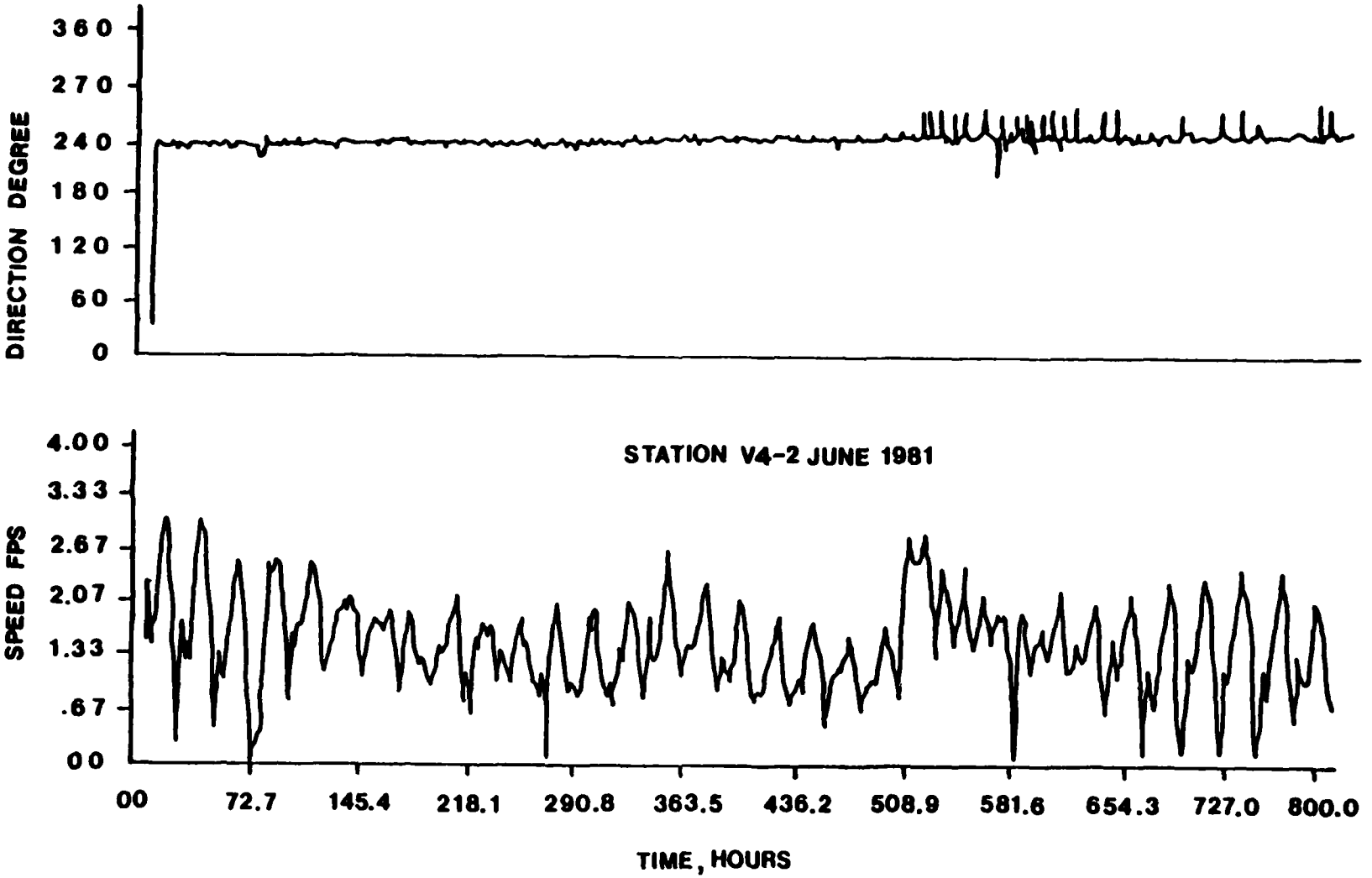

Figure 22. Current velocity and direction for the Atchafalaya River Outlet (WES 1982)

130. As shown in Figure 12, the variations of water and sediment discharge at the Lower Atchafalaya River Outlet follow the same pattern through time. Thus, for all practical purposes, the mean sediment concentration can be reasonably assessed. A mean water discharge of 300,000 cfs (8,500 cms) and a mean suspended sediment load of 200,000 metric tons per day are shown by Figure 12 for the period 1973-75. From these values, an average sediment concentration of 0.27 kg/m^3 (270 ppm) is derived.

131. For a water discharge of 300,000 cfs, Equation 83 gives a mean sediment concentration of 275,000 tons/day (0.34 kg/m^3), which is close to the value of 0.27 kg/m^3. In the following computations, the mean sediment concentration (c_0), varying from 100 ppm to 600 ppm, is taken into consideration for our study.

Sediment settling velocity and deposition

132. The sediment deposition rate, which depends on the shear stress of the flow (Krone 1962), is assumed to be proportional to the velocity of the sediment particles. In general, this velocity depends on the shape, size, and weight of the particle, as well as on hydrodynamic conditions. To define the settling velocity of cohesive sediments in a real situation is a difficult task, because these particles have the tendency to adhere to each other and form large aggregated flocs. Laboratory measurements made by the Waterways Experiment Station on Atchafalaya River sediments (Figure 23) have shown a settling velocity from 0.01 mm/sec to < 1.0 mm/sec (WES Preliminary Field Data Report 1982).

133. The freshly deposited sediments are initially in a very loose state. However, as new sediment layers are superimposed, the low density large aggregates are crushed down to smaller flocs, and denser and stronger bed layers are formed. As a result of this consolidation effect, the bulk density of the bed (ρ_s) may be of high value (Krone 1978). Wells and Roberts (1980) used a density of 375 kg/m^3 to estimate the sediment transported in the Atchafalaya mud stream. In our analysis, a value of ρ_s equal to 400 kg/m^3 is used.

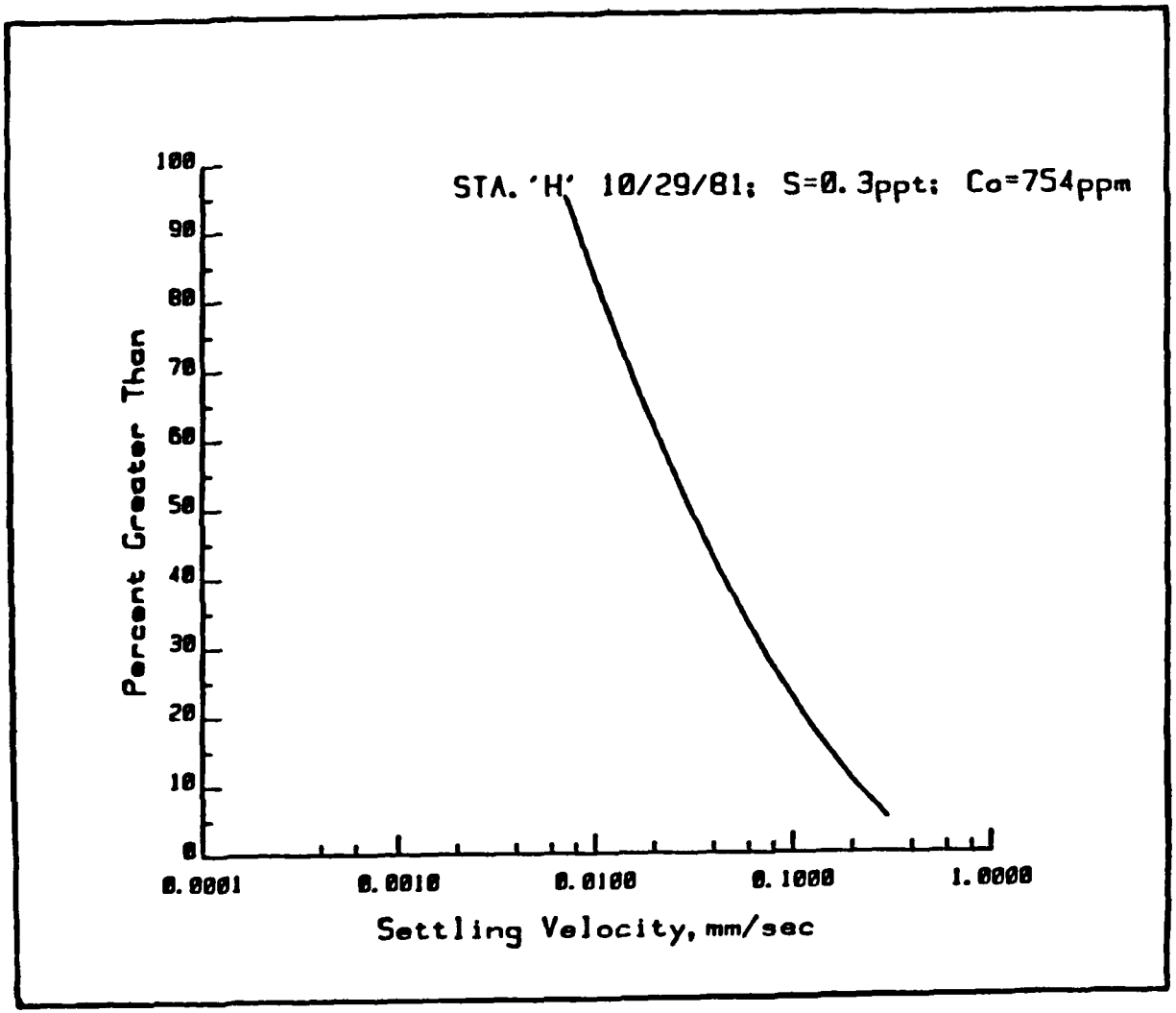

Figure 23. Settling velocities of Atchafalaya Bay sediments (WES 1982)

134. The active development of the river deltas in Atchafalaya Bay indicates that the deposition rate in the area is much faster than the rate of erosion. Normally, the combined effect of both deposition and erosion should be considered. In our analytical model it is assumed that the sediment is subjected only to transportation and deposition, and that each particle that hits the bottom adheres to it. Supressing the resuspension effects is acceptable, since the sediment deposition is estimated based on average values of the water discharge and the sediment concentration.

Bottom resistance and lateral entrainment

135. The predominance of silt, clay, and fine sand in the bottom materials of the bay causes the bed surface to be smooth, with relatively small friction resistance. In the absence of field data, the Darcy-Weisbach coefficient of friction (f) is assumed to vary from 0.001 to 0.006 in this study. It is further assumed that the friction coefficient is time-independent.

136. The riverine waters entering Atchafalaya Bay are well mixed with the receiving waters. Because of the shallowness of the bay, there is no density stratification, and the only entrainment of the receiving bay waters to the sediment-laden river waters is through the sides of the jet. The lateral entrainment coefficient (e) has proven to be a function of Richardson's number (Ellison and Turner 1959). Engelund (1976) used a value of 0.075 in the case of a very small Richardson number. In our analysis, a range of e varying from 0.0375 to 0.300 is considered.

Procedures for Closed-Form Analytical Solutions

Idealization of the Atchafalaya River-Bay system

137. The physical features of the Atchafalaya River-Bay system are approximated by simple geometry for the domain of the closed-form analytical solution. Using the data of the previous section, the nominal values of dependent variables (h, b, u, and c) can be deduced for our study.

138. The cross sections of the Lower Atchafalaya River and Wax Lake Outlet (Figures 21a and 21b) are found to be equal to 66,000 ft^2 (6,200 m^2) and 29,000 ft^2 (2,700 m^2), respectively. Considering a mean annual water discharge of 300,000 cfs (8,500 cms) at Simmesport and the 70-30 percentage split of discharge (Letter 1982), the flows in the Lower Atchafalaya River Outlet and the Wax Lake Outlet are 210,000 cfs and 90,000 cfs, respectively. Both flows exhibit a velocity of 3.10 cfs (~ 1 mps)(WES 1981).

139. Basically, the river mouth is the point at which fresh water leaves the confined channel and mixes with ambient water. In the Atchafalaya River-Bay system, the river outlet discharges a part of its flow into the bay through a navigation channel. The bottom of the navigation channel is much deeper than the bottom of the ambient bay. In this study, those flow and sediment discharges through the navigation channel are assumed not to have significant influence on jet characteristics, and are assumed to deliver directly to the Gulf of Mexico.

140. The Atchafalaya Bay is relatively flat, with a uniform depth of 6.0 ft (~2 m) (Figure 13). This depth, measured below mean sea level, is referenced to the bathymetry conditions of the year 1977 (Adams and Baumann 1980). In a shallow bay, the formation of delta lobes depends on the bathymetry of the receiving bay rather than the geometry of the river itself (Wells, Chinburg, and Coleman 1984). This fact leads us to assume that the river outlet can be approximated by a rectangular cross section. Using the bathymetry map of Adams and Baumann (1980), the inferred width is about 4,000 ft (1,200 m) for the Lower Atchafalaya River Outlet, and about 3,300 ft (1,000 m) for the Wax Lake Outlet. The nominal water depth at both outlets, h_0 = 6.5 ft (2 m), is used in this study.

Values of various parameters used in the analytical study

141. As previously mentioned, the rate of sediment deposition depends on the shear stress of the flow (Krone 1962). In this study, a linear relationship between the shear stress and mean square velocity is assumed (Equation 81). The center-line velocity at the

river outlet is used as a critical velocity ($u_{cr} = u_0$) under which deposition occurs. Equation 81 implies that at the middle point of the river outlet no deposition occurs. Table 4 summarizes the range of the values for various parameters to be used in our analytical study.

Computer graphics and numerical integration used for analytical solutions

142. The SAS/GRAPH (1981), a computer graphic system, is used to display the values of dependent variables (u, b, c, d) for various cases. The GPLOT PROCEDURE graphs one variable against another, producing a two-dimensional plane. The G3D PROCEDURE plots the value of three variables and produces a three-dimensional surface. The variables to be plotted are specified in a PLOT statement. Both the GPLOT and G3D PROCEDURES can automatically scale the axes, or the user can specify the scale. Use of computer graphics provides flexibility in displaying information meaningfully. Examples for use of computer graphic programs are listed in Appendix C.

143. A numerical integration technique is needed for the computation of integrals, $\int_0^r \frac{1}{HU}\,dr$ and $\int_0^r \frac{U}{H}\,dr$, appearing in Equation 79. The orthogonal collocation method is used for numerical integration (Villadsen and Michelson 1978). The method consists of expanding the normalized center-line velocity U, a dependent variable, in terms of a n^{th} order Jacobi polynomial. The n roots of this orthogonal polynomial are chosen as the n collocation points (Kuu and Polack 1982). The integration of the profile of the dependent variable is approximated by the Radau quadrature formula (Villadsen and Michelsen 1978). The Radau quadrature weights at the n collocation points (the abscissas) are determined (see Appendix D). The integral is approximated by the summation of the product of the weight and the value of the function at the collocation points. Quadrature integration is explained in detail in Appendix D.

Base Results of Analytical Solutions

144. This section presents a basic computation using nominal values of variables to obtain the closed-form analytical solution. This base result will serve as a guideline for the comparison of the results of various cases and for the sensitivity analysis of various parameters.

145. The following nominal values are used in the basic computations to obtain the base results:

b_0	= 500 m	w_0	= 0.05 mm/sec
h_0	= 2.0 m	a	= 0.0001
u_0	= 1.0 mps	f	= 0.001
u_{cr}	= 1.0 mps	e	= 0.075
c_0	= 300 ppm	ρ_s	= 400 kg/m^3

The dimensionless variables are defined as

r	$= x_1/b_0$	U_{cr}	$= u_{cr}/u_0$
s	$= x_2/b$	C	$= c_c/c_0$
B	$= b/b_0$	F	$= fb_0/h_0$
H	$= h/h_0$	W	$= b_0w_0/h_0u_0$
U	$= u_c/u_0$	D	$= f/a$

and the values of the integrals are

$I_1 = 0.948$
$I_2 = 1.397$
$I_3 = 0.760$

Results of constant depth without entrainment (Case 1: E = 0, H = 1)

146. The normalized (dimensionless) jet center-line velocity (U) and jet width (B) are obtained by substituting A = 0 into Equations

54 and 55. The center-line concentration (C) is given in Equation 66. The equations for each of these variables are

$$U = \exp(-Fr) \tag{84}$$

$$B = \exp(Fr) \tag{85}$$

$$C = \exp\left\{\frac{I_2}{I_1}\frac{W}{F}[1 - \exp(Fr)] + \frac{I_3}{I_1}\frac{W}{F}\frac{1}{U_{cr}^2}[1 - \exp(-Fr)]\right\} \tag{86}$$

147. The dimensional form of jet velocity (u), jet width (b), and center-line concentration (c) are derived straightforwardly as:

$$\begin{aligned} u(r, s) &= u_c G(s) = u_0 G(s) U \\ &= u_0(1 - s^2)\exp(-s^2)U \end{aligned} \tag{87}$$

$$b(r) = b_0 B \tag{88}$$

$$\begin{aligned} c(r, s) &= c_c R(s) = c_0 R(s) C \\ &= c_0(1 - s^2)^{\frac{1}{2}} \exp(-\tfrac{1}{2}s^2)C \end{aligned} \tag{89}$$

The deposited sediment (c_d) and its thickness (d) are computed from Equations 81 and 82, respectively:

$$c_d(r, s) = w_0 c\left(1 - u^2/u_{cr}^2\right)t \tag{90}$$

$$d(r, s) = c_d/\rho_s \tag{91}$$

The results of the calculations of u, c, and d are displayed three-dimensionally in Figures 24, 25, and 26, respectively (and Plate 1), with the aid of computer graphics (see Appendix C). Each of the variables is plotted versus the normalized longitudinal (r) and lateral (s) coordinates.

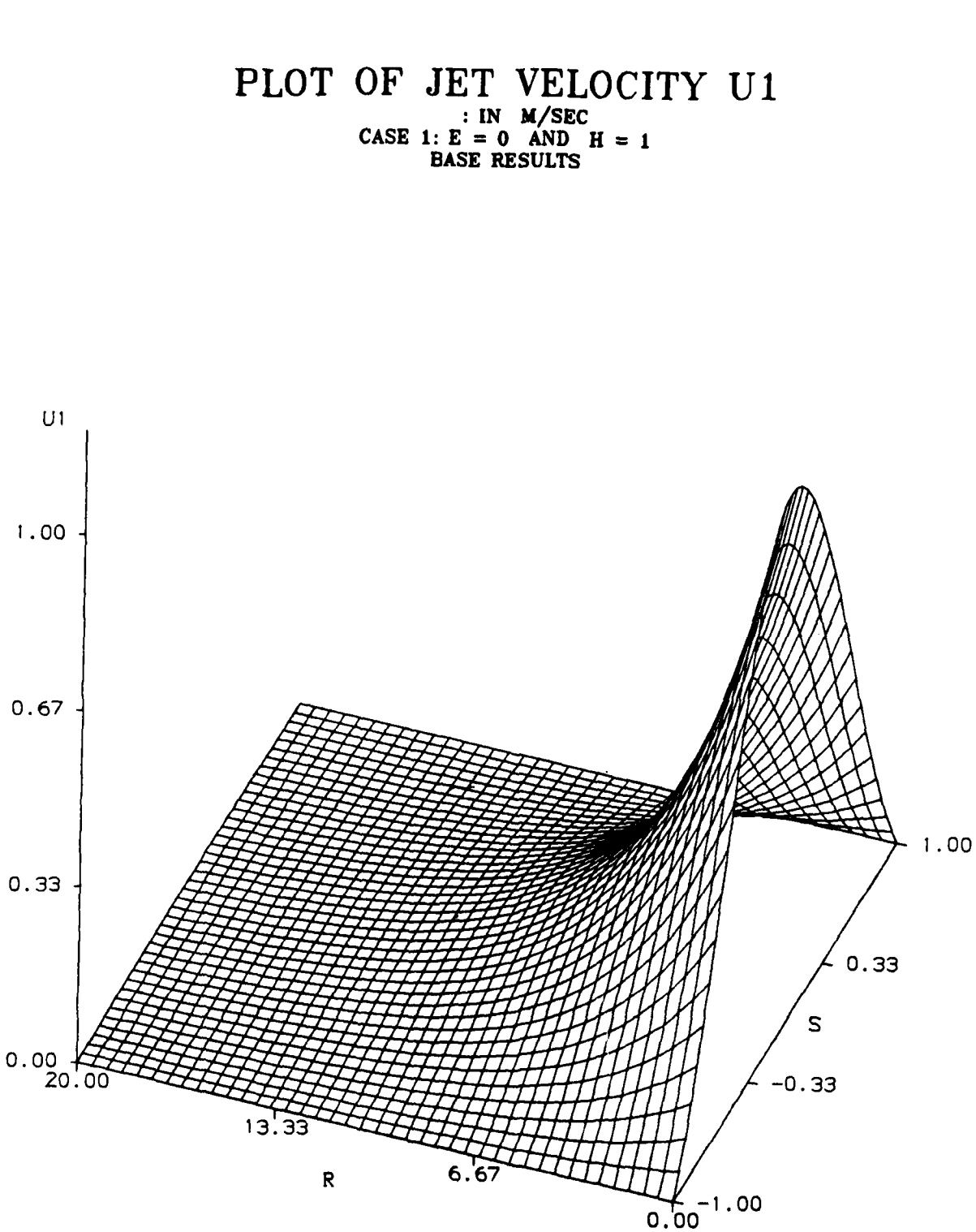

Figure 24. Case 1: Base results for jet velocity u

PLOT OF SEDIMENT CONCENTRATION C1

: IN PPM
CASE 1: E = 0 AND H = 1
BASE RESULTS

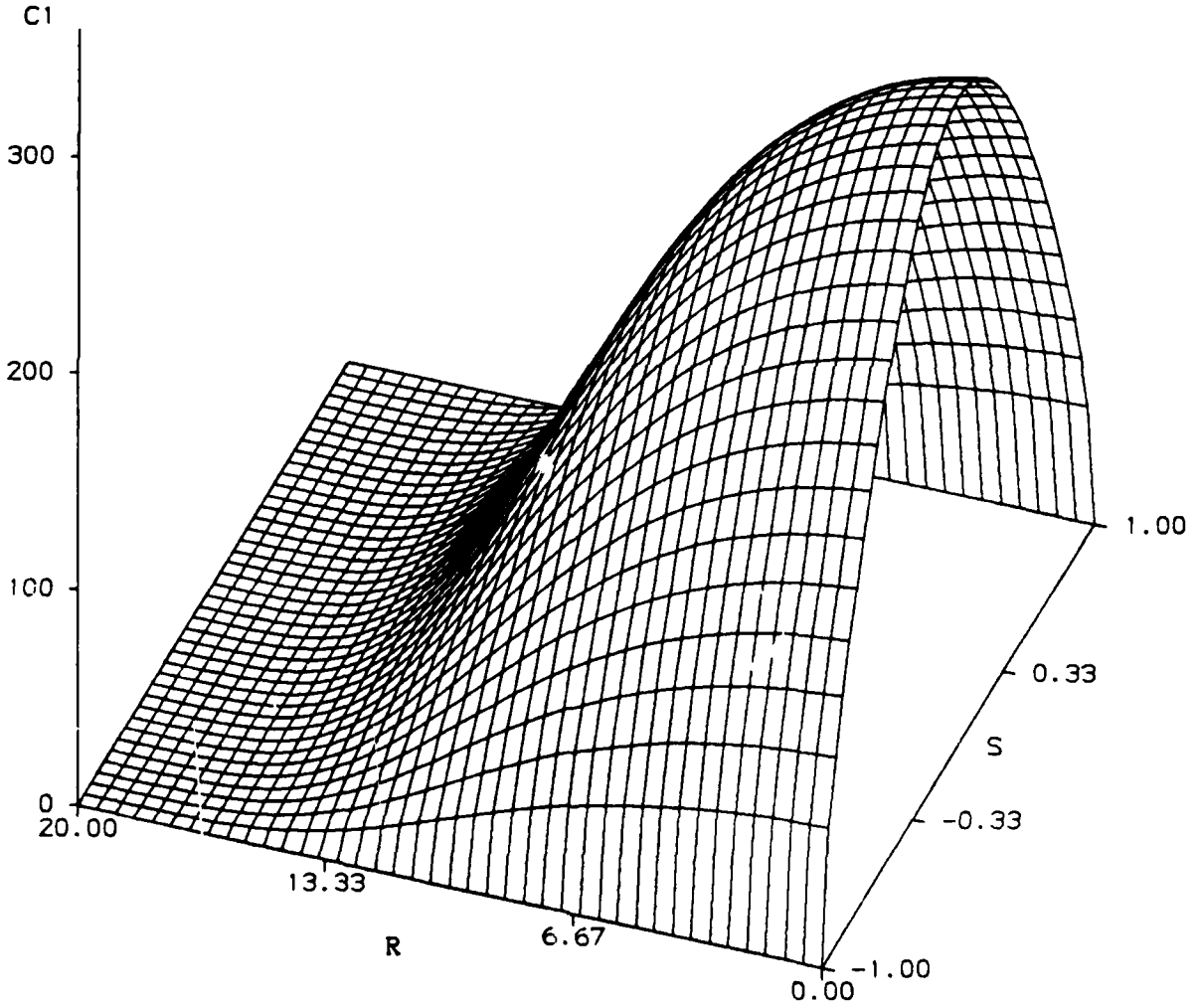

Figure 25. Case 1: Base results for sediment concentration c

PLOT OF SEDIMENT THICKNESS

: IN CM
CASE 1: E = 0 AND H = 1
BASE RESULTS

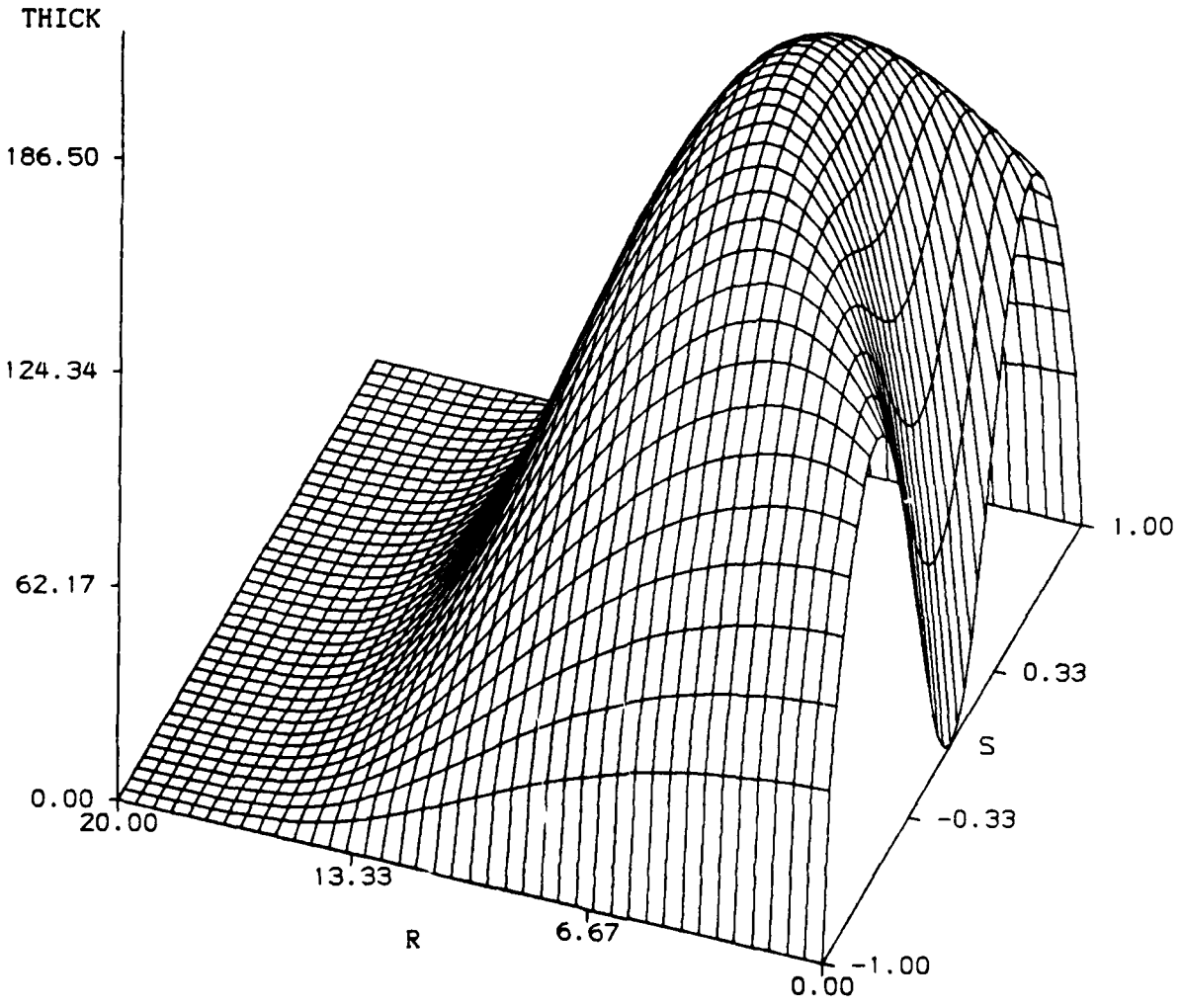

Figure 26. Case 1: Base results for sediment thickness d

Results of linearly varying depth
without entrainment (Case 2: $E = 0$, $H \neq 1$)

148. For linearly varying depth ($H = 1 + arb_0/h_0$) and no entrainment ($A = 0$), the nondimensional continuity equation, Equation 35, becomes

$$\frac{d}{dr}(HUB) = 0 \tag{92}$$

Using the boundary conditions stated in Equation 36, Equation 92 implies that

$$HUB = \text{constant} = 1 \tag{93}$$

or

$$UB = H^{-1} \tag{94}$$

Similarly, the nondimensional momentum equation, Equation 41, can be written as

$$H\frac{d}{dr}(U^2B) + \left(a\frac{b_0}{h_0} + F\right)U^2B = 0 \tag{95}$$

Solving for U^2B, we obtain

$$U^2B = H^{-(1 + D)} \tag{96}$$

Combining Equations 94 and 96, we get

$$U = H^{-D} \tag{97}$$

$$B = H^{-1 + D} \tag{98}$$

and finally

$$HUB = (H)\ (H^{-D})\ (H^{-1+D}) = 1 \tag{99}$$

149. The nondimensional form of sediment conservation is given by Equation 48. Substituting Equations 97, 98, and 99 into Equation 48, we obtain

$$\frac{dC}{C} = \frac{WD}{F}\left(-\frac{I_2}{I_1}H^{-1+D} + \frac{I_3}{I_1}\frac{1}{U_{cr}^2}H^{-1-D}\right)dH \tag{100}$$

or

$$C = \exp\left[-\frac{W}{F}\left(\frac{I_2}{I_1}H^{D} + \frac{I_3}{I_1}\frac{1}{U_{cr}^2}H^{-D}\right) + Y\right] \tag{101}$$

where

$$Y = \frac{W}{F}\left(\frac{I_2}{I_1} + \frac{I_3}{I_1}\frac{1}{U_{cr}^2}\right) \tag{102}$$

or

$$C = \exp\left[\frac{I_2}{I_1}\frac{W}{F}(1 - H^{D}) + \frac{I_3}{I_1}\frac{W}{F}\frac{1}{U_{cr}^2}(1 - H^{-D})\right] \tag{103}$$

150. The dimensional form of jet velocity (u), width (b), concentration (c), the deposited sediment (c_d), and the sediment thickness (d) for Case 2 are computed using exactly the same procedure as Case 1 with Equations 87, 88, 89, 90, and 91. The three-dimensional graphs for u, c, and d for this case are plotted in Plate 2.

Results of constant depth
with entrainment (Case 3: $E \neq 0$, $H = 1$)

151. As shown in PART V and presented again in this section, Equations 54, 55, and 61 are the expressions for the normalized center-line velocity (U), jet width (B), and center-line concentration (C), respectively:

$$U = \left[- \frac{2A}{F} \exp (Fr) + \left(1 + \frac{2A}{F}\right) \exp (2Fr) \right]^{-\frac{1}{2}} \tag{104}$$

$$B = - \frac{2A}{F} + \left(1 + \frac{2A}{F}\right) \exp (Fr) \tag{105}$$

and

$$C = \exp \left[- \frac{I_2}{I_1} W \int_0^r \frac{1}{U} dr + \frac{I_3}{I_1} \frac{W}{U_{cr}^2} \int_0^r U dr - \ell n(UB) \right] \tag{106}$$

152. The integrals appearing in Equation 106 have to be evaluated numerically. In this case, the lower end point (U = 1 at r = 0) of both integrals is known, thus the Radau quadrature formula (Appendix D) is used.

153. Again, the dimensional form of jet velocity (u), width (b), concentration (c), the deposited sediment (c_d) and its thickness (d) are computed straightforwardly by using Equations 87, 88, 89, 90, and 91, respectively. Plate 3 contains the plots for u, c, and d.

Results of linearly varying depth
with entrainment (Case 4: E ≠ 0, H ≠ 1)

154. The general solution of linearly varying depth with entrainment for the normalized center-line velocity (U), jet width (B), and center-line concentration (C) are given in Equations 74, 75, and 79 in PART V:

$$U = (2A)^{-\frac{1}{2}} H^{-D} \left[\frac{h_0}{ab_0} \frac{1}{2-D} (H^{2-D} - 1) - \frac{1}{2A} \right]^{-\frac{1}{2}} \tag{107}$$

$$B = 2AH^{D-1} \left[\frac{h_0}{ab_0} \frac{1}{2-D} (H^{2-D} - 1) + \frac{1}{2A} \right] \tag{108}$$

and

$$C = \exp\left[- \frac{I_2}{I_1} W \int_0^r \frac{1}{HU}\, dr + \frac{I_3}{I_1} \frac{W}{U_{cr}^2} \int_0^r \frac{U}{H}\, dr - \ell n(HUB) \right] \quad (109)$$

155. Again, the lowest limit (H = 1, U = 1, at r = 0) of both integrals appearing in Equation 109 is known, and the Radau integration technique (Appendix D) is used. Similarly, the dimensional form of jet velocity (u), jet width (b), concentration (c), the deposited sediment (c_d), and the sediment thickness (d) are computed by using Equations 87, 88, 89, 90, and 91, respectively. The three-dimensional graphs of u, c, and d are displayed in Figures 27, 28, and 29, respectively (and Plate 4).

Prediction of Delta Front Advancement

156. The rate of delta growth depends on the amount of sediment supplied by the riverine waters and reworking by current forces in the receiving bay (Coleman and Wright 1975). The areal and mass extent of deltaic evolution is governed by the relative roles of inertial and frictional forces. Thus sediment deposition patterns are determined by various physical parameters that are formulated in the analytical solutions for the four different cases.

Sediment deposition patterns under quasi-steady state

157. In this study, a quasi-steady state for sediment deposition is assumed (Engelund 1976). The deposited sediment and its thickness are computed as a linear function with time (Equation 90). The deposition patterns of Case 4 for the time interval of 1.5 years, 1.0 year, and 0.5 year are given in Plate 5. From these figures, it is shown that the deposited sediment forms a saddle-shaped bottom. The rapid accumulation of suspended sediment near the river outlet and the abrupt decline of sediment deposition away from the outlet are observed. As the central portion of the sediment accumulates, it

PLOT OF JET VELOCITY U1

: IN M/SEC
CASE 4: E ≒ 0 AND LINEAR H
BASE RESULTS

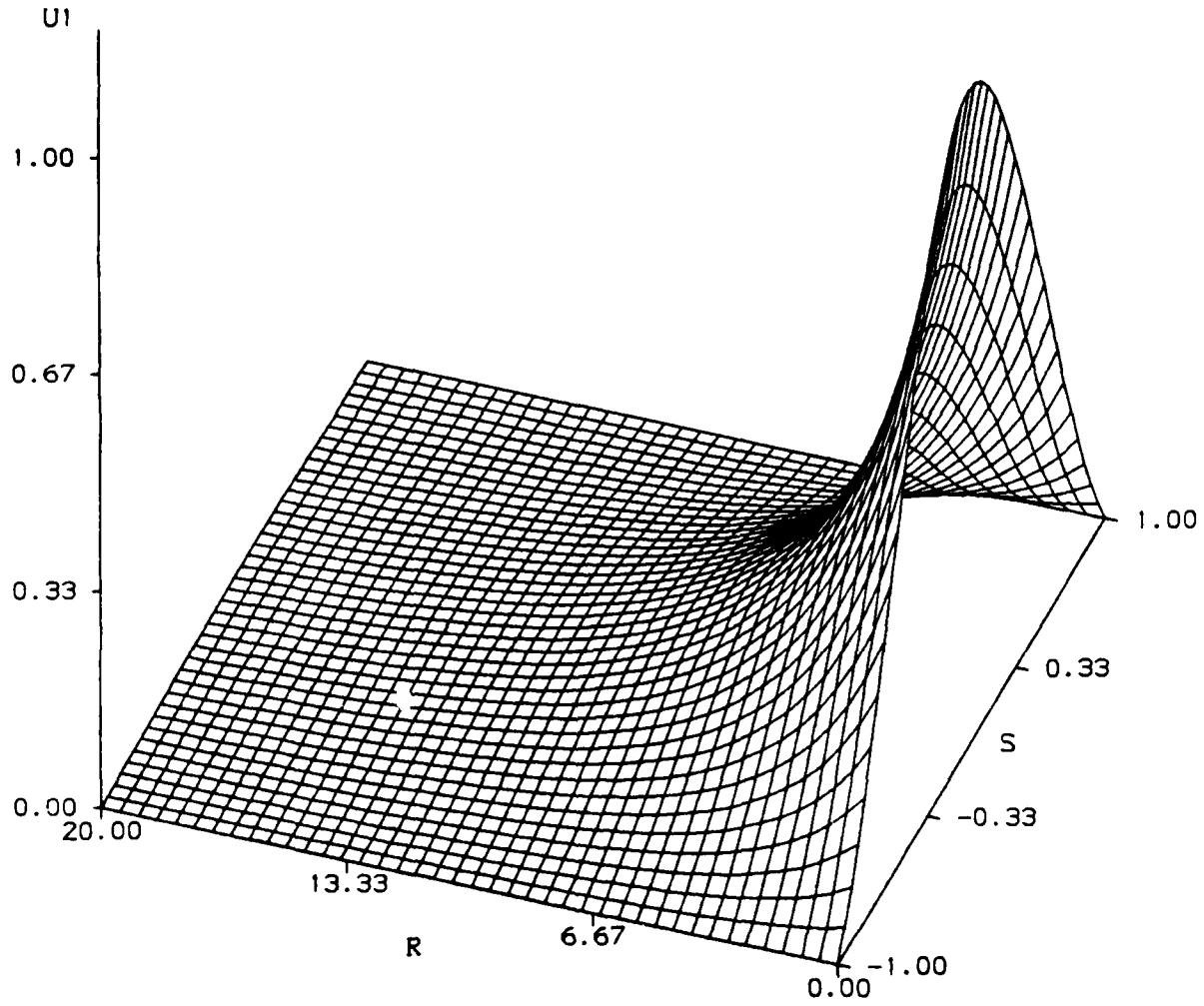

Figure 27. Case 4: Base results for jet velocity u

PLOT OF SEDIMENT CONCENTRATION C1

: IN PPM
CASE 4: E ≠ 0 AND LINEAR H
BASE RESULTS

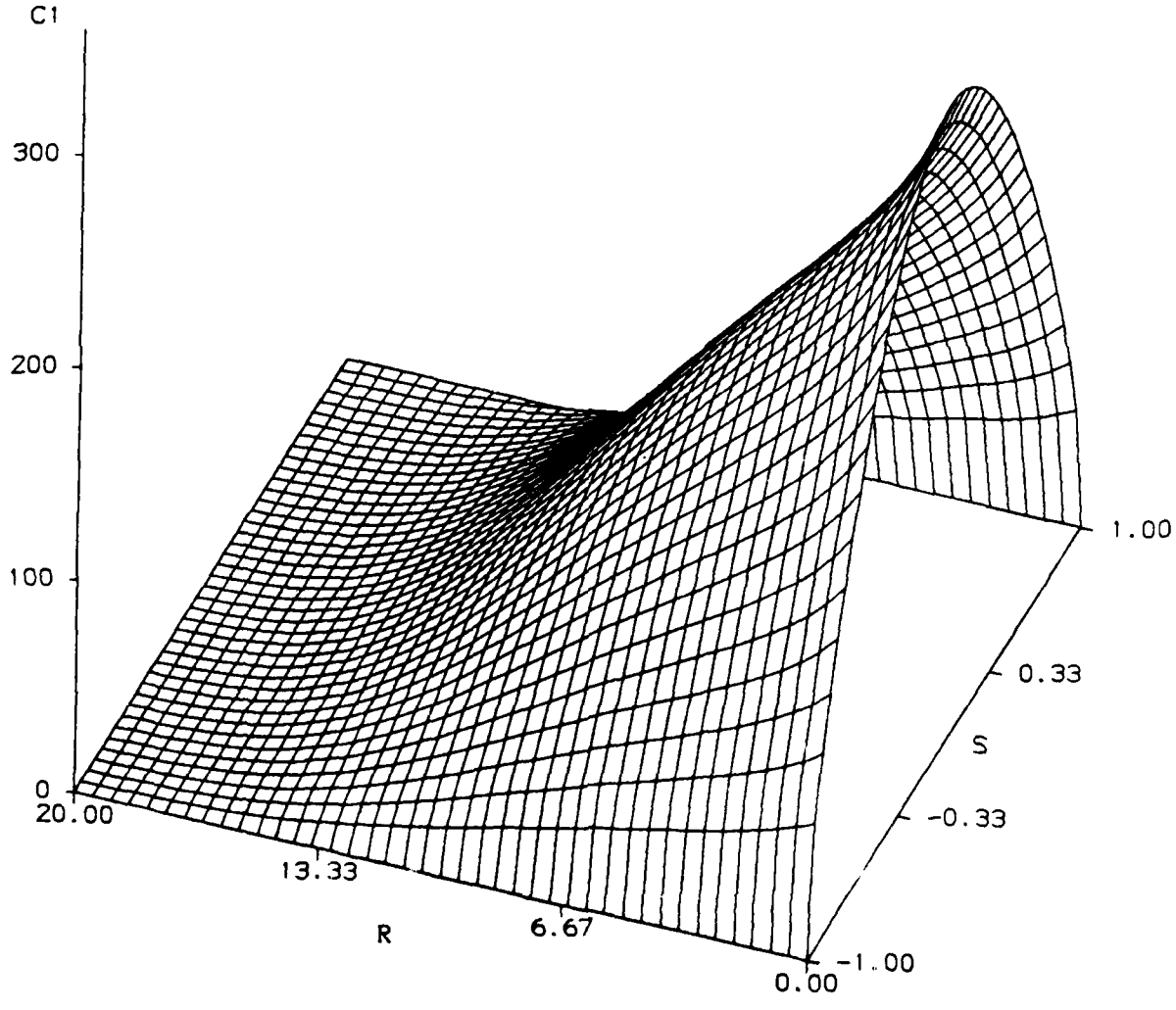

Figure 28. Case 4: Base results for sediment concentration c

PLOT OF SEDIMENT THICKNESS

: IN CM

CASE 4: E ≠ 0 AND LINEAR H

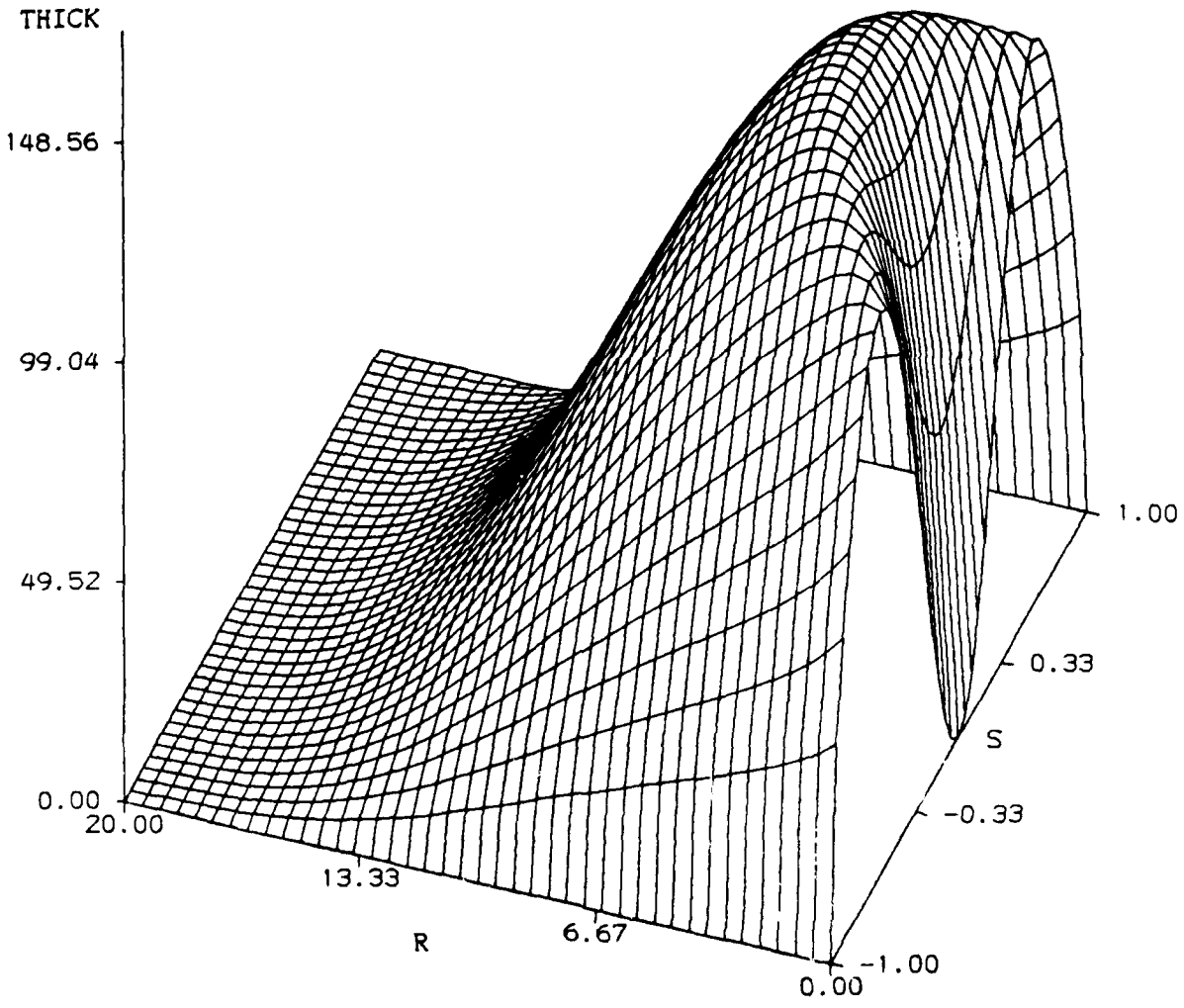

Figure 29. Case 4: Base results for sediment thickness d

AD-A164 931 THE ATCHAFALAYA RIVER DELTA REPORT 7 ANALYTICAL ANALYSIS OF THE DEVELOPME..(U) LOUISIANA STATE UNIV BATON ROUGE COASTAL ECOLOGY LAB F C WANG SEP 85 WES/TR/HL-82-15 DAC339-81-C-0004 F/G 8/8 NL

2/3

UNCLASSIFIED

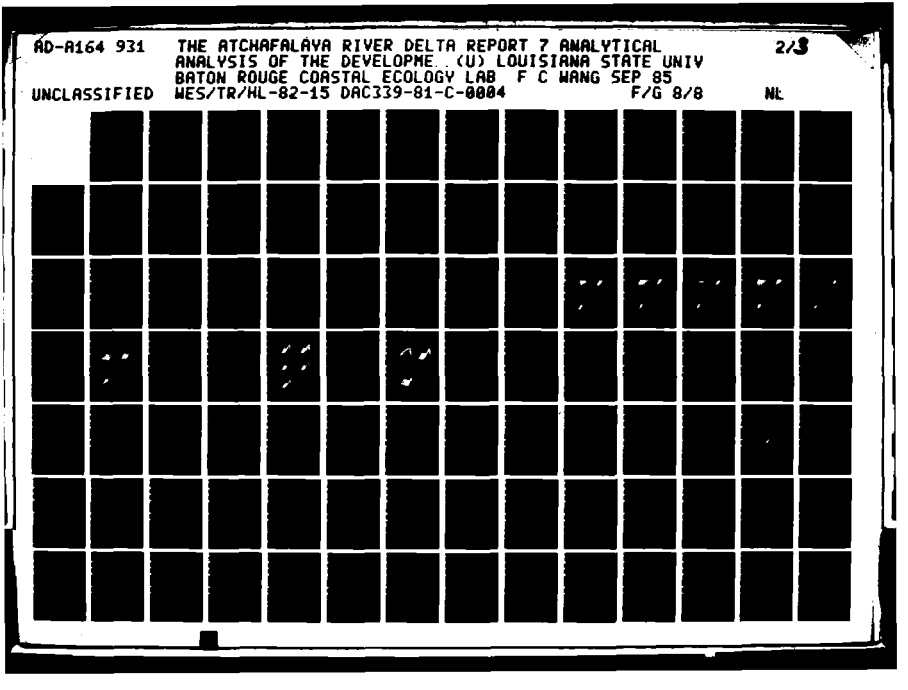

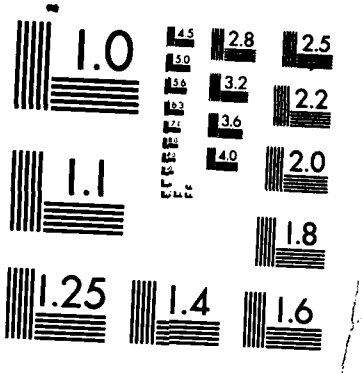

causes the river mouth channel to separate into arms known as bifurcating channels (Coleman 1976).

158. Therefore, until subaerial land has emerged, it can be inferred that the riverine input has limited influence within a certain longitudinal distance; and that as the deposition process is completed in this level of development the river mouth advances to the end of the subaerial land and begins the process of bifurcation.

Conceptualization of delta-channel development

159. The geometry of river-mouth sandbars is determined by riverine flow conditions. When river outflow velocities are high and water depths seaward of the mouth are shallow, the rapid rate of effluent expansion provides, initially, a broad radial sandbar and later on develops a distributary network. Coleman (1976) documented three major types of existing delta channel patterns (Figure 30). In an environment having a high subsidence rate, low wave and tide energy, low offshore slope, and a fine grain sediment load, the development of bifurcating channels is typical. Deltas developing this distributary pattern are characterized by a large number of river mouths (Figure 30).

160. Channel bifurcations and crevasse discharges have influenced the shape of subaerial land in Atchafalaya Bay. Adams and Baumann (1980) identified five levels of bifurcation that have been taking place in the Lower Atchafalaya River delta (Figure 31). The branching channels discharge water and suspended sediments that form subdeltas along the distributary channels. The shoaling at the branching river mouth is repeated and new bifurcations develop at the new channel outlets to form a complex branching pattern (Adams and Baumann 1980).

Stepwise procedure for delta growth prediction

161. A stepwise procedure, formulated to estimate the areal and volume extent of the delta in both space and time, is the means by which delta growth is predicted. The space steps are selected at the beginning of the computation and guided by the dimensional plot of sediment deposition. The time-steps are not known a priori, but

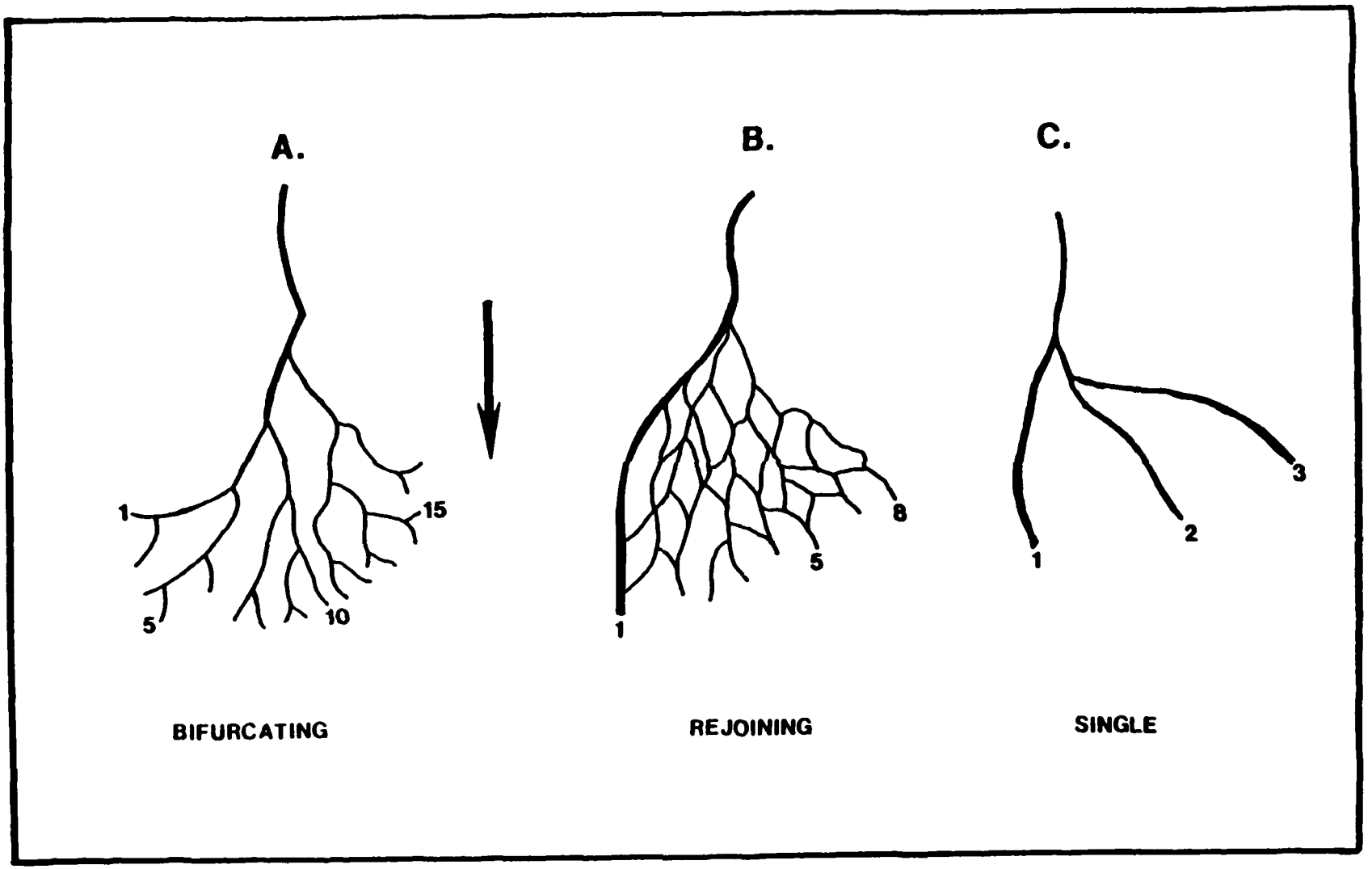

Figure 30. Types of distributary channel patterns (Coleman and Wright 1975)

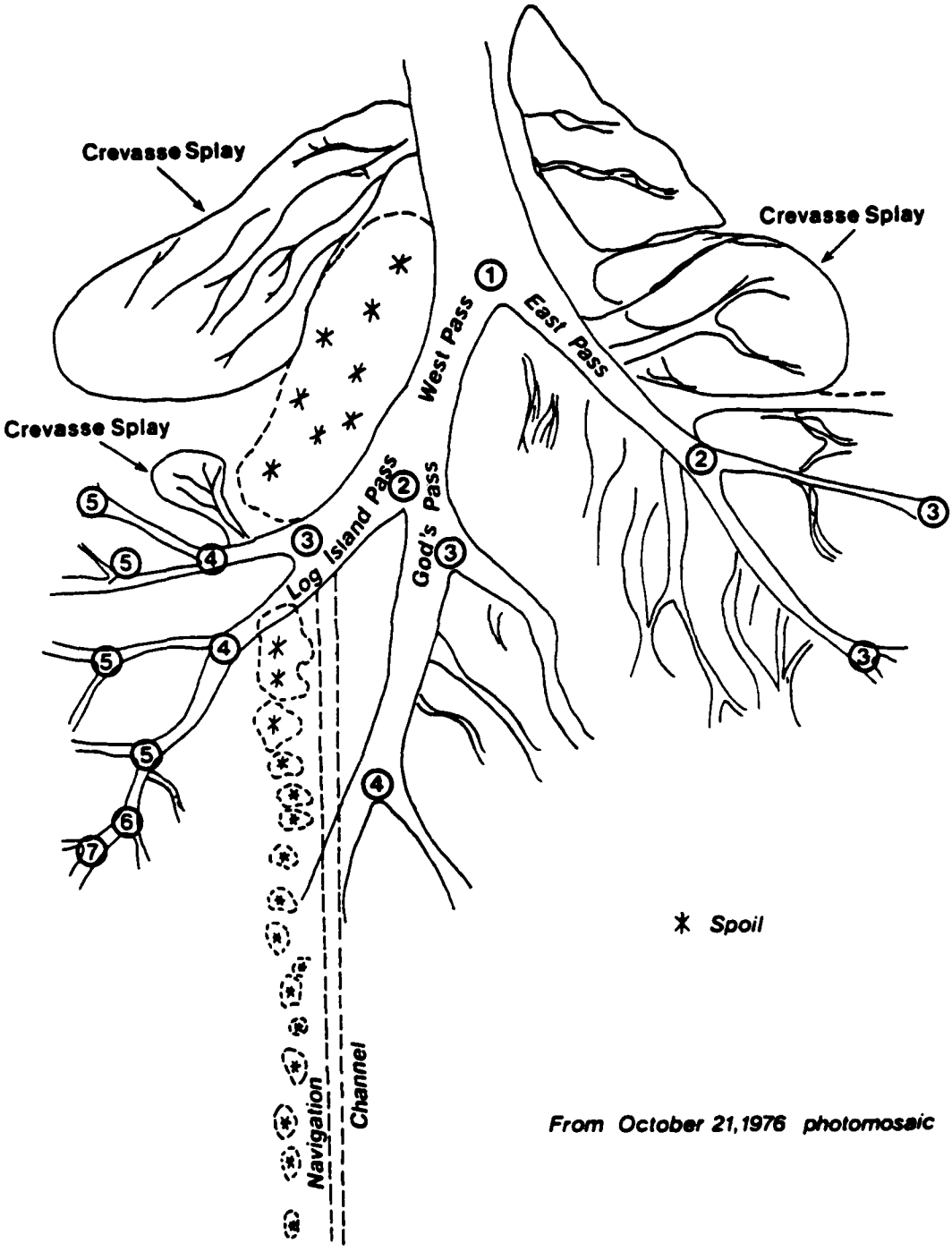

Figure 31. Lower Atchafalaya River Delta (Adams and Baumann 1980)

depend upon the analytical solutions themselves and are obtained by the numerical procedure (Appendix E).

162. In order to simulate the process of bifurcation, it is assumed that at each level of bifurcation the branching channels achieve a stage of development similar to their parent channel, and that the subdelta is produced by turbulent jets with the same riverine flow conditions. An idealized bifurcation scheme is displayed in Figure 32.

163. In this study, our predictions are based on mean sea level, which is used as the determining elevation for subaerial land. Plate 6 is a two-dimensional plot of sediment thickness for Case 4. The total sediment volume is computed by analytical integration. The time required to fill the known volume of sediment to an average thickness h is obtained by the method of Bisection Search (Scheid 1968). The numerical procedures are explained in detail in Appendix E.

Prediction for the Lower Atchafalaya River Outlet delta

164. River delta development depends on the quantity of sediment that is delivered to and retained in the receiving bay. In Atchafalaya Bay, much of the flow through both the Lower Atchafalaya River Outlet and Wax Lake Outlet enters the Gulf of Mexico via the navigation channels. Adams and Baumann (1980) estimated that 40 to 50 percent of the total volume of suspended sediment delivered to the bay through the river outlets will be retained in Atchafalaya Bay and the rest will be dispersed in peripheral marshes and offshore regions.

165. For predictive purposes, it is assumed that the volume of sediment is proportional to the volume of discharge. Based upon the 70-30 percentage split of discharge for the two outlets (Letter 1982), the Lower Atchafalaya River delta is expected to grow to a much greater extent than the Wax Lake Outlet delta.

166. The Lower Atchafalaya River delta can be divided into an eastern and a western component (Adams and Baumann 1980), areas that are associated with East Pass and West Pass (Figure 31). Van Heerden (1980) conducted an extensive field study in the eastern half of the

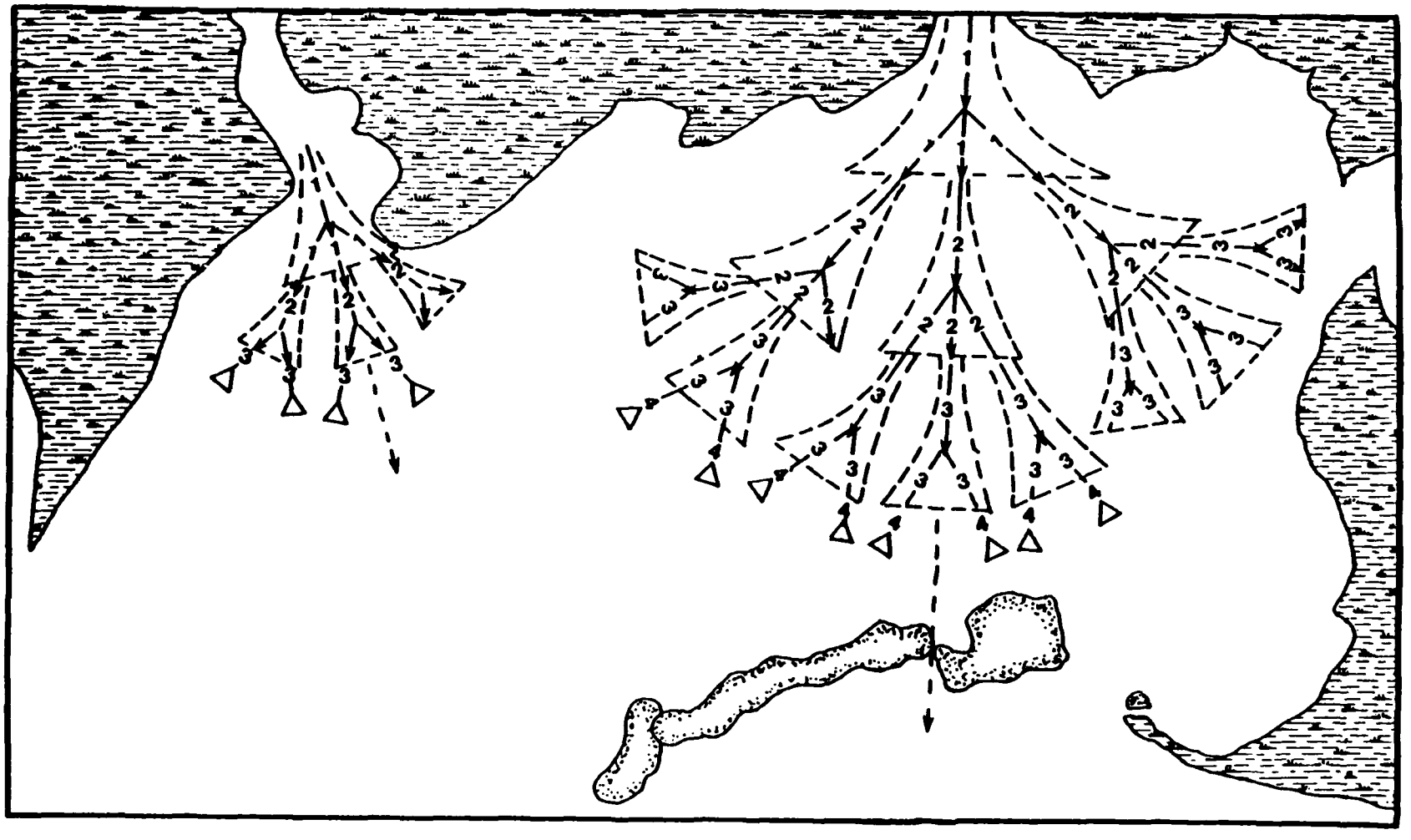

Figure 32. An idealized pattern of bifurcating channels

Lower Atchafalaya River delta from 1973 to 1979. The total area of the eastern half of the subdeltas was 4.56 mi^2 (11.67 km^2) with an average growth rate of 0.76 mi^2/year (2 km^2/year).

167. In contrast, subdelta development on the western side is more complex. Adams and Baumann (1980) indicated that if it were not for the navigation channel, God's Pass and Log Island Pass (Figure 31), which developed from second-order bifurcation, along with East Pass would represent the three major river outlets.

168. To simulate the growth of river deltas in this physical domain, a stepwise procedure described in the previous section is used and the simulation is done as follows:

a. In the first order bifurcation, the total river discharge and suspended sediments are divided into three equal amounts representing the three major outlets.

b. A space step is selected at the onset of computation; the subdelta area (jet length and width) at each outlet is calculated.

c. The time-step is searched by the numerical procedure (Appendix E).

The numerical procedure is repeated in the same manner for the sequential order of bifurcation processes. The results of each computation are summarized in Table 5. The average growth rate is about 5 km^2/year.

Prediction for the Wax Lake Outlet delta

169. The bifurcation process is not as evident on the Wax Lake Outlet delta. Most of the delta development has occurred west of the main channel (Adams and Baumann 1980). A few branching channels have developed on the western side of the outlet and subdeltas have formed along the subchannels.

170. Wells, Chinburg, and Coleman (1984) reported that during the 1980-81 flood year, the Wax Lake Outlet delta represented 17 percent of total subaerial land in Atchafalaya Bay, and approximately 10 percent of the total if averaged over a 6-year period from 1975 to 1981 covering an area of 2 km^2 to 3 km^2. The average growth rate ranged from 0.3 to 0.5 km^2/year.

171. To simulate the natural bifurcation pattern in the absence of field observation is a difficult task. Thus the same branching scheme presented earlier is used for modeling the growth of the Wax Lake Outlet delta. The stepwise numerical procedure is again used to estimate the growth of delta lobes. The results are listed in Table 6. The average growth rate is about 2.6 km^2/year.

Estimation of Atchafalaya River delta growth

172. Aerial photographs (Wells, Chinburg, and Coleman 1984) and photomosaics (Adams and Baumann 1980) show that the Atchafalaya River deltas have grown by developing parabolic lobes of fine-grain sediments that radiate from the network of branching channels. These delta lobes are evolved from shallow sandbars that rose above mean sea level and emerged as subaerial land.

173. Adams and Baumann (1980) indicated that in Atchafalaya Bay the central area between two deltas is apparently broad and deep enough to transport the riverflow it receives without forming a discrete channel. This fact suggests that in our study, the analytical results derived from numerical procedures for the Lower Atchafalaya River Outlet and the Wax Lake Outlet separately can be combined linearly to represent the total delta growth in the bay. This is similar to Letter's (1982) approach, in which the bay area was roughly divided into two areas, one for each of the two outlets. Figure 33 shows an estimation of the total subaerial land in Atchafalaya Bay derived from our analytical approach. Figure 34 presents the prediction of volume extent of Atchafalaya River delta growth.

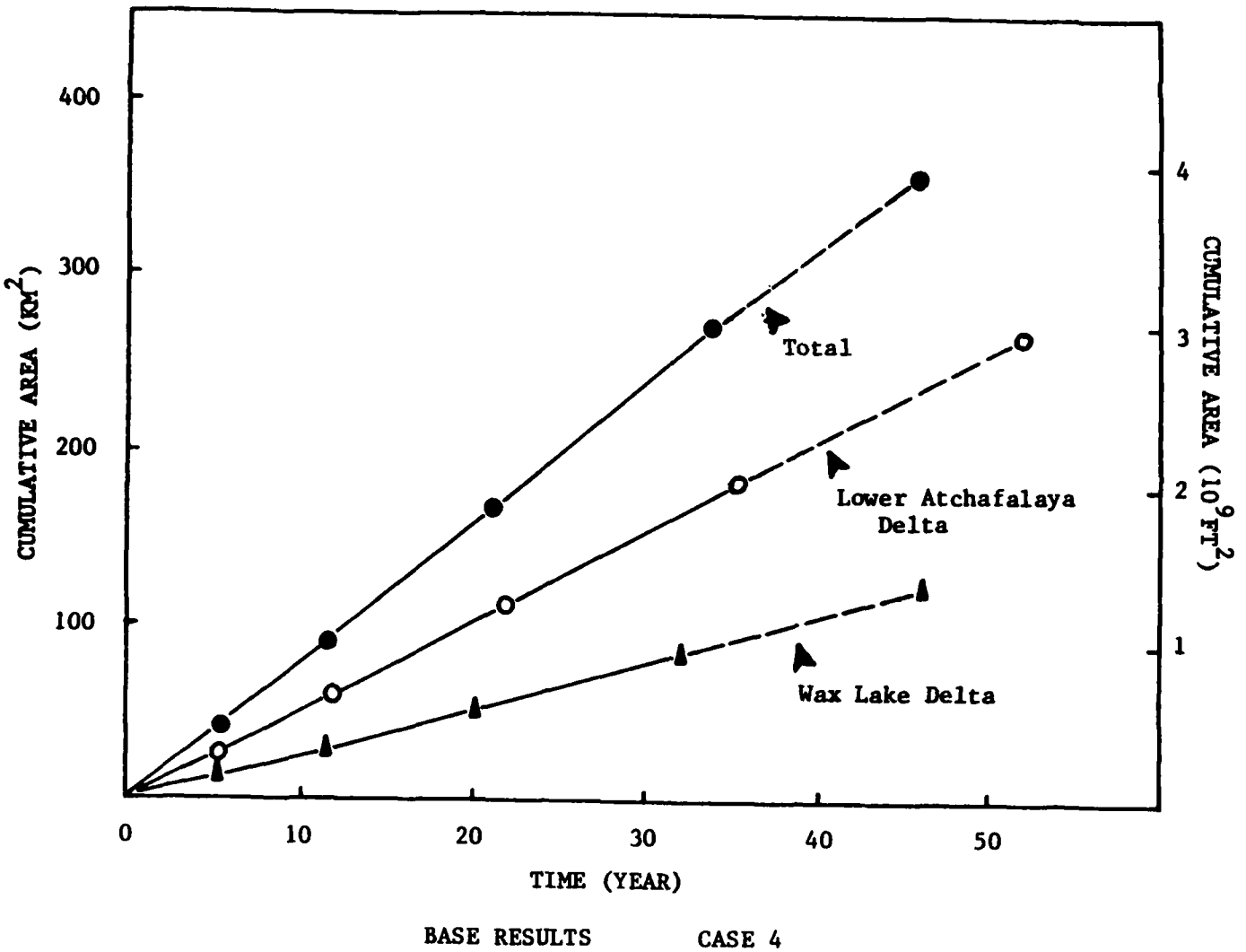

Figure 33. Analytical prediction of subaerial land in Atchafalaya Bay (Case 4)

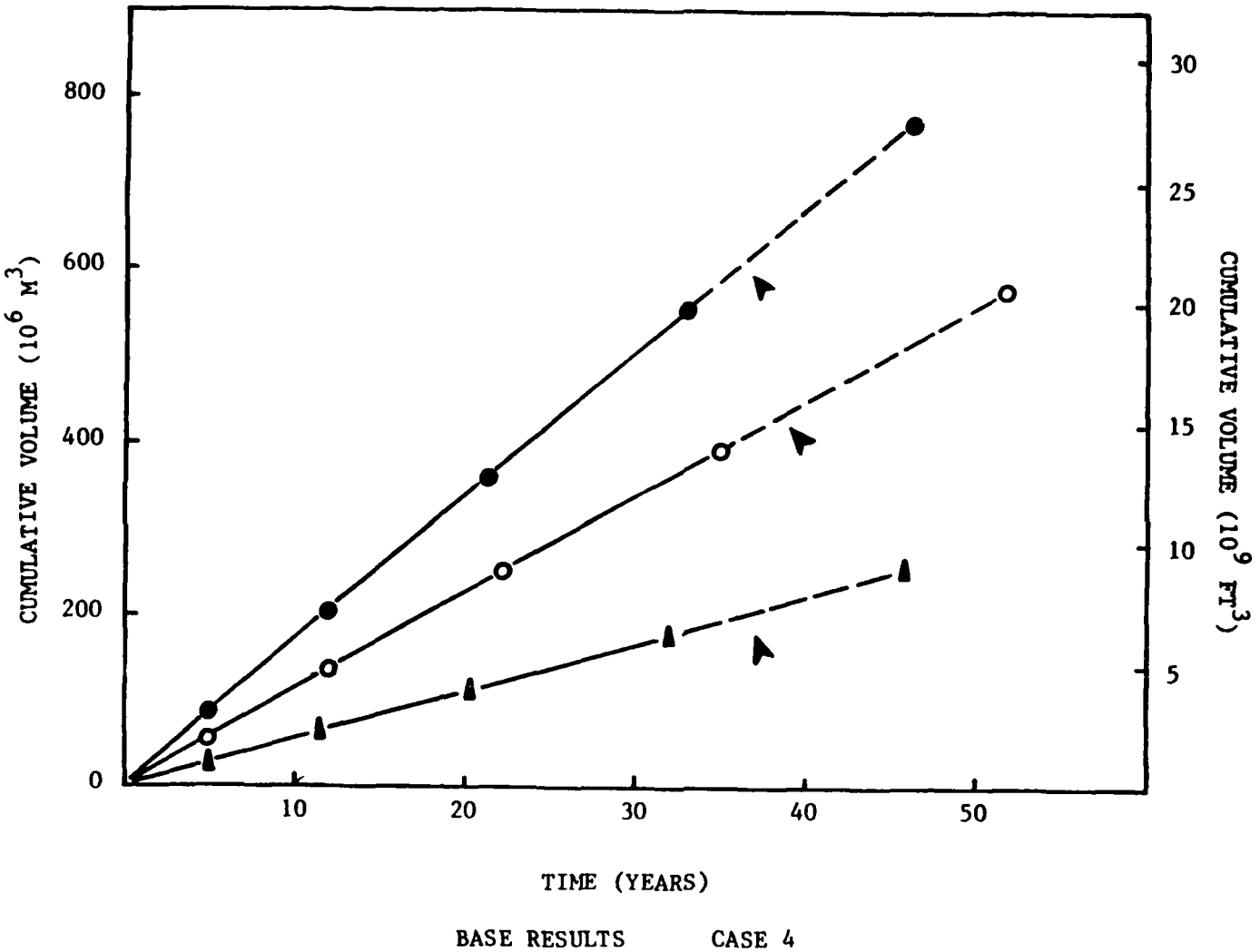

igure 34. Analytical prediction of volume extent of Atchafalaya River Delta growth (Case 4)

PART VII: SENSITIVITY ANALYSIS AND RESULTS

Sensitivity Analysis of Various Parameters

174. The analytical solutions of jet characteristics derived in PART V are based on the theory of turbulent plane jet under a number of assumptions. The numerical approaches to predict the delta growth presented in PART VI depend upon a number of estimated parameters. It is thus essential to study the importance of various physical parameters in the problem formulation and to show the balance between the numerical procedures and the physical environment.

175. The sensitivity analysis is used to aid in the understanding of the dynamics of river-delta interaction; to identify the relative importance of various variables in deltaic processes; and to test the effects of the distributary network on the outcome of predictions. The sensitivity tests to be conducted are:

a. River outlet conditions (h_0, b_0, u_0).

b. Sediment concentration and settling velocity (c_0, w_0).

c. Bay bottom slope, friction, and lateral entrainment (a, f, e).

176. The sensitivity analysis is performed in two phases. First, each parameter is analyzed independently by holding other variables constant, under the same conditions as in the base results. Second, several parameters are examined conjunctively to show their interrelated effects.

River outlet conditions (h_0, b_0, u_0)

177. In this study, the water depth of the receiving bay is taken as the same as the water depth at the river outlet. To examine the influence of the outlet depth (h_0) on the growth of delta, three different water depths of 1.5 m, 1.0 m, and 0.5 m for Case 4 (linear depth with entrainment, $E \neq 0$ and $H \neq 1$) are considered. That is, in the sensitivity test, only the outlet water depth (h_0) in Case 4 is changed from 2.0 m to 1.5 m, 1.0 m, and 0.5 m, while all other variables remain constant. The suspended sediment distributions are given in Plate 7 as

three-dimensional plots. The results demonstrate that at shallower water depths, delta buildup is sharper in shape and is limited to a much smaller area close to the river outlet.

178. The remaining outlet conditions are studied by observing simulated jet behavior under the influence of width of the outlet (b_0) and outlet velocity (u_0). A sensitivity test is made for the half-width at values of 250 m, 500 m, 750 m, and 1000 m while other variables in Case 4 remain constant. The results of the effects on jet width, jet velocity, and sediment concentration are plotted in Plate 8. It is concluded that the larger the river outlet, the faster the jet spreads laterally and the faster the current velocity and sediment concentration diminish longitudinally. Also, from Plate 9 it is shown that as the outlet velocity (u_0) exceeds 0.5 m/sec, the sediment concentration (c) is not substantially influenced by higher values of u_0 (u_0 = 1.0, 1.5 m/sec).

Sediment concentration and settling velocity (c_0, w_0)

179. A continous point source of sediment issuing from the river outlet is assumed in this study. The supply of sediment to Atchafalaya Bay has been changing both in volume and character over the past decade. In a regressional analysis, Letter (1982), based on the 50-year extrapolation hydrograph at Simmesport, computed the maximum and minimum sediment yield (113 and 38 million tons/year) corresponding to the maximum and minimum discharges (310,000 and 139,000 cfs) and obtained maximum and minimum sediment concentrations of 365 ppm and 275 ppm.

180. A sensitivity test is conducted for the mean concentration (c_0) (c_0 = 100, 200, 300, 400, and 600 ppm) in Case 4. The three-dimensional plots of sediment distributions are given in Plate 10. The deposited sediments become thicker as the sediment concentrations are increased; however, delta growth in all instances is restricted to the proximity area of the outlet.

181. The settling velocity of suspended sediment (w_0) is in part a function of particle size (Figure 23); the situation is further complicated by the aggregation of the suspended cohesive materials (Van Heerden, Wells, and Roberts 1981). The influence of the settling velocity is

investigated for w_0 = 0.01, 0.05, 0.1, 0.5, and 1.0 mm/sec. The results for the dimensional center-line concentration are given in Plate 11. The dependence of w_0 on c is shown. The sediment deposition pattern for settling velocities of 0.01, 0.1, and 1.0 mm/sec are presented in Plate 12. It demonstrates that smaller settling velocities result in more uniform deposition patterns, and that larger settling velocities produce patterns sharper in shape and limited to a smaller area close to the river outlet.

Bay bottom slope, friction,and lateral entrainment (a, f, e)

182. In Atchafalaya Bay, Adams and Baumann (1980) estimated that the bay has a slight slope of 0.00015, approximately 0.8 ft per mile. In this study, a sensitivity test is made using slope values of 0.00001, 0.00005, 0.0001, 0.0002, and 0.001 with other parameters in Case 4 remaining constant. The results of the effects on jet width, jet velocity, and sediment concentration are shown in Plate 13. The plots demonstrate that the influence of the bottom slope is minor except for a value of 0.001.

183. The dimensional jet width (B), the center-line velocity (U), and sediment concentration (C) are displayed in Plate 14 for Case 1 (E=0, H=1), Case 2 (E=0, H≠1), Case 3 (E≠0, H=1), and Case 4 (E≠0, H≠1). It is seen that increasing the bottom slope causes a narrower and elongated riverine jet (Case 1 vs Case 2; Case 3 vs Case 4), and that the effect of bottom slope counteracts the effect of the lateral entrainment (Case 1 vs Case 4). The velocity, however, does not exhibit any significant variation among the cases. The sediment concentration is affected both by the bottom slope and the lateral entrainment.

184. The analytical solutions of jet width, center-line velocity, and sediment concentration all show a strong dependence on the bottom friction (f). In fact, the jet width grows and jet velocity decays exponentially along the longitudinal distance. The values of the Darcy-Weisbach's coefficient are taken as 0.001, 0.002, 0.003, 0.004, and 0.006 in the sensitivity test while all other parameters remain the same as in Case 4. The plots of jet width, center-line velocity, and concentration are shown in Plate 15. It is inferred from these figures that the bottom

friction plays an important role in the jet dynamics. When the friction is larger, the jet expands laterally much faster as it faces the bottom resistance and loses its momentum much more quickly. It also indicates a rapid decrease in the sediment concentration with increasing values for the bottom friction.

185. Ozsoy (1977) stressed the importance of the effects of lateral entrainment on tidal inlet characteristics. To study the effects of entrainment on the characteristics of the river delta, four values of the entrainment coefficient e = 0.0375, 0.075, 0.150, and 0.300 are examined. Results are shown in Plate 16 for jet width, center-line velocity, and concentration, respectively. It is seen that for a river-delta system the entrainment mechanism also plays a role.

The Relative Role of Physical Parameters

186. The sensitivity analyses conducted in previous sections shed some light on the relative importance of various parameters in the study of river-delta interaction. Their orders of apparent importance are listed below:

a. The bottom friction (f) influences jet flow to the greatest extent. The jet loses its momentum due to high friction, and expands its width at a faster rate than in the case of low friction.

b. The settling velocity (w_0) affects the transport of suspended sediment to a large extent. With higher settling velocity, the center-line sediment concentration drops more rapidly and the delta lobe is smaller and closer to the river outlet.

c. The width of the outlet (b_0), as considered in simulating the process of branching channels, has significant influence on the shape of subaerial land. The wider the outlet, the more rapidly current velocity diminishes with increasing longitudinal distance, which results in much faster lateral spreading of the jet, a natural cause of delta buildup.

d. The lateral entrainment (e) affects the jet characteristics. Jet width increases with increasing entrainment. Consequently, the jet velocity and sediment concentration decrease as the jet width expands.

e. The influence of the outlet depth (h_0) on jet characteristics can be examined by utilizing the aspect ratio (Jirka 1981), defined as the ratio depth to width, "h_0/b_0". Higher values of this ratio, increasing h_0 or decreasing b_0, result in a much narrower and more elongated delta form.

f. Increasing the center-line velocity (u_0) and the sediment concentration (c_0) will develop delta lobes with thicker and more elongated shapes.

Growth Curves of Subaerial Land in Atchafalaya Bay

187. In this study, the values used in the base runs are mean values of various physical parameters taken from the available literature (PARTS II and VI). These quantities may vary throughout the period of predicted growth depending on the nature of the system under consideration. To circumvent this situation, the most sensitive parameters are used to simulate the greatest and least potential growth of subaerial land.

Simulated growth of Atchafalaya River deltas

188. The physical quantities that are of major importance to the Atchafalaya River-Bay system are the coefficient of bottom friction (f), the settling velocity of sediment particles (w_0), and the sediment concentration (c_0). Since high friction causes the jet to spread laterally, high settling velocity results in smaller delta lobes, and low sediment concentration develops a thinner subdelta, the environment for least growth can be simulated by increasing f and w_0 and decreasing the c_0 value. In contrast, the high growth environment can be best simulated by low f, low w_0, and high c_0 values.

189. The following environments are simulated for the growth of subaerial land in Atchafalaya Bay:

a. Base results

$f = 0.001$

$w_0 = 0.05$ mm/sec

$c_0 = 300$ ppm

b. Slow growth

$f = 0.004$

$w_0 = 0.1$ mm/sec

$c_0 = 200$ ppm

c. Fast growth

$f = 0.001$

$w_0 = 0.03$ mm/sec

$c_0 = 400$ ppm

The results of the simulated growth patterns are summarized in Tables 7, 8, 9, and 10 and plotted in Plate 17.

Comparison with other predictions

190. The growth of the Atchafalaya River deltas has been predicted by various investigators. Shlemon (1972), based on sediment measurements made in the outlets, predicted a growth rate of 5.5 to 7.5 mi^2/year (14 to 18 km^2/year), with the delta covering an area of 290 to 350 mi^2 (750 to 900 km^2) by the year 2020. His prediction was referred to a -3 ft mean low gulf contour.

191. Adams and Baumann (1980), following the same empirical approach as Shlemon, estimated that the Atchafalaya Bay will be filled to an average depth of 2 ft below mean sea level in a time period of approximately 40 years.

192. Wells, Chinburg, and Coleman (1984), based on the generic analysis of existing deltas, projected that by the year 2030 a new subaerial land mass will be created in the bay ranging from 59 to 132 mi^2 (150 to 337 km^2) with 81 mi^2 (208 km^2) representing the expected land in 50 years under average flood conditions. They estimated a growth rate of 1.6 mi^2/year (4.0 km^2/year); their study was referred to the mean sea level.

193. Letter (1982) developed a regressional model and predicted that within 50 years (by the year 2027) the delta will evolve gulfward of Eugene Island. The total volume of the deposited sediment is estimated at 58 billion ft^3; and the delta mass volume (based on the -3 ft NGVD) is about 17.6 billion ft^3.

194. The total subaerial land development predicted analytically in this study is displayed in Figure 35 together with the prediction

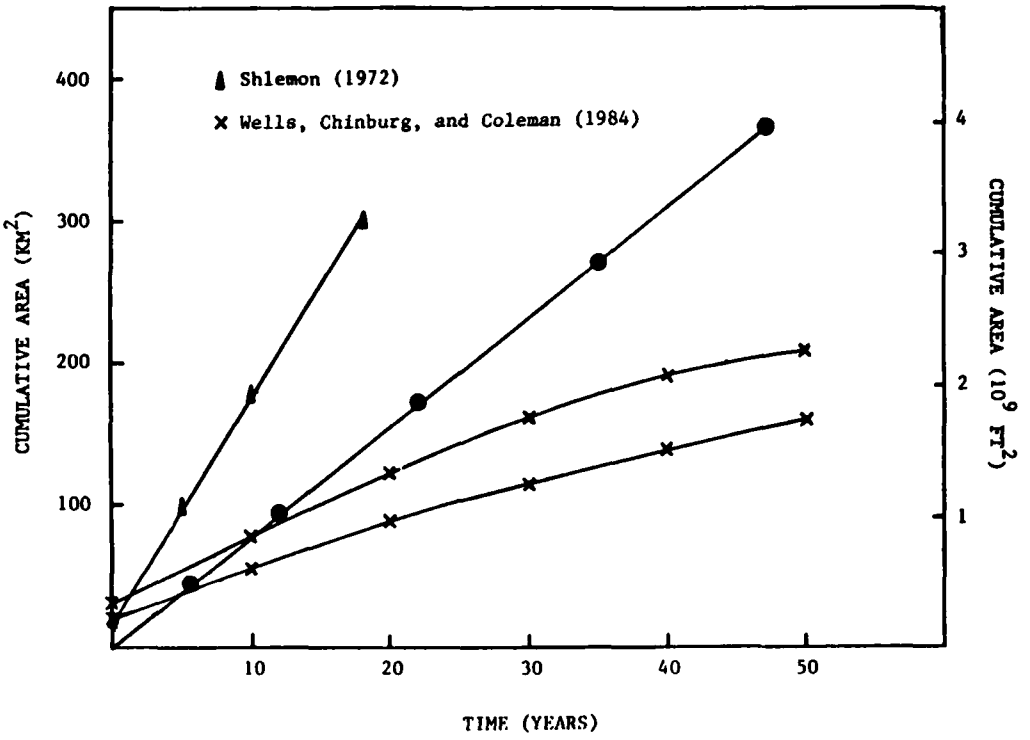

Figure 35. Prediction of subaerial land in Atchafalaya Bay

curves developed by Shlemon (1972) and Wells, Chinburg, and Coleman (1984). A contour-type map for approximate delta front advancement is depicted in Figure 36. Our prediction, based on analytical results, shows an average growth rate of 7.6 km^2/yr, ranging from 6.0 to 10.0 km^2/yr as simulated for the slow growth and fast growth environments, respectively. On a volume basis, the average volume of sediment deposition is predicted at 16 x 10^6 m^3/yr, with a range of 12 x 10^6 m^3/yr to 23 x 10^6 m^3/yr.

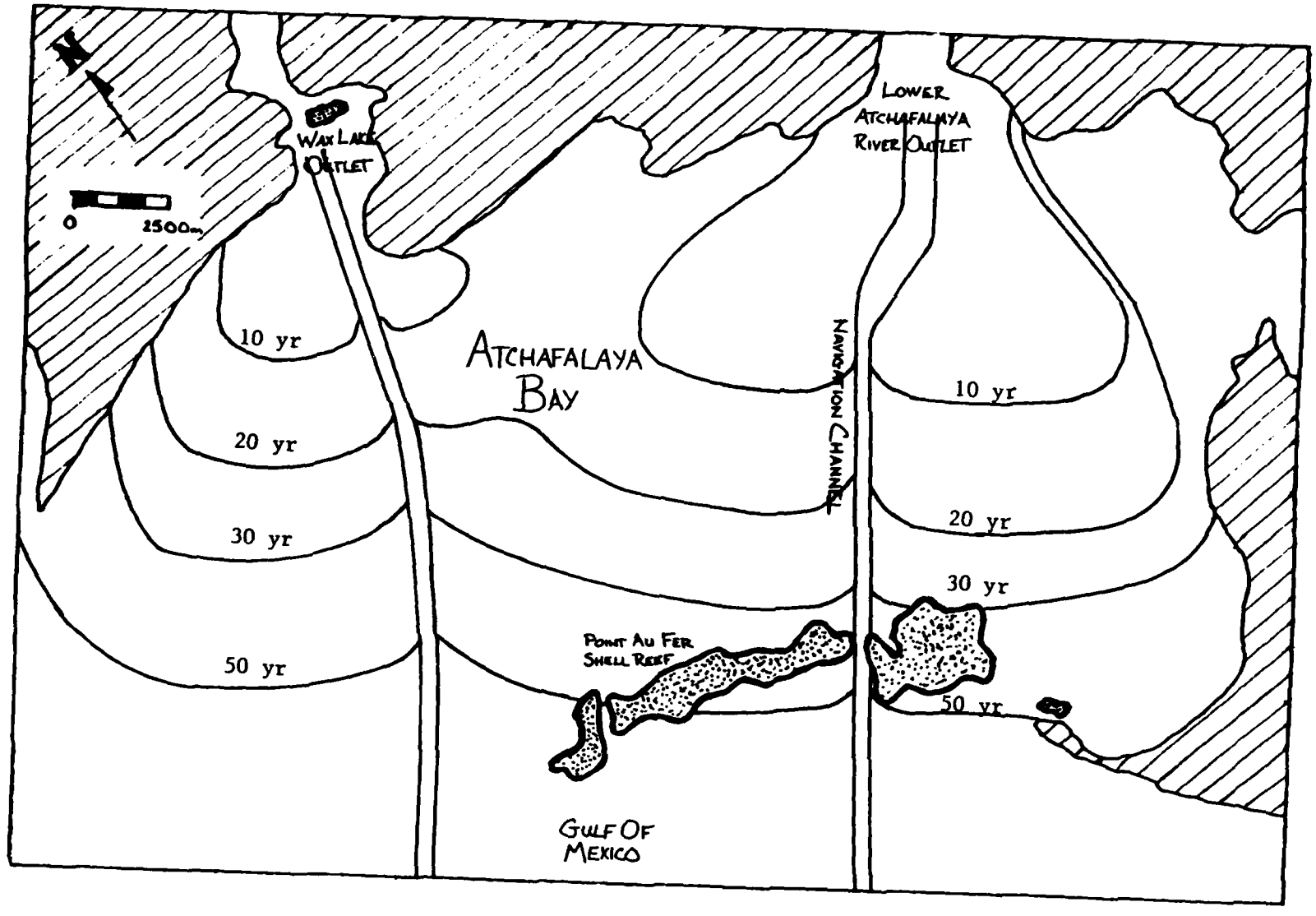

Figure 36. Predicted Atchafalaya Bay subaerial delta configuration

PART VIII: SUMMARY, LIMITATIONS, AND CONCLUSIONS

Summary

195. An analysis has been made to aid in understanding the various phenomena associated with turbulent plane jets issuing from river outlets and discharging into a quiescent receiving bay. An integrated form of the hydrodynamic equations of flow continuity and momentum balance, coupled with the mass transport equation, has been formulated into a two-dimensional spatial and quasi-steady temporal domain.

196. A similarity function in the form of exponential and polynomial expressions was chosen for the velocity and sediment concentration profiles. The lateral entrainment is expressed as a function of the jet center-line velocity. A closed-form analytical solution is obtained in terms of the normalized dependent variables of the jet width, the center-line jet velocity, and the center-line sediment concentration. The solutions for cases of constant depth and of linearly varying depth, both with and without entrainment, are presented.

197. From these normalized solutions, the thickness of deposited sediment is calculated under quasi-steady state conditions. The Statistical Analysis System of computer graphics (SAS/GRAPH 1981) is used to display the three-dimensional sediment deposition patterns. These sediment patterns, together with a stepwise numerical procedure simulating the process of branching channels, are then used to estimate the areal extent and the volume of deposition for the Atchafalaya deltas under a variety of conditions. Sensitivity analyses are performed to assess the relative importance of various parameters in the river-delta system.

Limitations

198. There are certain limitations inherent in the application of the analytical model:

a. The governing equations for flow and mass transport are developed for a shallow-water environment in the absence of tidal and wave currents. Therefore the simplified equations for turbulent jets will not be representative of a regime subjected to tidal and wave action.

b. The similarity profiles for the velocity and sediment concentration must be used in order to obtain a set of closed-form analytical solutions.

c. The deposition function used for sediment dispersion and settling in shallow water does not take the erosion process into consideration. The analytical approach is not capable of addressing the problem of the resuspension of sediment in the bay and the reworking of delta deposits by physical processes offshore.

d. In studying the river delta development, the sediment deposition is assumed to be quasi-steady state; the thickness of the deposited sediment layer is assumed to vary linearly with time.

e. The bifurcation processes are simulated in the form of turbulent jets at the new channel outlets; at each level of bifurcation, an equal amount of flow and sediments is assumed to be distributed to the branching channels.

f. The values of various parameters are based on time-averaged quantities. The analysis is projected to yield a gross estimate of areal and volume extent of the Atchafalaya River delta.

g. The analytical results are generated from local data within the bay. Predicting the delta development beyond the bay will be less accurate, since the governing equations of turbulent plane jets derived for shallow receiving waters will not be applicable to the deeper water offshore.

Conclusions

199. The primary sources of energy for the development of the Atchafalaya River's deltas in the bay are the natural resources of the river, that is, the suspended sediments that form the delta and the river discharge that carries the sediment load. The river-delta interaction is a complicated phenomenon. The analytical work reported herein is a simplified representation of complexity in predicting the evolution of

the Atchafalaya River delta. It covers the essential features of natural processes leading to the growth of the delta.

200. The following conclusions are drawn from this study:

a. The depth of the river outlet and the bottom friction in the bay play an important role in determining the spreading of river effluents.

b. The process of channel bifurcation has significant influence in the shape and the area of subaerial land.

c. The settling velocity of sediment particles has the most impact on the volume of delta lobes.

d. The center-line velocity and sediment concentration control both the area extent and volume deposition of river deltas.

e. The lateral entrainment also plays a role in the development of river deltas in the shallow and wide Atchafalaya Bay.

f. The predictions of the future growth of the Atchafalaya River deltas in this study are:

(1) The Lower Atchafalaya River Outlet Delta will grow approximately 5.0 km^2/yr; the Wax Lake Outlet Delta will grow at a rate of 2.6 km^2/year.

(2) The total growth of subaerial land of the Atchafalaya River deltas is expected to be 7.6 km^2/year.

g. It will take about 50 years for the Atchafalaya River deltas to reach the Point Au Fer Shell Reef.

h. The results of delta growth predicted in this analytical study are commensurate with the predictions made by others.

LITERATURE CITED

Abraham, G. 1976. "Entrainment Solutions for Jet Discharge into Deep Water," Thermal effluent disposal from power generation. Z. P. Zaric, ed., Hemisphere Publishing Corp. pp 11-44.

Abramovich, G. N. 1964. The theory of turbulent jets. MIT Press.

Adams, R. D., and Baumann, R. H. 1980. Land building in coastal Louisiana: emergence of the Atchafalaya Bay delta, Sea Grant Publication No. LSU-T-80-02. Center for Wetland Resources, Louisiana State University, Baton Rouge, La.

Ariathurai, R., MacArthur, R. C., and Krone, R. B. 1977. Mathematical model of estuarial sediment transport, Technical Report D-77-12, Contract No. DACW39-75-C-0080. US Army Engineer Waterways Experiment Station, Vicksburg, Miss.

Bates, C. C. 1953. Rational theory of delta formation. Amer. Assoc. Petr. Geol. Bull., Vol. 37: pp 2119-2162.

Beyer, W. H. 1978. Handbook of mathematical science. 5th edition. CRC Press.

Bowman, M. J. and Iverson, R. L. 1978. "Estuarine and Plume Fronts," Oceanic Fronts in Coastal Processes. M. J. Bowman and W. E. Esaias, eds., Springer-Verlag, New York, pp 87-104.

Coleman, J. M. 1976. Deltas: processes of deposition and models for exploration. Continuing Education Publication Company, Inc.

Coleman, J. M., and Wright, L. D. 1975. "Modern River Deltas: Variability of Processes and Sand Bodies," Deltas: models for exploration. M. L. Broussard, ed. Houston Geol. Soc., Houston, Tex., pp 99-149.

Cratsley, D. W. 1975. Recent deltaic sedimentation, Atchafalaya Bay, Louisiana, M.S. Thesis. Louisiana State University, Baton Rouge, La.

Dronkers, J. J. 1964. Tidal computations in rivers and coastal waters. North-Holland Publishing Co., Amsterdam, The Netherlands.

Ellison, T. H. and Turner, J. S. 1959. Turbulent entrainment in stratified flows. Fluid Mech., Vol. 6: pp 423-448.

Engelund, F. 1976. Hydraulics of surface jet. J. Hydraul. Div., ASCE. Vol. 102 (HY9) Proc. Paper 12409: pp 1315-1325.

Engelund, F. and Pederson, F. B. 1973. Surface jet at small Richardson numbers. J. Hydraul. Div., ASCE. Vol. 99 (HY3) Proc. Paper 9588: pp 405-416.

Fox, D. G. 1970. Forced plume in a stratified fluid. J. Geophys. Res. Vol. 75 (33): pp 6818-6835.

French, J. L. 1960. Tidal flow in entrances, US Army Corps of Engineers, Committee on Tidal Hydraulics, Technical Bull. No 3. Waterways Experiment Station, Vicksburg, Miss.

Garrett, B., Hawxhurst, P., and Miller, J. 1969. Atchafalaya Bay, Louisiana, Lower Atchafalaya River and Wax Lake Outlets, 66th Meeting of the Committee on Tidal Hydraulics, July 15-15, 1969. New Orleans, La.

Hayashi, T. and Shuto, N. 1967. Diffusion of warm water jets discharged horizontically at the water surface. Proc. 12th Congr. IAHR, Fort Collins, Colo.: pp 47-55.

Hirst, E. 1971. Buoyant jets discharged to quiescent stratified ambients. J. Geophys. Res., Vol. 76 (30) October: pp 7375-7384.

Hoopes, J. A., Zeller, R. W. and Rohlich, G. A. 1967. Heat dissipation and induced circulations from condensor cooling water discharge into Lake Monona, Report No 35. Department of Civil Engineering, Univ. of Wisconsin.

Jirka, G. H., Abraham, G. and Harleman, D. R. F. 1975. An assessment of techniques for hydrothermal prediction, R. M. Parsons Lab., Report No 203. MIT.

Jirka, G. H., Adams E. E. and Stolzenbach, K. D. 1981. Buoyant surface jets. J. Hydraul. Div., ASCE. Vol. 107 (HY11) Proc. Paper 16660: pp 1467-1487.

Kantha, L. H., Phillips, O. M. and Azad, R. S. 1979. On turbulent entrainment at a stable density interface. J. Fluid Mech., Vol. 79: pp 753-768.

Kato, H. and Phillips, O. M. 1969. On the penetration of a turbulent layer into a stratified fluid. J. Fluid Mech., Vol. 37: pp 643-665.

Keffer, J. F. and Baines, W. D. 1963. The round turbulent jet in a crosswind. J. Fluid Mech., Vol. 15 (4): pp 481-496.

Koh, R. C. Y. and Fan, L. N. 1970. Mathematical models for the prediction of temperature distribution resulting from the discharge of heated water in large bodies of water, EPA Water Pollution Control Research Series 16130 DWO.

Krone, R. B. 1962. Flume studies of the transport of sediment in estuarial shoaling processes. Technical Report, Hydraulic Engineering Lab, University of California. Berkeley, Calif.

Krone, B. B. 1978. "Aggregation of Suspended Particles in Estuaries," Estuarine transport processes. Bjorn Kjerfve, ed. University of South Carolina Press. Columbia, S. C.

Kuu, W. Y., and Polack, J. A. 1982. Kinetic parameter estimation for reaction systems of immoblized cells and enzymes, Paper No. 86b. 75th Ann. AICHE Meeting, Los Angeles, Calif. 14-18 November 1982.

Letter, J. V., Jr. 1982. The Atchafalaya River Delta. Report 3: extrapolations of delta growth, Technical Report HL-82-15. US Army Engineer Waterways Experiment Station, Vicksburg, Miss.

McAnally, W. H., Jr., and Heltzel, S. B. 1978. A plan for predicting the evolution of Atchafalaya Bay, Louisiana. US Army Engineers, Waterways Experiment Station, Vicksburg, Miss.

Motz, L. and Benedict, B. 1970. Heated surface jet discharged into a flowing ambient stream, Report No. 4. Department of Environmental and Water Resources Engr., Vanderbilt Univ. Nashville, Tenn.

Nihoul, J. C. J. 1975. "Hydrodynamic Models," Modeling of marine systems, J. C. J. Nihoul, ed. Elsevier Scientific Publishing Co., Amsterdam, The Netherlands.

Ozsoy, E. 1977. Flow separation and related phenomena at tidal inlets, Ph.D. Diss. Univ. of Flordia, Gainesville, Fla.

Pai, S.-I. 1954. Fluid dynamics of jets, D. Van Nostrand Co., Inc.: pp 98-137.

Policastro, A. J. and Dunn, W. E. 1976. "Evaluation of Integral and Phenomenological Models for Heated Surface Plumes with Field Data," Thermal effluent disposal from power generation. Z. P. Zaric, ed., Hemisphere Publishing Corp. pp 45-59.

Price, J. F. 1979. On the scaling of stress-driven entrainment experiments. J. Fluid Mech., Vol. 90 (3): pp 509-529.

Rajaratnam, N. 1976. Turbulent jets. Elsevier Scientific Publ. Co., Amsterdam, The Netherlands.

Rajaratnam, N. and Stalker, M. J. 1982. Circular wall jets in co-flowing streams. J. Hydraul. Div., ASCE. Vol. 108 (HY82) Proc. Paper 16851, February: pp 187-198.

Roberts, H. H., Adams, R. D., and Cunningham, R. H. W. 1980. Evolution of sand-dominated subaerial phase, Atchafalaya Delta, Louisiana. Amer. Assoc. Petr. Geol. Bull., Vol. 64 (2): pp 264-279.

Safaie, B. 1979. Mixing of buoyant surface jet over sloping bottom. Waterways, Port, Coast and Ocean Div., ASCE. Vol. 105(WW4): pp 357-373.

SAS/GRAPH. 1981. User's guide. Statistical Analysis System SAS Institute Inc., Cary, N. C.

Scheid, F. 1968. Numerical analysis. Schaum's Outline Series, Schaum Publishing Co., New York.

Schlichting, H. 1968. Boundary layer theory. McGraw-Hill, New York.

Shirazi, M. A. and Davis, L. R. 1974. Workbook of thermal plume prediction, Vol. 2: Surface discharge, EPA Technology Series EPA-R2-72-005b, May.

Shlemon, R. J. 1972. Development of the Atchafalaya Delta, Louisiana. Hydrologic and Geologic Studies of Coastal Louisiana, Report No 13. Center for Wetland Resources, Louisiana State University, Baton Rouge, La.

Sill, B. L., Fisher, J. S. and Whiteside, S. D. 1981. "Laboratory Investigation of Ebb Tide Shoals," J. WPCO Engr. Div., ASCE. Vol. 107 (WW4) Proc. Paper 16674: pp 233-242.

Stolzenbach, K. D. and Harleman, D. R. F. 1971. An analytical and experimental investigation of surface discharges of heated water, R. M. Parsons Lab., Report No 156. MIT.

Townsend, A. A. 1956. The structure of turbulent shear flow. Cambridge Univ. Press, New York.

US Army Corps of Engineers. 1974. Preliminary draft environmental impact statement, Atchafalaya Basin floodway. New Orleans, La.

US Fisheries and Wildlife Service. 1976. A progress report: fish, wildlife, and related resources, Atchafalaya River Basin, Louisiana. US Dept. of the Interior. 347 pp.

Van Heerden, I. L. 1980. Sedimentary response during flood and non-flood conditions, New Atchafalaya Delta, Louisiana, M.S. Thesis. Louisiana State Univeristy, Baton Rouge, La.

Van Heerden, I. L., Wells, J. T., and Roberts, H. H. 1981. Evolution and Morphology of Sedimentary Environments, Atchafalaya Delta, Louisiana. Trans. Gulf Coast Assoc. of Geol. Soc. 31st Ann. Meeting, 21-23 October 1981, Corpus Christi, Tex., pp 399-408.

Villadsen, J., and Michelson, M. L. 1978. Solutions of differential equation models by polynomial approximation. Prentice-Hall, Englewood Cliffs, N. J.

Waterways Experiment Station. 1981. Hydrographic analysis data, 1974-1976. US Army Corps of Engineers, New Orleans, La.

Waterways Experiment Station. 1982. Preliminary field data report, Vicksburg, Miss.

Wells, J. T., Chinburg, S. J., and Coleman, J. M. 1984. The Atchafalaya River Delta. Report 4: generic analysis of delta development, Technical Report HL-82-15; prepared for Waterways Experiment Station, Contract DACW 39-80-C-00082. Coastal Studies Institute, Center for Wetland Resources, Louisiana State University, Baton Rouge, La.

Wells, J. T., and Kemp, P. 1981. Atchafalaya mud stream and recent mudflat progradation: Louisiana Chenier Plain. Trans. Gulf Coast Assoc. of Geol. Soc. 31st Ann. Meeting, 21-23 October 1981, Corpus Christi, Tex.: pp 409-416.

Wells, J. T., and Roberts, H. H. 1980. Fluid mud dynamics and shoreline stabilization, Louisiana Chenier Plain. Proc. 17th Conf. Coast. Engr., ASCE. Sydney, Australia, March 23-28, 1980: pp 1328-1401.

Wright, L. D. and Coleman, J. M. 1971. Effluent expansion and interfacial mixing in the presence of a salt wedge, Mississippi River Delta. J. Geophys. Res. Vol. 76 (36): pp 8649-8661.

Wright, L. D. and Coleman, J. M. 1974. Mississippi River mouth processes: effluent dynamics and morphologic development. J. Geol. Vol. 82: pp 751-778.

Wylie, C. R., Jr. 1951. Advanced engineering mathematics. McGraw-Hill, New York. 591 pp.

Table 1

Area and Thickness of Fill in Atchafalaya Bay, 1952-1962
(Area computed from isopachs, Figure 6)
(Shlemon 1972, Table 1)

Thickness ft	1	2	3	4	5	6
Area, square miles	46.89	23.60	9.20	2.14	1.00	0.60

Table 2

Average Annual Suspended Load Budget, Atchafalaya River
(Roberts, Adams, and Cunningham 1980, Table 1)

	Input 10^3 Ton		Distribution of Input 10^3 Ton					
	Simmesport (Near Diversion Point)	%	Basin Retention	%	Wax Lake Outlet	%	Lower Atchafalaya River	%
1967-1971								
Sand	19,342	22	14,491	75	1,153	6	6,698	19
Silt/Clay	67,905	78	10,179	15	15,590	23	42,136	62
Total	87,247	100	24,670	29	16,743	19	45,834	52
1973-1975								
Sand	37,506	25	3,668	10	5,748	15	28,090	75
Silt/Clay	100,704	75	21,256	19	21,789	20	67,650	61
Total	148,210	100	24,924	17	27,546	19	95,740	65

Note: Computations from measured data and sediment rating curves, USACOE files.

Table 3

Chronological Development of the Atchafalaya River Delta

Year	River Discharge (Simmesport)		Sediment Characteristics		Bay Bathymetry			References
	Maximum	Average	Size	Quantity	Deposition	Depth and Area	Profile	
Prior to 1950's			Clays and silty clays	Very little	Prodelta	6 ft	No change	Shlemon 1972 Cratsley 1975
1952-1962			Silt and Sand	1 ft thick	Subaqueous delta	47 sq mi		Shlemon 1972
1965-1967	325,000 cfs	165,000 cfs	25% sand 75% silt and clay		Distributary mouth bars			Garrett, Hawxhurst, and Miller 1969
1967-1972	303,000 cfs	208,000 cfs		63×10^6 tons/yr	Subaerial delta		Bathy profiles	USACOE 1974 Cratsley 1975
1973-1975	700,000 cfs	315,000 cfs	25% sand 75% silt	123×10^6 tons/yr				Van Heerden 1980 Roberts, Adams, and Cunningham 1980
1976-1978		165,000 cfs			Subaerial land	16 sq mi	Bathy map	Roberts, Adams, and Cunningham 1980 Adams and Baumann 1980
1979	500,000 cfs		250-400 mg/l					Van Heerden 1980 Wells and Kemp 1981
1970-2020					Subaerial land	290-350 sq mi	Bathy map	Shlemon 1972
1977-2027			Sand-dominated	$58 \times 10^9 ft^3$	Subaerial land	50 sq mi	Bathy map	Letter 1984
1980-2030				495×10^6 ft/yr	Subaerial land	60-130 sq mi	Bathy map	Wells, Chinburg, and Coleman 1984

Table 4

Values of Various Parameters Used for Analytical Solutions

Half Width of Outlet b_0 m	Water Depth at Outlet h_0 m	Flow Velocity at Outlet u_0 mps	Sediment Concentration at Outlet c_0 ppm	Settling Velocity of Sediment w_0 mm/sec	Bay Bottom Slope a	Friction Coefficient f	Lateral Entrainment Coefficient e
250	1.0	0.05	100	0.01	0.001	0.001*	0.0375
500*	1.5	1.0*	300*	0.05*	0.0001*	0.003	0.075*
1000	2.0*	1.5	600	1.00	0.00001	0.006	0.300

*Value used in the base results.

Table 5

Predicted Areal and Volume Extent of the Lower Atchafalaya River Outlet Delta

Case 4: h_0 = 2 m, u_0 = 1 mps, w_0 = 0.05 mm/sec, f = 0.001
c_0 = 300 ppm, p_s = 400 kg/m^3, e = 0.075

Bifurcation Level	b_0 m	r	x_1 km	x_2 km	Area 10^6 m^2	Volume 10^6 m^3	Time Year
1	500.0	9.36	4.68	6.95	26.65	59.58	5.34
2	166.7	24.28	4.05	3.60	35.54	78.28	7.04
3	55.6	59.48	3.31	2.10	51.54	111.4	10.06
4	27.8	102.4	2.85	1.55	66.54	142.5	12.90
5	13.9	173.4	2.41	1.16	85.80	182.1	16.60

Note: A three-branch distribution pattern is used for the second and third levels of bifurcation; for the fourth and fifth levels, the distributary networks are characterized by a two-branch channel pattern.

Table 6

Predicted Areal and Volume Extent of the Atchafalaya River Wax Lake Outlet Delta

Case 4: h_0 = 2 m, u_0 = 1 mps, w_0 = 0.05 mm/sec, f = 0.001
c_0 = 300 ppm, p_s = 400 kg/m^3, e = 0.075

Bifurcation Level	b_0 m	r	x_1 km	x_2 km	Area 10^6 m^2	Volume 10^6 m^3	Time Year
1	500.0	6.87	3.44	4.10	13.20	28.62	5.16
2	166.7	17.65	2.94	2.11	16.92	36.34	6.54
3	55.6	42.55	2.37	1.24	23.64	50.08	9.04
4	27.8	72.27	2.01	0.918	29.82	62.68	11.34
5	13.9	120.9	1.68	0.690	37.88	78.92	14.38

Note: A three-branch distribution pattern is used for the second and third level of bifurcation; for the fourth and fifth levels, the distributary networks are characterized by a two-branch channel pattern.

Table 7

Predicted Areal and Volume Extent of the Lower Atchafalaya River Outlet Delta

Slow Growth Environment

Case 4: h_0 = 2 m, u_0 = 1 mps, w_0 = 0.10 mm/sec, f = 0.004
c_0 = 200 ppm, p_s = 400 kg/m^3, e = 0.075

Bifurcation Level	b_0 m	r	x_1 km	x_2 km	Area 10^6 m^2	Volume 10^6 m^3	Time Year
1	500.0	3.02	1.51	10.74	10.62	22.02	2.98
2	166.7	8.58	1.43	4.44	12.46	25.88	3.48
3	55.6	23.19	1.29	2.10	16.44	33.78	4.56
4	27.8	42.29	1.18	1.42	20.74	42.68	5.76
5	13.9	75.69	1.05	0.999	26.92	55.18	7.46
6	7.0	132.5	0.928	0.723	35.56	72.88	9.80
7	3.5	230.4	0.806	0.531	47.12	96.24	12.98

Note: A three-branch distribution pattern is used for the second and third levels of bifurcation; for the remaining levels, the distributary networks are characterized by a two-branch channel pattern.

Table 8

Predicted Areal and Volume Extent of the Lower Atchafalaya River Outlet Delta

Fast Growth Environment

Case 4: h_0 = 2 m, u_0 = 1 mps, w_0 = 0.03 mm/sec, f = 0.001

c_0 = 400 ppm, p_s = 400 kg/m^3, e = 0.075

Bifurcation Level	b_0 m	r	x_1 km	x_2 km	Area 10^6 m^2	Volume 10^6 m^3	Time Year
1	500.0	11.47	5.74	10.48	44.85	102.69	6.92
2	166.7	30.02	5.00	5.43	61.20	137.64	9.30
3	55.6	74.52	4.14	3.15	90.70	200.22	13.56
4	27.8	129.4	3.60	2.31	118.2	257.76	17.56
5	13.9	221.96	3.09	1.72	155.2	334.28	22.88

Note: A three-branch distribution pattern is used for the second and third levels of bifurcation; for the fourth and fifth levels, the distributary networks are characterized by two-branch channel patterns.

Table 9

Predicted Areal and Volume Extent of the Atchafalaya River Wax Lake Outlet Delta

Slow Growth Environment

Case 4: h_0 = 2 m, u_0 = 1 mps, w_0 = 0.10 mm/sec, f = 0.004

c_0 = 200 ppm, p_s = 400 kg/m^3, e = 0.075

Bifurcation Level	b_0 m	r	x_1 km	x_2 km	Area 10^6 m^2	Volume 10^6 m^3	Time Year
1	500.0	2.37	1.18	5.90	5.42	11.18	3.02
2	166.7	6.68	1.12	2.41	6.19	12.70	3.42
3	55.6	17.88	0.994	1.16	7.98	16.32	4.40
4	27.8	32.23	0.896	0.788	9.88	20.20	5.46
5	13.9	56.89	0.791	0.558	12.58	25.64	6.94
6	7.0	98.07	0.686	0.408	16.34	33.24	8.96
7	3.5	167.8	0.587	0.303	21.30	43.24	11.66

Note: A three-branch distribution pattern is used for the second and third levels of bifurcation; for the remaining levels, the distributary networks are characterized by two-branch channel patterns.

Table 10

Predicted Areal and Volume Extent of the Atchafalaya River Wax Lake Outlet Delta

Fast Growth Environment

Case 4: h_0 = 2 m, u_0 = 1 mps, w_0 = 0.03 mm/sec, f = 0.001
c_0 = 400 ppm, p_s = 400 kg/m^3, e = 0.075

Bifurcation Level	b_0 m	r	x_1 km	x_2 km	Area 10^6 m^2	Volume 10^6 m^3	Time Year
1	500.0	8.66	4.33	6.02	22.10	49.06	6.62
2	166.7	22.38	3.73	3.12	29.18	63.90	8.64
3	55.6	54.51	3.03	1.82	41.82	89.86	12.20
4	27.8	93.52	2.60	1.34	53.72	114.36	15.58
5	13.9	157.9	2.19	1.01	69.04	145.72	19.96

Note: A three-branch distribution pattern is used for the second and third levels of bifurcation; for the fourth and fifth levels, the distributary networks are characterized by two-branch channel patterns.

PLOT OF JET VELOCITY U1

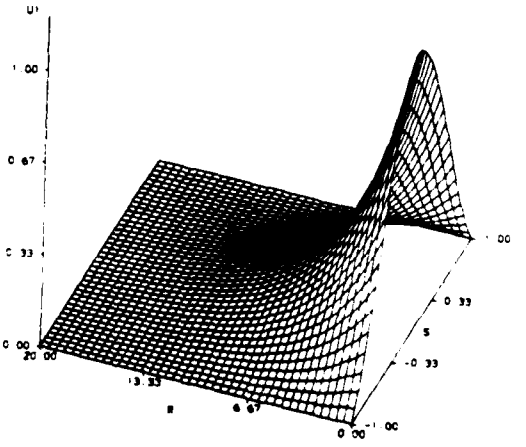

PLOT OF SEDIMENT CONCENTRATION C1

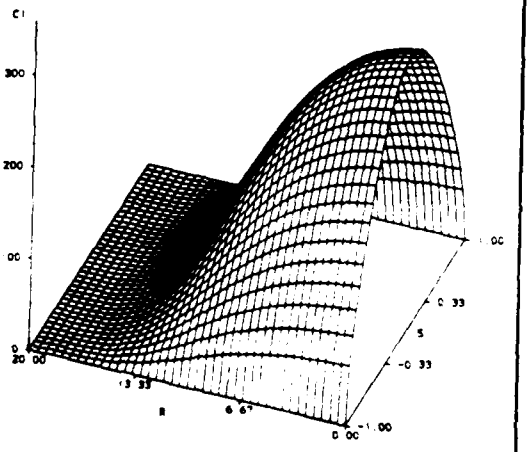

PLOT OF SEDIMENT THICKNESS

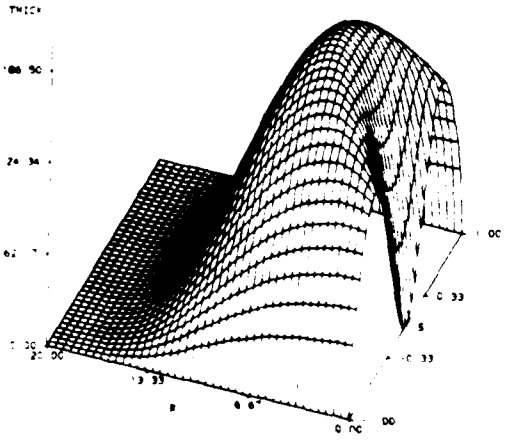

BASE RESULTS

CASE 1

E = 0 AND H = 1

PLATE 1

PLOT OF JET VELOCITY U1

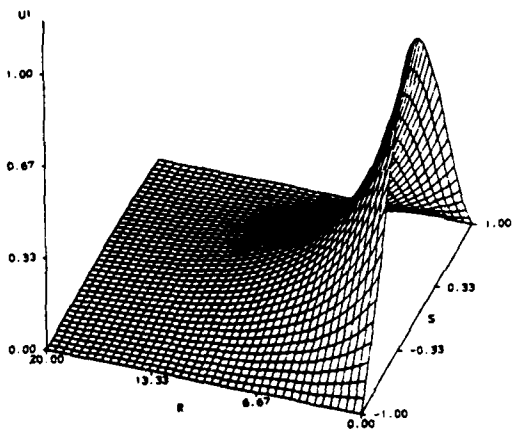

PLOT OF SEDIMENT CONCENTRATION C1

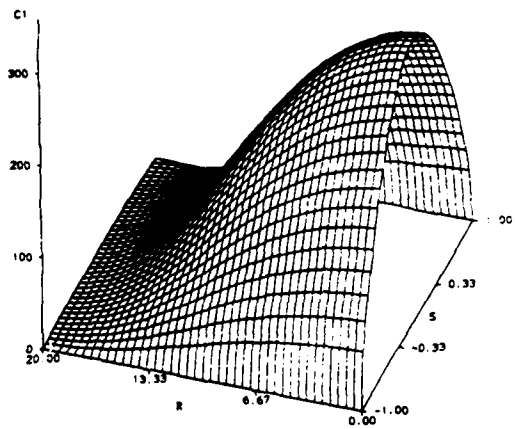

PLOT OF SEDIMENT THICKNESS

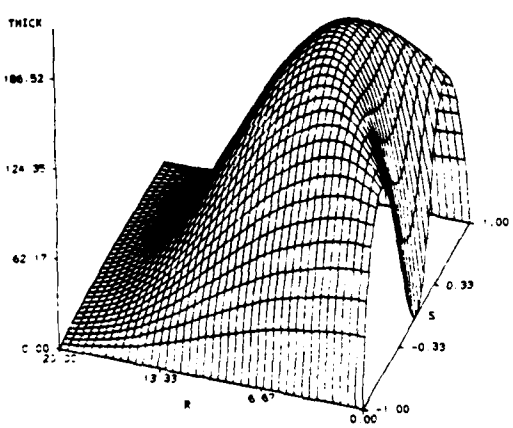

BASE RESULTS

CASE 2

E = 0 AND LINEAR H

PLATE 2

PLOT OF JET VELOCITY U1

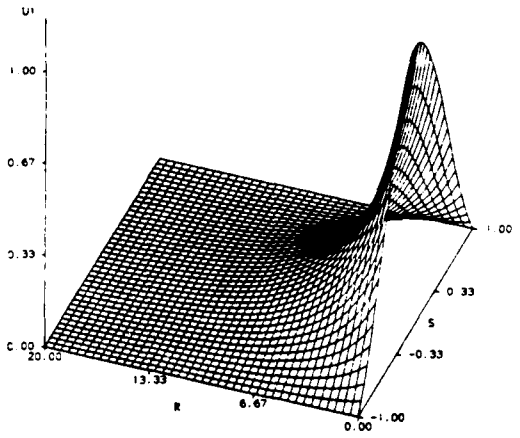

PLOT OF SEDIMENT CONCENTRATION C1

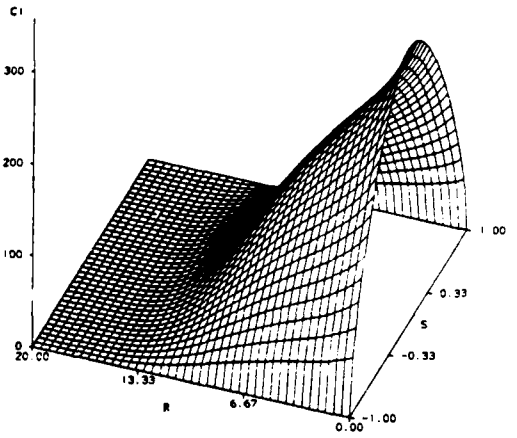

PLOT OF SEDIMENT THICKNESS

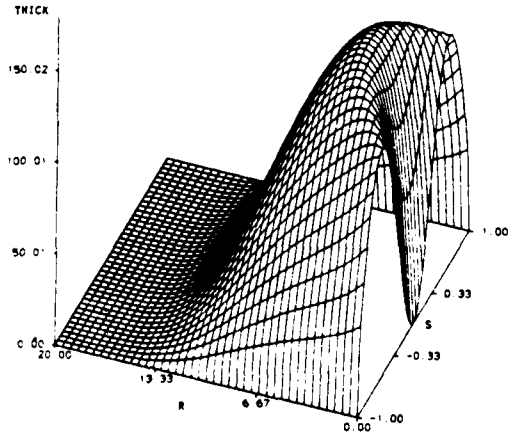

BASE RESULTS

CASE 3

E/= 0 AND H = 1

PLATE 3

PLOT OF JET VELOCITY U1

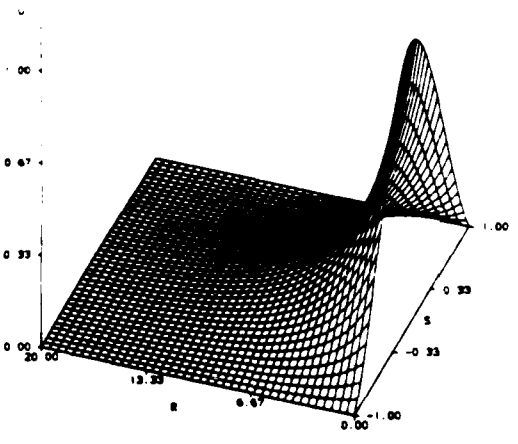

PLOT OF SEDIMENT CONCENTRATION C1

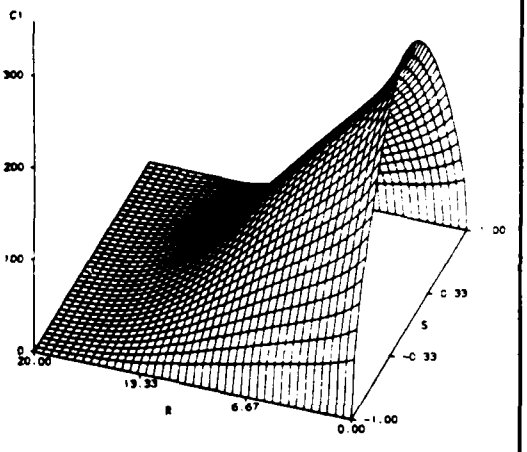

PLOT OF SEDIMENT THICKNESS

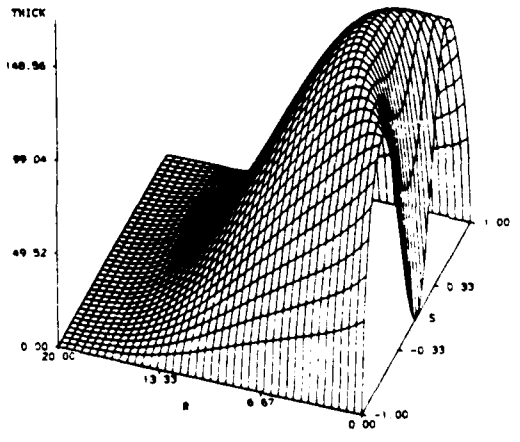

BASE RESULTS

CASE 4

E/= 0 AND LINEAR H

PLATE 4

PLOT OF SEDIMENT THICKNESS

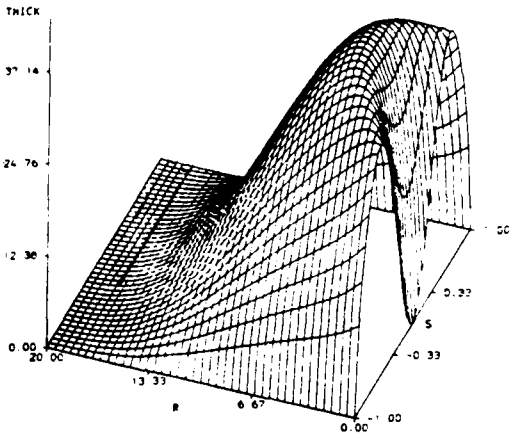

PLOT OF SEDIMENT THICKNESS

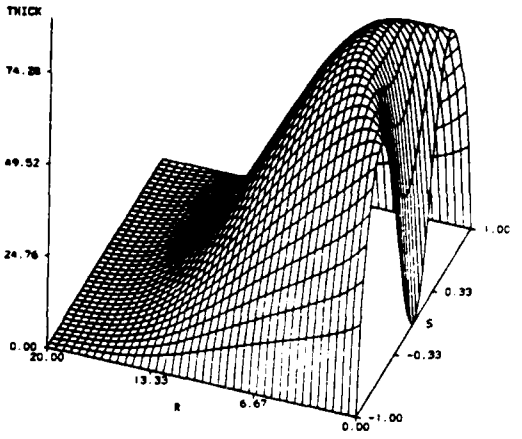

PLOT OF SEDIMENT THICKNESS

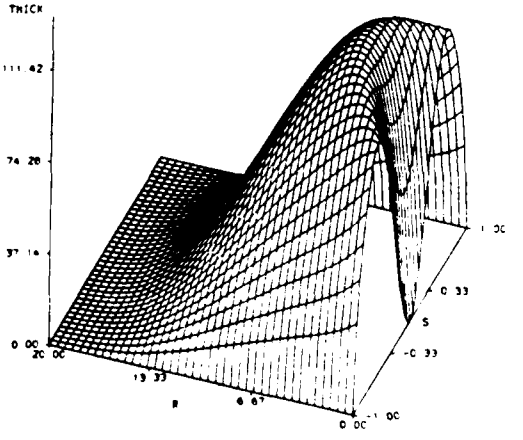

BASE RESULTS

CASE 4

SEDIMENT THICKNESS
T = 0.5, 1.0, 1.5 YEARS

PLATE 5

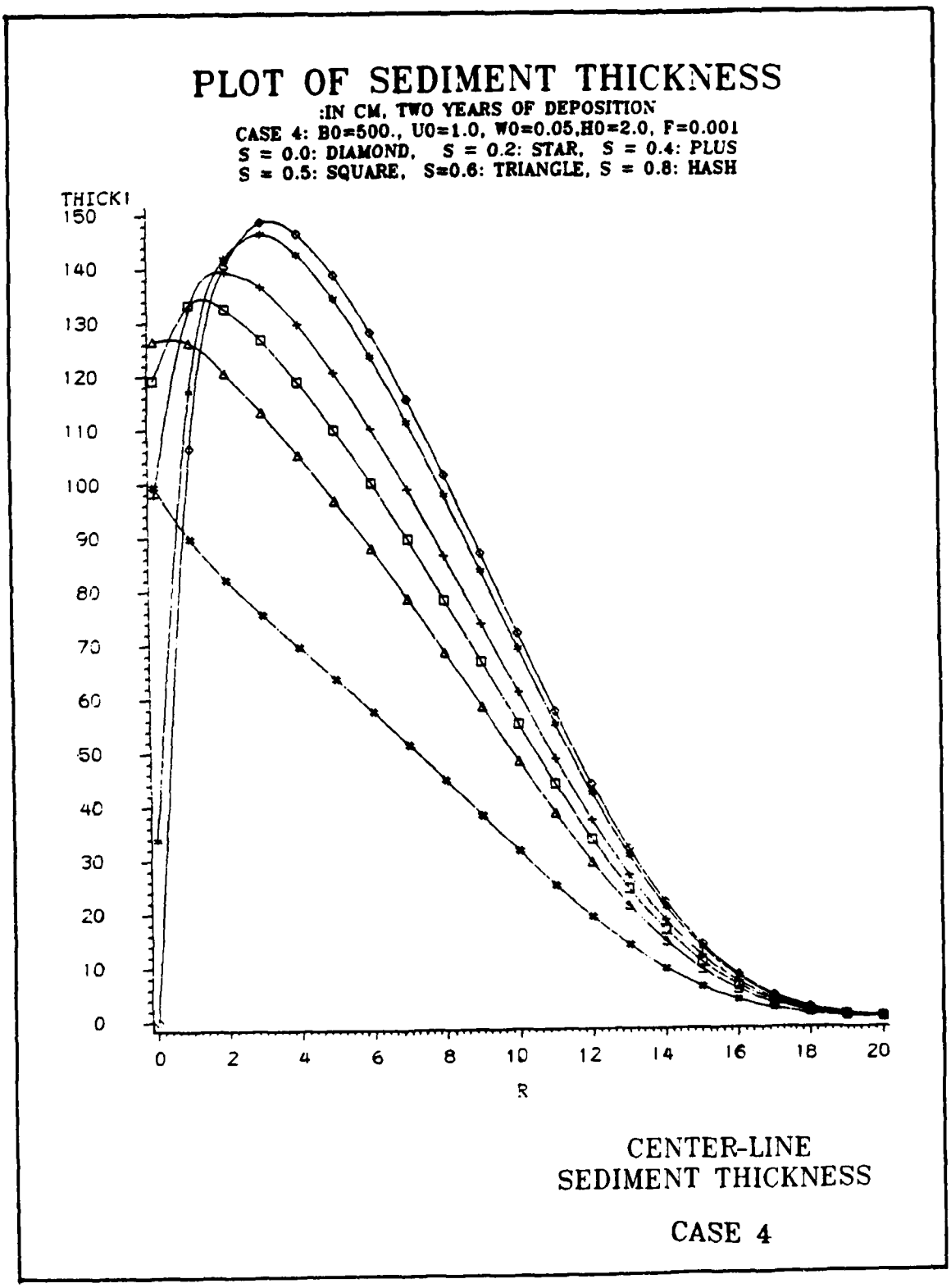
PLOT OF SEDIMENT THICKNESS
:IN CM, TWO YEARS OF DEPOSITION
CASE 4: B0=500., U0=1.0, W0=0.05,H0=2.0, F=0.001
S = 0.0: DIAMOND, S = 0.2: STAR, S = 0.4: PLUS
S = 0.5: SQUARE, S=0.6: TRIANGLE, S = 0.8: HASH
THICK!
150
140
130
120
110
100
90
80
70
60
50
40
30
20
10
0
0
2
4
6
8
10
12
14
16
18
20
R
CENTER-LINE
SEDIMENT THICKNESS
CASE 4

PLATE 6

PLOT OF SEDIMENT THICKNESS

IN CM

CASE 4 E = 0 AND LINEAR H
BASE RESULTS EXCEP H0 = 0.5 M
TWO YEARS OF DEPOSIT

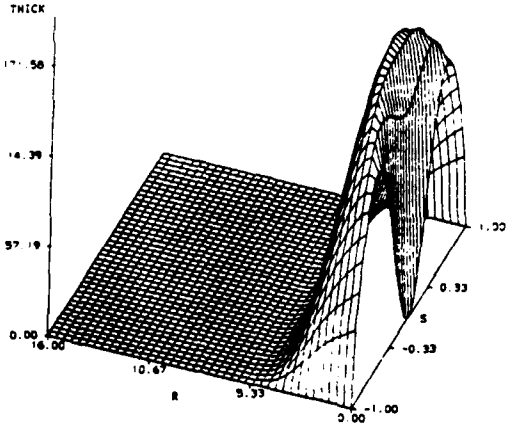

PLOT OF SEDIMENT THICKNESS

IN CM

CASE 4 E = 0 AND LINEAR H
BASE RESULTS EXCEP H0 = 1.0 M
TWO YEARS OF DEPOSIT

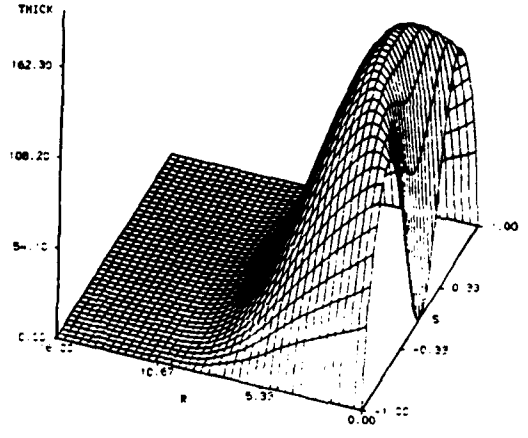

PLOT OF SEDIMENT THICKNESS

IN CM

CASE 4 E = 0 AND LINEAR H
BASE RESULTS EXCEP H0 = 1.5 M
TWO YEARS OF DEPOSIT

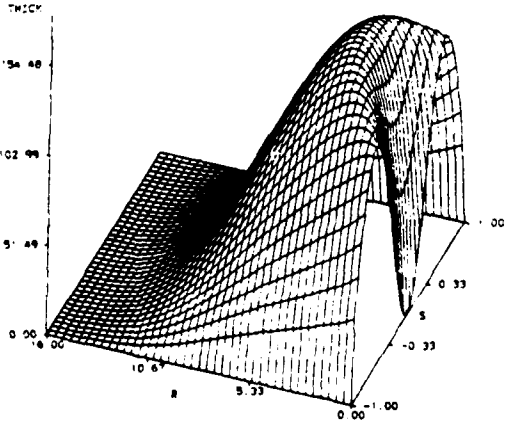

SEDIMENT THICKNESS

CASE 4

VARIED WATER DEPTH AT OUTLET

TWO YEARS OF DEPOSIT

PLATE 7

PLOT OF DIMENSIONAL JET WIDTH B

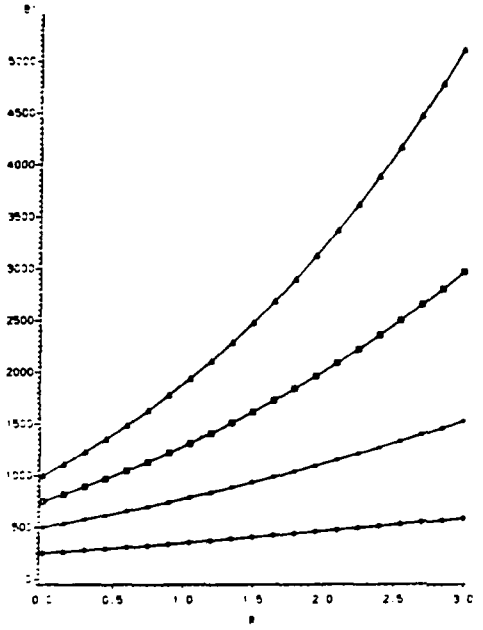

PLOT OF DIMENSIONAL JET VELOCITY U

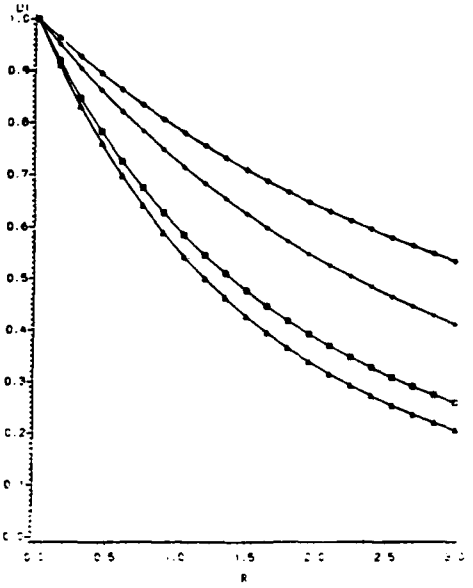

PLOT OF DIMENSIONAL SEDIMENT CONC. C

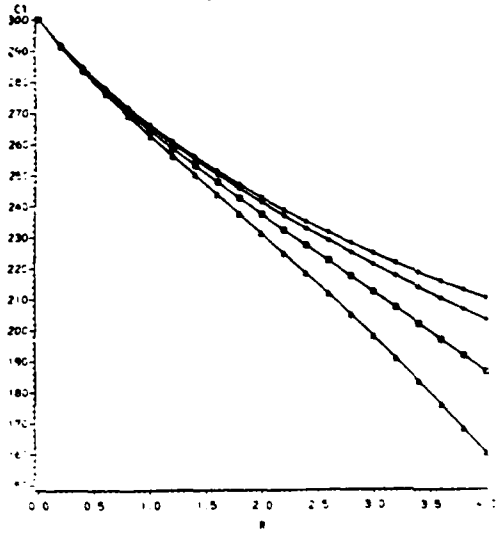

CENTER-LINE VALUES

JET WIDTH

VELOCITY

SEDIMENT CONCENTRATION

CASE 4

VARIED JET HALF-WIDTH AT OUTLET

PLATE 8

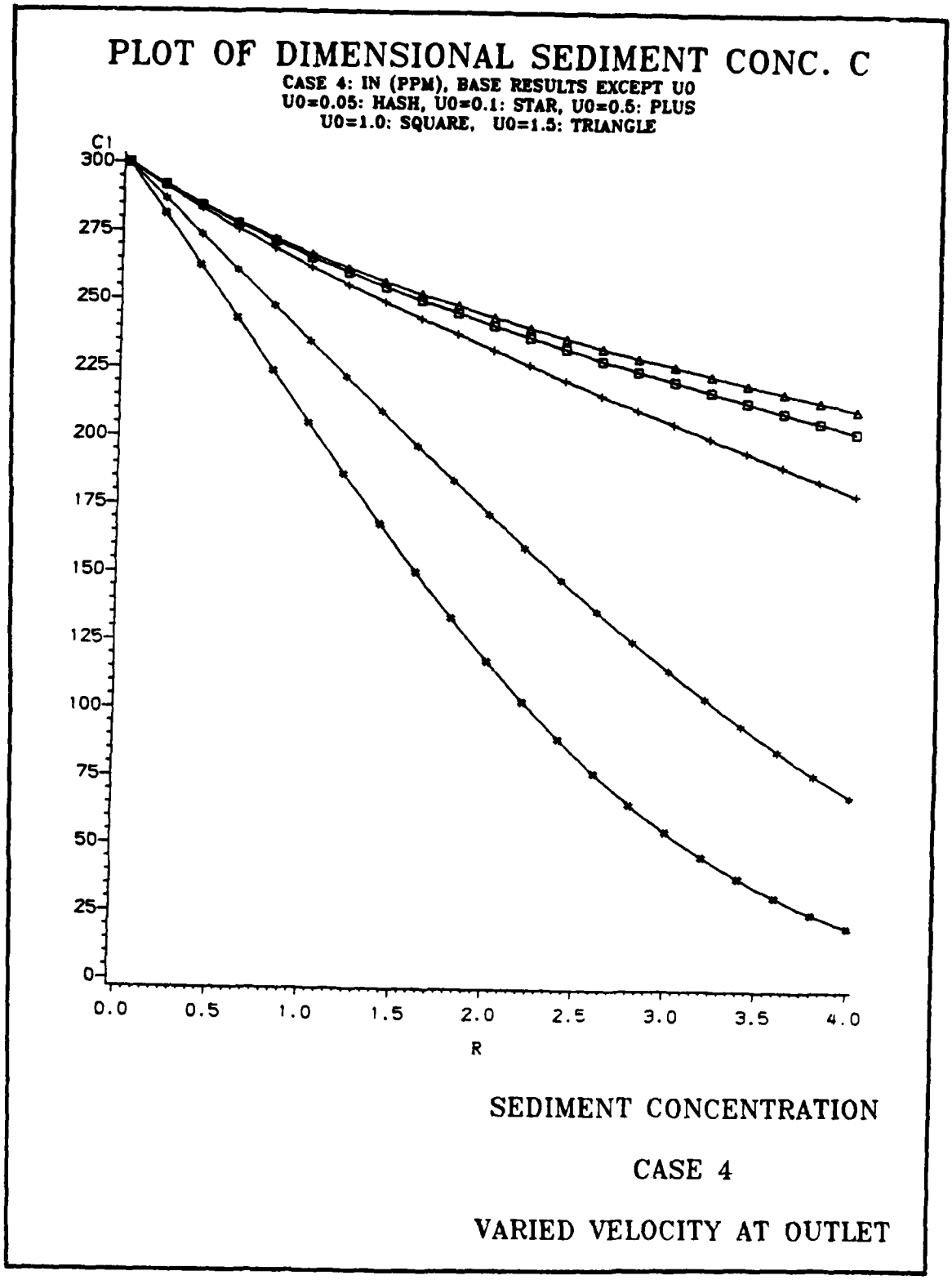
PLOT OF DIMENSIONAL SEDIMENT CONC. C
CASE 4: IN (PPM), BASE RESULTS EXCEPT U0
U0=0.05: HASH, U0=0.1: STAR, U0=0.5: PLUS
U0=1.0: SQUARE, U0=1.5: TRIANGLE
C1
300
275
250
225
200
175
150
125
100
75
50
25
0
0.0
0.5
1.0
1.5
2.0
2.5
3.0
3.5
4.0
R
SEDIMENT CONCENTRATION
CASE 4
VARIED VELOCITY AT OUTLET

PLATE 9

PLOT OF SEDIMENT THICKNESS

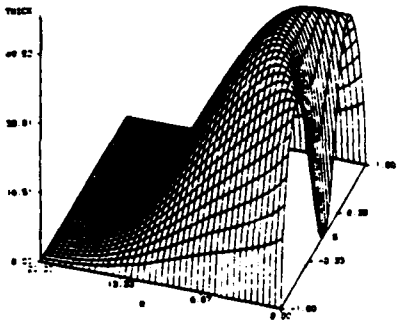

PLOT OF SEDIMENT THICKNESS

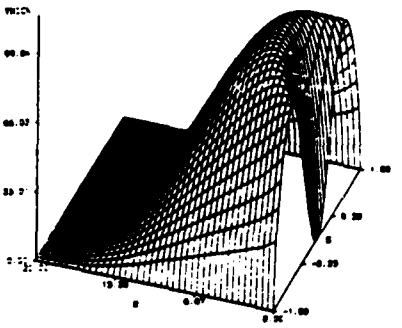

PLOT OF SEDIMENT THICKNESS

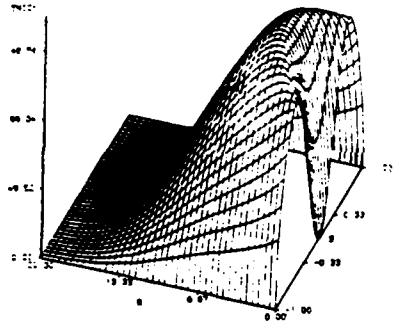

PLOT OF SEDIMENT THICKNESS

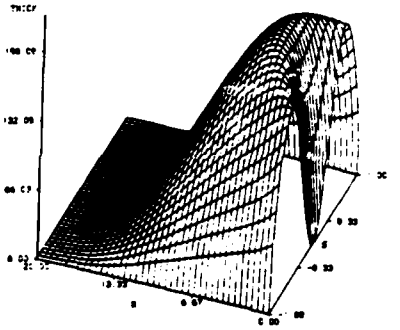

PLOT OF SEDIMENT THICKNESS

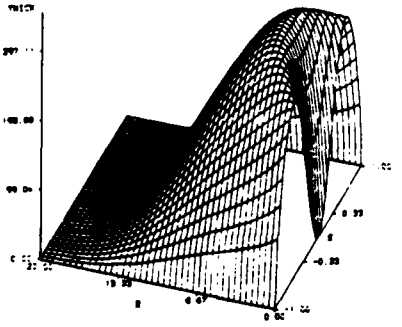

SEDIMENT THICKNESS

CASE 4

VARIED SEDIMENT CONCENTRATION AT OUTLET

100 TO 600 PPM

PLATE 10

PLOT OF DIMENSIONAL SEDIMENT CONC. C

CASE 4: IN (PPM), BASE RESULTS EXCEPT W0
W0=0.01E-3:HASH,W0=0.05E-3:STAR,W0=0.1E-3:PLUS
W0=0.5E-3: SQUARE, W0=1.0E-3: TRIANGLE

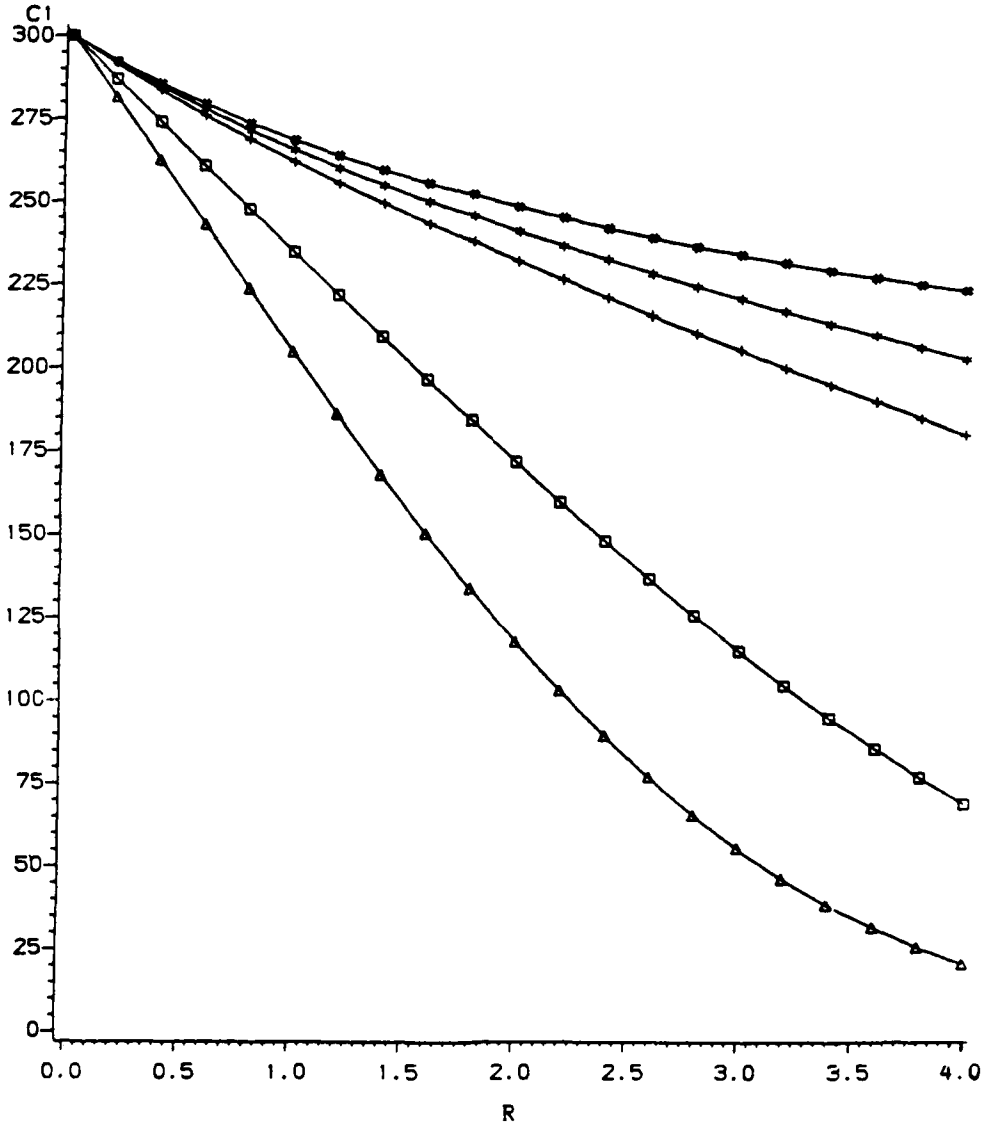

CENTER-LINE SEDIMENT CONCENTRATION

CASE 4

VARIED SEDIMENT SETTLING VELOCITY AT OUTLET

PLATE 11

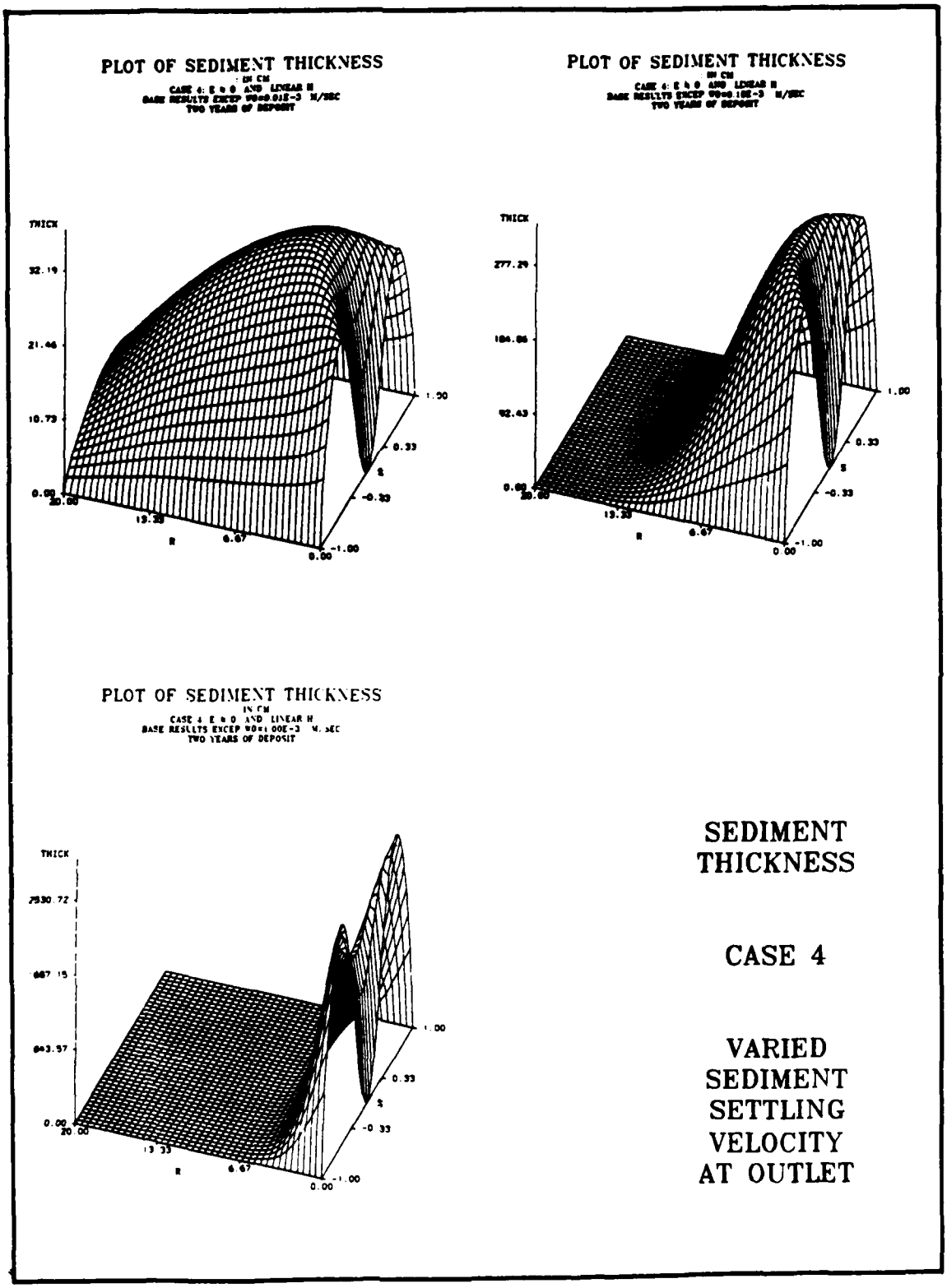
PLOT OF SEDIMENT THICKNESS
IN CM
CASE 4: E & D AND LINEAR H
BASE RESULTS EXCEP WS=0.01E-3 M/SEC
TWO YEARS OF DEPOSIT
THICK
32.19
21.46
10.73
0.00
20.00
13.33
6.67
0.00
R
1.00
0.33
-0.33
-1.00
S
PLOT OF SEDIMENT THICKNESS
IN CM
CASE 4: E & D AND LINEAR H
BASE RESULTS EXCEP WS=0.10E-3 M/SEC
TWO YEARS OF DEPOSIT
THICK
277.29
184.86
92.43
0.00
20.00
13.33
6.67
0.00
R
1.00
0.33
-0.33
-1.00
S
PLOT OF SEDIMENT THICKNESS
IN CM
CASE 4: E & D AND LINEAR H
BASE RESULTS EXCEP WS=1.00E-3 M/SEC
TWO YEARS OF DEPOSIT
THICK
2530.72
1687.15
843.57
0.00
20.00
13.33
6.67
0.00
R
1.00
0.33
-0.33
-1.00
S
SEDIMENT THICKNESS
CASE 4
VARIED SEDIMENT SETTLING VELOCITY AT OUTLET

PLATE 12

PLOT OF DIMENSIONAL JET WIDTH B

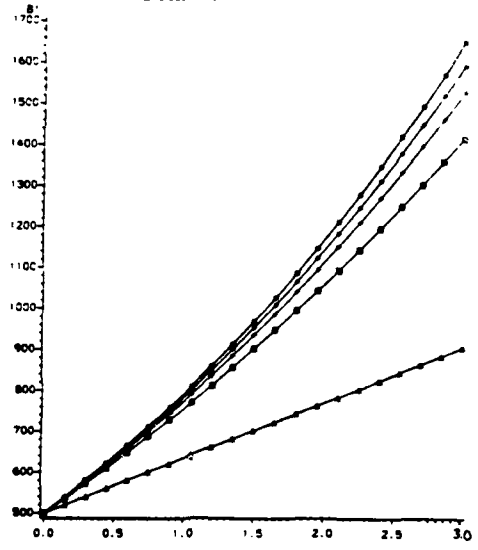

PLOT OF DIMENSIONAL JET VELOCITY U

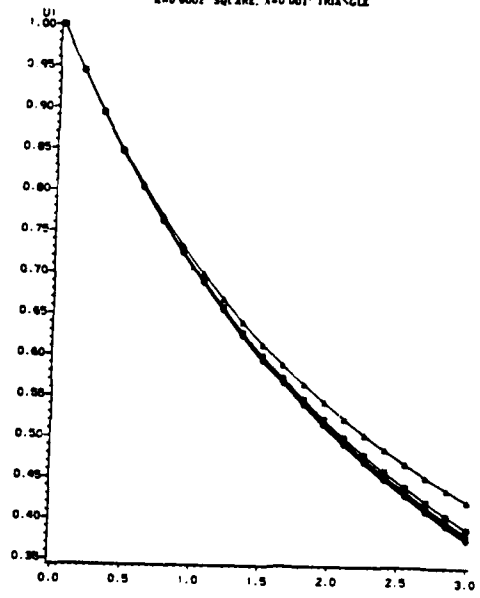

PLOT OF DIMENSIONAL SEDIMENT CONC. C

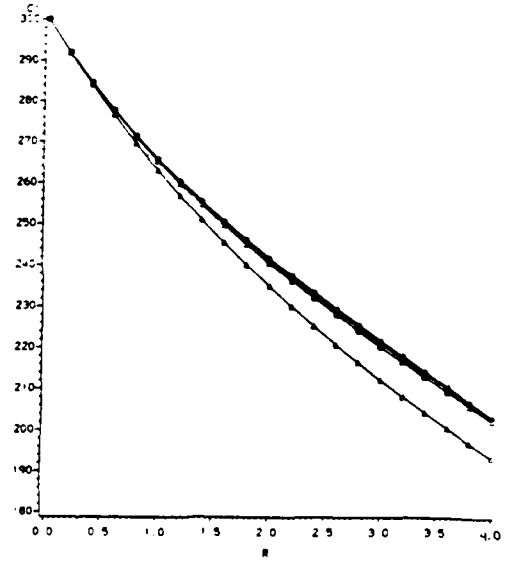

JET WIDTH

CENTER-LINE VELOCITY

CENTER-LINE SEDIMENT CONCENTRATION

CASE 4

VARYING BOTTOM SLOPE

PLATE 13

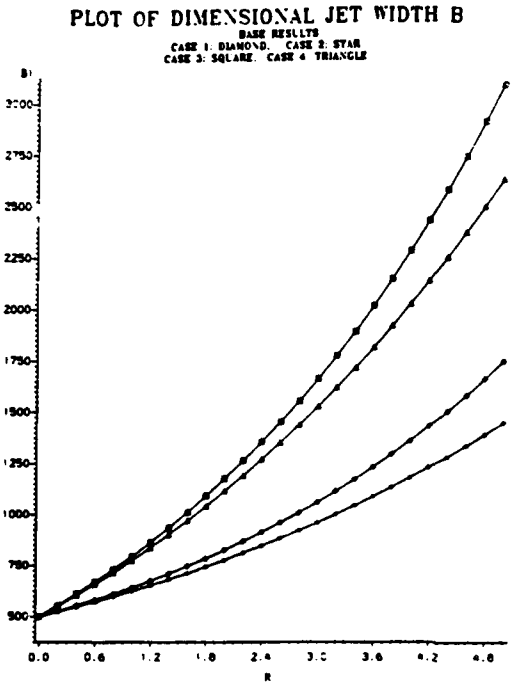

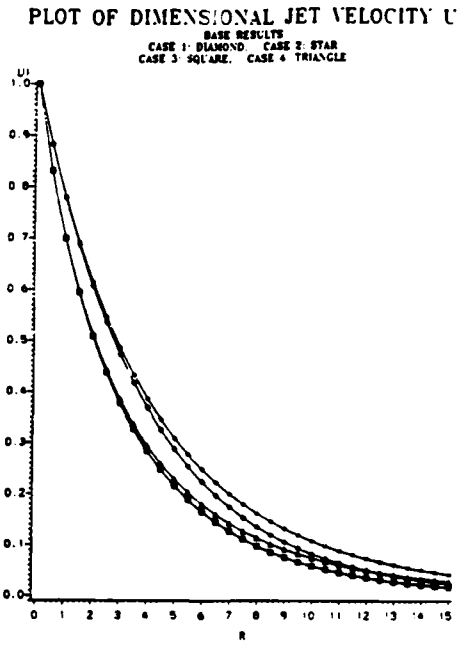

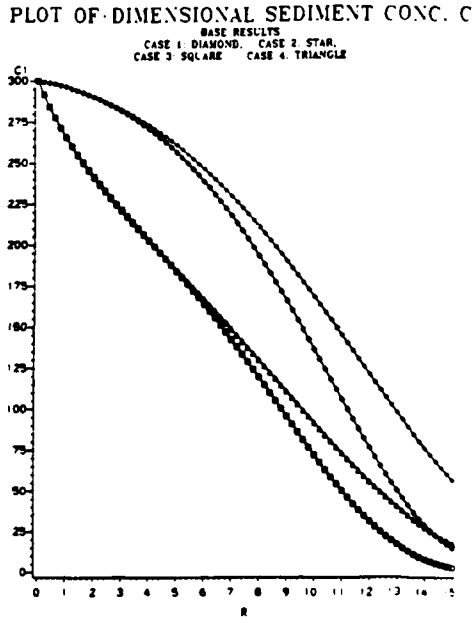

JET WIDTH

CENTER-LINE VELOCITY

CENTER-LINE SEDIMENT CONCENTRATION

CASES 1, 2, 3, AND 4

PLATE 14

PLOT OF DIMENSIONAL JET WIDTH B

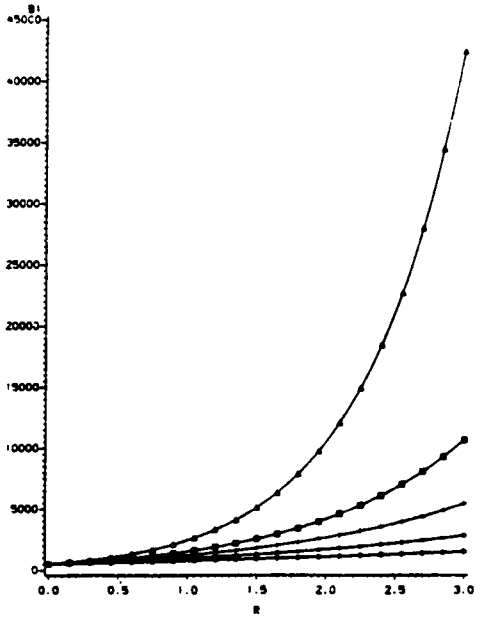

PLOT OF DIMENSIONAL JET VELOCITY U

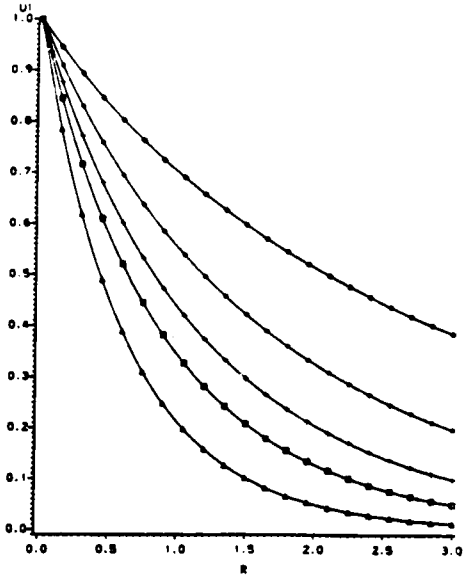

PLOT OF DIMENSIONAL SEDIMENT CONC. C

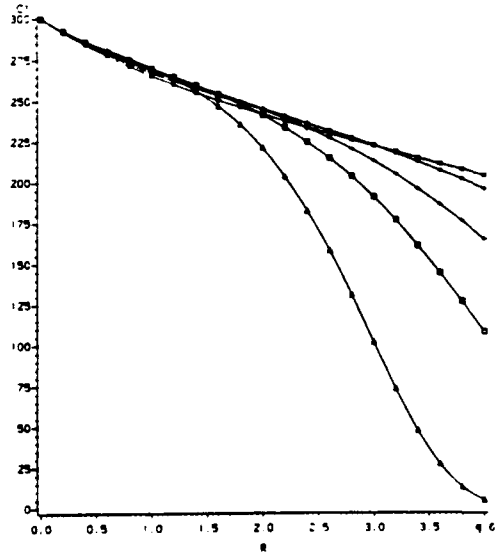

JET WIDTH

CENTER-LINE VELOCITY

CENTER-LINE SEDIMENT CONCENTRATION

CASE 4

VARYING BOTTOM FRICTION

PLATE 15

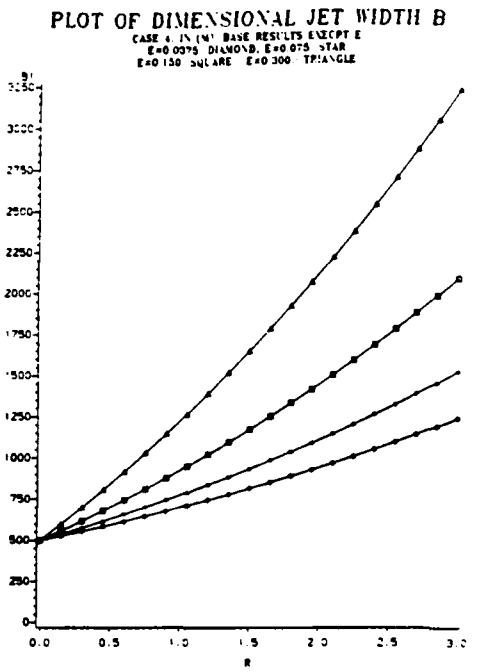

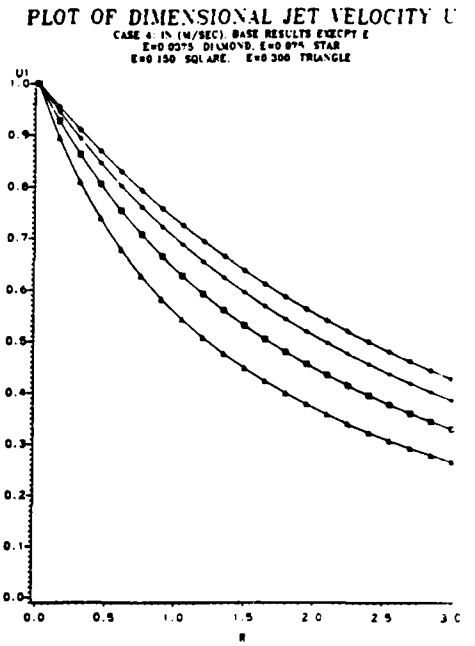

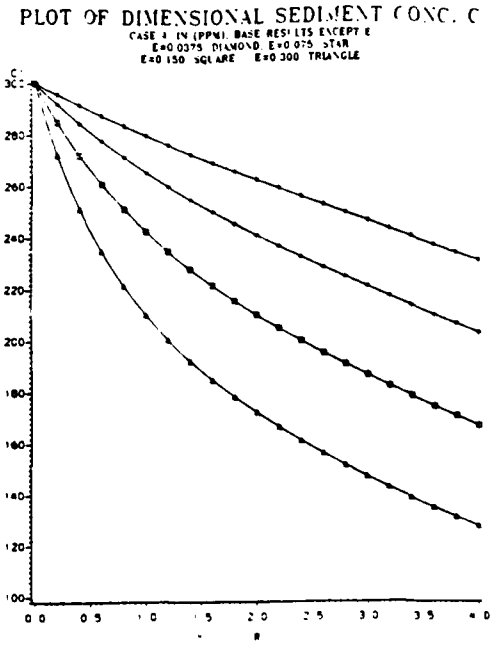

JET WIDTH

CENTER-LINE VELOCITY

CENTER-LINE SEDIMENT CONCENTRATION

CASE 4

VARYING DEGREES OF ENTRAINMENT

PLATE 16

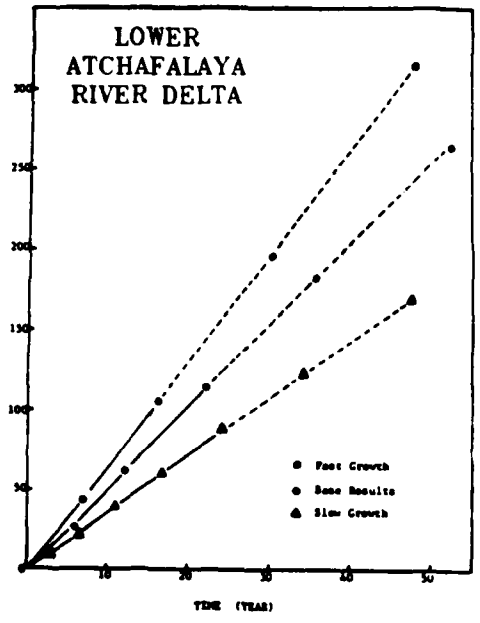

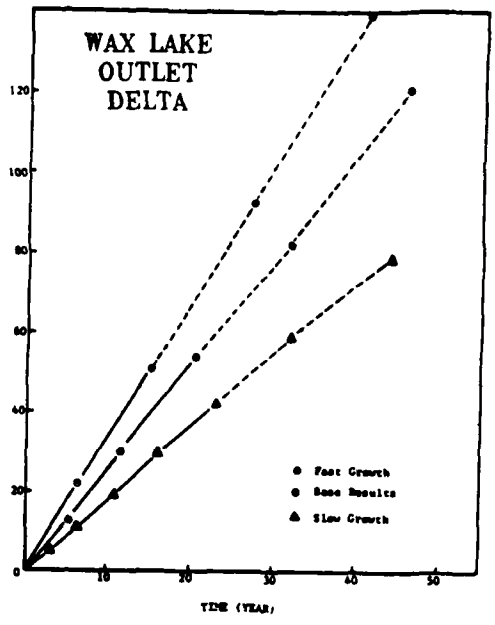

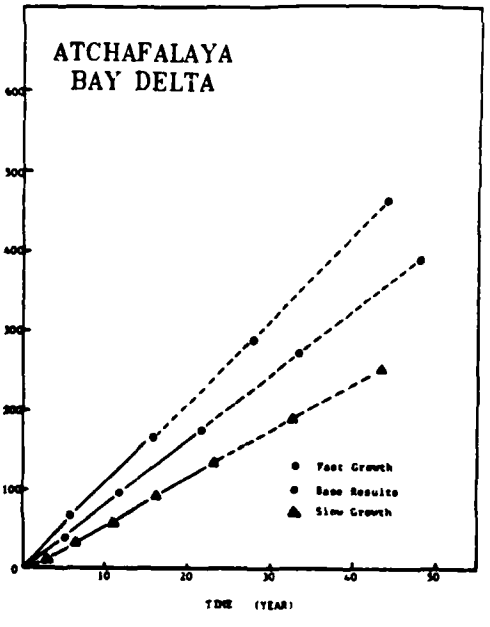

CUMULATIVE
SUBAERIAL
SEDIMENT

PLATE 17

APPENDIX A: GAUSSIAN QUADRATURE NUMERICAL INTEGRATION

1. To evaluate the integral of a function, f(x), over a finite interval (-1,1), Gaussian quadrature numerical integration (Beyer 1978)* is used. The Gaussian quadrature formula has the form

$$\int_{-1}^{1} f(x)dx = \sum_{i=i}^{n} [H_i f(x_i)] \qquad \text{(A1)}$$

where H_i are the weights; the abscissas, x_i, occur in pairs symmetrically placed with respect to the origin.

2. For an eight-point numerical integration (n = 8), the values for x_i and H_i are given as follows:

x_i	H_i
± 0.9602899	0.1012285
± 0.7966665	0.2223810
± 0.5255324	0.3137066
± 0.1834346	0.3626838

3. A simple FORTRAN coding for the Gaussian quadrature formula is listed in Table A1. The values of the following integrals, cited in PART V, are found:

$$\int_{-1}^{1} (1 - s^2) \exp(-s^2)\, ds = 1.1147022$$

$$\int_{-1}^{1} (1 - s^2)^{\frac{3}{2}} \exp\left(-\frac{3}{2}s^2\right) ds = 0.9494728$$

$$\int_{-1}^{1} (1 - s^2)^{\frac{1}{2}} \exp\left(-\frac{1}{2}s^2\right) ds = 1.3974447$$

$$\int_{-1}^{1} (1 - s^2)^{\frac{5}{2}} \exp\left(-\frac{5}{2}s^2\right) ds = 0.7597358$$

*References cited in the appendices are included with those for the main body of the report, starting on page 113.

Table A1

Computer Source Program of Gaussian Quadrature

Eight-Point Numerical Integration

```
GAUSSIAN QUADRATURE EIGHT POINT NUMERICAL INTEGRATION
REFERENCE:  BEYER, W.H., 1978.  "HANDBOOK OF MATHEMATICAL
            SCIENCE", 5TH EDITION, CRC PRESS.

GAUSSIAN QUADRATURE FORMULA:

    WHERE X = ABSCISSAS AND H = WEIGHTS

      DIMENSION X(8),H(8),X1(8),H1(8)
      DATA F1,F2,F3,F4/4*0.0/
      REAL*8 X1/0.9602899,0.7966665,0.5255324,0.1834346,
      -0.1834346,-0.5255342,-0.7966665,-0.9602899/,
      H1/0.1012285,0.2223810,0.3137066,0.3626838,
      0.3626838,0.3137066,0.2223810,0.1012285/
      DO 9 I=1,8
        X(I)=X1(I)
    9   H(I)=H1(I)
      WRITE(6,1)
    1 FORMAT(5X,'THE FOLLOWING INTEGRALS ARE COMPUTED:')
      DO 11 I=1,8
   11  F1=F1+H(I)*(1.-X(I)*X(I))*EXP(-X(I)*X(I))
      WRITE(6,10)F1
      DO 12 I=1,8
   12   F2=F2+H(I)*(1.-X(I)*X(I))**1.5*EXP(-1.5*X(I)*X(I))
      WRITE(6,20)F2
      DO 13 I=1,8
   13   F3=F3+H(I)*(1.-X(I)*X(I))**0.5*EXP(-0.5*X(I)*X(I))
      WRITE(6,30)F3
      DO 14 I=1,8
   14   F4=F4+H(I)*(1.-X(I)*X(I))**2.5*EXP(-2.5*X(I)*X(I))
      WRITE(6,40)F4
      STOP
   10 FORMAT(10X,'I(1)   =',F10.7)
   20 FORMAT(10X,'I(3/2) =',F10.7)
   30 FORMAT(10X,'I(1/2) =',F10.7)
   40 FORMAT(10X,'I(5/2) =',F10.7)
      END

THE FOLLOWING INTEGRALS ARE COMPUTED:
      I(1)   = 1.1147020
      I(3/2) = 0.9494730
      I(1/2) = 1.3974440
      I(5/2) = 0.7597359
```

APPENDIX B: SOLUTION FOR BERNOULLI-TYPE EQUATIONS

1. This appendix shows the procedure for reducing a Bernoulli-type equation into a linear first-order differential equation. Bernoulli-type equations have the form

$$\frac{dy}{dx} + p(x)y = q(x)y^n \tag{B1}$$

This basic equation is modified by setting

$$z = y^{1-n} \tag{B2a}$$

which transforms into the equation

$$y = z^{\frac{1}{1-n}} \tag{B2b}$$

The first term of Equation B1 can then be expressed as

$$\frac{dy}{dx} = \frac{dy}{dz}\frac{dz}{dx} = \frac{1}{1-n} z^{\frac{n}{1-n}} \frac{dz}{dx} \tag{B3}$$

Substituting Equations B2a and B3 into Equation B1 and simplifying, we have

$$\frac{dz}{dx} + (1 - n)p(x)z = (1 - n)q(x) \tag{B4a}$$

or

$$\frac{dz}{dx} + P(x)z = Q(x) \tag{B4b}$$

2. Equation B4b is the general form of a linear first-order differential equation. By the method of integrating factors (Wylie 1951), the general solution of Equation B4b is

$$z = \frac{1}{\mu}\left[\int \mu Q(x)dx + C\right] \tag{B5}$$

where

$$\mu = \text{integrating factor} = \exp\int P(x)dx \tag{B6}$$

and

$$C = \text{constant of integration}$$

3. Finally, using the relationship of Equation B2b, the standard solution for the Bernoulli-type equation is obtained:

$$y = z^{\frac{1}{1-n}}$$

$$y = \left\{\left[\exp\int P(x)dx\right]^{-1}\left[\exp\int P(x)dx\, Q(x)dx + C\right]\right\}^{\frac{1}{1-n}} \tag{B7}$$

where

$$P(x) = (1 - n)p(x) \tag{B8a}$$

$$Q(x) = (1 - n)q(x) \tag{B8b}$$

The Solution of Equation 53 in PART V

In PART V, Equation 53 is a Bernoulli-type ordinary differential equation:

$$\frac{dU}{dr} + FU = - A \exp(Fr)\, U^3 \tag{B9}$$

The solution of the above equation can be obtained by equating

$$y \equiv U$$

$$x \equiv r$$

$$n = 3$$

$$P(x) = (1 - n)p(x) = -2F \tag{B10a}$$

$$Q(x) = (1 - n)q(x) = 2A \exp(Fr) \tag{B10b}$$

and computing the integrating factor

$$\mu = \exp \int P(x)dx \tag{B11a}$$

$$= \exp \int -2Fdr \tag{B11b}$$

$$= \exp(-2Fr) \tag{B11c}$$

Thus

$$U = \{\exp(2Fr)\,[-\frac{2A}{F} \exp(-Fr) + C]\}^{-\frac{1}{2}} \tag{B12}$$

Utilizing the initial condition

$$U|_{r=0} = 1 = -\frac{2A}{F} + C \tag{B13}$$

we obtain

$$C = 1 + \frac{2A}{F} \tag{B14}$$

Finally, the solution of the Bernoulli equation is

$$U = \{\exp(2Fr)[-\frac{2A}{F} \exp(-Fr) + 1 + \frac{2A}{F}]\}^{-\frac{1}{2}} \tag{B15}$$

or

$$U = \left[-\frac{2A}{F}\exp(Fr) + \left(1 + \frac{2A}{F}\right)\exp(2Fr)\right]^{-\frac{1}{2}} \tag{B16}$$

This is the jet velocity in nondimensional form for the case of constant depth. It is cited as Equation 54 in PART V.

The Solution of Equation 72 in PART V

Equation 72, appearing in PART V, is also a Bernoulli-type ordinary differential equation:

$$\frac{d(HU)}{dr} + a\frac{b_0}{h_0}(D - 1)H^{-1}(HU) = -AH^{D-1}(HU)^3 \tag{B17}$$

The solution is obtained as in the previous example, using

$$y \equiv HU$$

$$x \equiv r$$

$$n = 3$$

$$P(x) = (1 - n)p(x) = -2a\frac{b_0}{h_0}(D - 1)H^{-1} \tag{B18a}$$

$$Q(x) = (1 - n)q(x) = 2AH^{D-1} \tag{B18b}$$

The integrating factor is computed as

$$\mu = \exp\int P(x)dx \tag{B19a}$$

$$= \exp\int -2a\frac{b_0}{h_0}(D - 1)H^{-1}dr \tag{B19b}$$

Note that

$$H = 1 + a\frac{b_0}{h_0}r$$

and

$$dH = a\frac{b_0}{h_0}dr$$

Thus

$$\mu = \exp\int -2(D - 1)\frac{dH}{H} = H^{-2(D-1)} \tag{B20}$$

and

$$HU = [H^{2(D-1)}(\frac{2A}{2 - D}\frac{h_0}{ab_0}H^{2-D} + C)]^{-\frac{1}{2}} \tag{B21}$$

Utilizing the initial conditions

$$HU|_{r=0} = 1 = \frac{2A}{2 - D}\frac{h_0}{ab_0} + C \tag{B22}$$

the constant of integration is found to be

$$C = 1 - \frac{2A}{2 - D}\frac{h_0}{ab_0} \tag{B23}$$

The final solution of this Bernoulli equation is

$$HU = [H^{2(D-1)}(\frac{2A}{2 - D}\frac{h_0}{ab_0}H^{2-D} + 1 - \frac{2A}{2 - D}\frac{h_0}{ab_0})]^{-\frac{1}{2}} \tag{B24}$$

or

$$HU = (2A)^{-\frac{1}{2}}H^{1-D}[\frac{h_0}{ab_0}\frac{1}{2 - D}(H^{2-D} - 1) + \frac{1}{2A}]^{-\frac{1}{2}} \tag{B25}$$

The above equation appears as Equation 73 in PART V.

APPENDIX C: COMPUTER GRAPHICS

1. Behavior of variables used in the system of equations employed to describe sedimentation patterns in Atchafalaya Bay is illustrated in the report by the use of Statistical Analysis System plotting subroutines (SAS/GRAPH 1981). Two-dimensional plots are used to display changes in jet center-line values of selected variables as distance from the outlet increases; three-dimensional plots are used to depict values of the variables over the entire jet.

2. The GPLOT procedure, a subprogram of SAS/GRAPH, was used to produce the majority of the two-dimensional plots. Variables, entered as x and y coordinate pairs, are plotted exactly; the plotting routine includes an interpolation feature (SPLINE) that produces a smooth curve fit to the data values.

3. A second SAS/GRAPH subprogram, the G3D procedure, plots the values of three variables and generates a three-dimensional surface. The three variables used to illustrate deposition patterns are jet velocity, sediment concentration, and sediment thickness. Each of these variables is plotted versus normalized longitudinal (r) and lateral (s) coordinates by the program, which again interpolates to produce a smooth surface fit to the input data.

Computer Program C1

4. This computer program contains plotting instructions for the generation of a two-dimensional center-line sediment thickness profile using the GPLOT procedure. The data used to create the plot were taken from the Case 4 conditions for delta development ($E \neq 0$ and linear H), after two years of deposit, with varying sediment concentrations. Predicted sediment thickness at forty equidistant locations along the center line of the jet was entered with corresponding longitudinal distance from the outlet; data points are indicated on the plot by designated symbols representing different sediment concentrations. The resulting plot is shown in Figure C1.

COMPUTER PROGRAM C1

```
//STEP1  EXEC SAS
//SYSIN DD *
 DATA ONE;
 U0=1;  W0=0.05E-3; F=0.001; B0=500;
 H0=2.0; A=0.0001; AI1=0.948; AI2=1.397; AI3=0.76;
 TIME=2.0*365.*86400.; DS=0.4;
 ARRAY ROOT (I) ROOT1 - ROOT11;
 ARRAY WT (I) WT1 - WT11;
    ROOT1=0.00533697; ROOT2=0.04735263; ROOT3=0.12782106;
    ROOT4=0.23991861; ROOT5=0.37413950; ROOT6=0.51910186;
    ROOT7=0.66251286; ROOT8=0.79221088; ROOT9=0.89719596;
    ROOT10=0.96855602; ROOT11=1.00000000;
    WT1=0.29169804; WT2=0.28548098; WT3=0.27317938;
    WT4=0.25505539; WT5=0.23149529; WT6=0.20300115;
    WT7=0.17018012; WT8=0.13373121; WT9=0.09442893;
    WT10=0.05309150; WT11=0.00865801;
 UCR = U0;
 D = F/A;
 W = B0*W0/U0/H0;
 D = F/A; E=0.075;
 AA = 1.794*E;
 ARRAY C0(I) C01 - C05;
 C01=100.; C02=200.; C03=300.; C04=400.; C05=600.;
 ARRAY CA(I) CA1 - CA5;
 ARRAY CD(I) CD1 - CD5;
 ARRAY UD(I) UD1 - UD5;
 ARRAY H (I) H1 - H11;
 ARRAY CFU (I) CFU1 - CFU11;
 ARRAY U (I) U1 - U11;
 ARRAY SA (I) SA1 - SA11;
 ARRAY SB (I) SB1 - SB11;
     DO R = 0.0 TO 20.0 BY 0.50;
 HH = 1. + A*B0/H0*R;
 CF =  H0/A/B0/(2.-D)*(HH**(2.-D) - 1.) + 0.5/AA;
 UU = 1./SQRT(2.*AA) /HH**D / SQRT(CF);
 BB = 2.*AA*HH**(D-1) * CF;
 DO OVER ROOT; H = 1. + A*B0/H0*R*SQRT(ROOT); END;
 DO OVER H; CFU= H0/A/B0/(2.-D)*(H**(2.-D) - 1.) + 0.5/AA; END;
     DO I = 1 TO 11;
 U =1./SQRT( 2.*AA) / H**D/SQRT(CFU);
     END;
 G1= -AI2*W/AI1*R/2.;
 G2= AI3*W/AI1/1.0/1.0*R/2.;
     DO I = 1 TO 11;
 SA = WT/H/U ;
 SB = WT*U/H ;
     END;
 SUM1 = SUM(OF SA1 - SA11);
 SUM2 = SUM(OF SB1 - SB11);
```

```
C = EXP( G1*SUM1 + G2*SUM2 - LOG(HH*UU*BB) );
    DO I = 1 TO 5;
CA = C0 * C;
UD=U0*UU;
CD = W0*100.*CA*1.0E-6*(1. - UD*UD/UCR/UCR)*TIME;
    END;
TA = CD1/DS;
TB = CD2/DS;
TC = CD3/DS;
TD = CD4/DS;
TE = CD5/DS;
OUTPUT;END;
PROC GPLOT; PLOT TA*R TB*R TC*R TD*R TE*R/OVERLAY;
SYMBOL1 I=SPLINE V=DIAMOND;
SYMBOL2 I=SPLINE V=TRIANGLE;
SYMBOL3 I=SPLINE V=STAR;
SYMBOL4 I=SPLINE V=PLUS;
SYMBOL5 I=SPLINE V=HASH;
TITLE1 ;
TITLE2 ;
TITLE3 .F=TRIPLEX .H=2 CENTERLINE SEDIMENT THICKNESS PROFILE;
TITLE4 .F=TRIPLEX .H=1 IN CM, TWO YEARS DEPOSIT;
TITLE5 .F=TRIPLEX .H=1 CASE 4: E ≠ 0  AND  LINEAR H;
TITLE6 .F=TRIPLEX .H=1 C0=100: DIAMOND, C0=200: TRIANGLE;
TITLE7 .F=TRIPLEX .H=1 C0=300: STAR, C0=400: PLUS, C0=600: HASH;
/*
//
```

CENTER-LINE SEDIMENT THICKNESS PROFILE

IN CM, TWO YEARS DEPOSIT
CASE 4: E ≠ 0 AND LINEAR H
C0=100: DIAMOND, C0=200: TRIANGLE
C0=300: STAR, C0=400: PLUS, C0=600: HASH

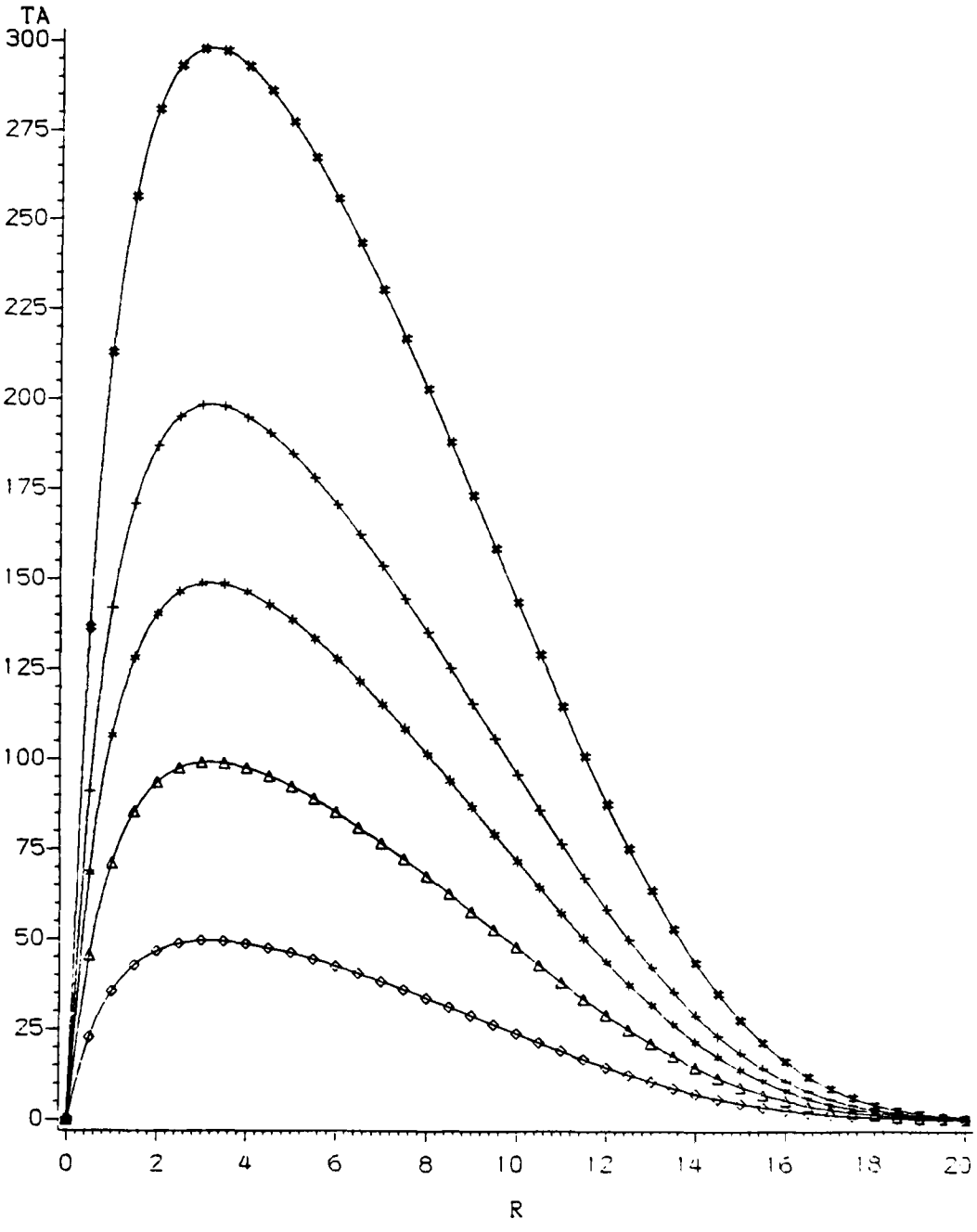

Figure C1. Plot of center-line sediment thickness profile

Computer Program C2

5. Computer program C2 contains plotting instructions for generation of a three-dimensional representation of sediment thickness using the G3D procedure; the resulting plot is shown in Figure C2. The sediment deposition pattern shown was predicted by the closed-form analytical solutions of the two-dimensional system of equations describing sedimentation for Case 4 ($E \neq 0$ and linear H) after two years of deposit. These equations are used by the G3D subroutine to produce 1651 data points for generation of the final three-dimensional plot.

COMPUTER PROGRAM C2

```
//STEP1  EXEC SAS
//SYSIN DD *
 DATA ONE;
 U0=1;  W0=0.05E-3; F=0.001; B0=500; C0=300.;
 H0=2.0; A=0.0001; AI1=0.948; AI2=1.397; AI3=0.76;
 TIME=2.0*365.*86400.; DS=0.4;
 ARRAY ROOT (I) ROOT1 - ROOT11;
 ARRAY WT (I) WT1 - WT11;
    ROOT1=0.00533697; ROOT2=0.04735263; ROOT3=0.12782106;
    ROOT4=0.23991861; ROOT5=0.37413950; ROOT6=0.51910186;
    ROOT7=0.66251286; ROOT8=0.79221088; ROOT9=0.89719596;
    ROOT10=0.96855602; ROOT11=1.00000000;
    WT1=0.29169804; WT2=0.28548098; WT3=0.27317938;
    WT4=0.25505539; WT5=0.23149529; WT6=0.20300115;
    WT7=0.17018012; WT8=0.13373121; WT9=0.09442893;
    WT10=0.05309150; WT11=0.00865801;
 UCR = U0;
 D = F/A;
 W = B0*W0/U0/H0;
 D = F/A; E=0.075;
 AA = 1.794*E;
 ARRAY H (I) H1 - H11;
 ARRAY CFU (I) CFU1 - CFU11;
 ARRAY U (I) U1 - U11;
 ARRAY SA (I) SA1 - SA11;
 ARRAY SB (I) SB1 - SB11;
     DO R = 0.0 TO 20.0 BY 0.50;
     DO S = -1 TO 1 BY 0.05;
 HH = 1. + A*B0/H0*R;
 CF =  H0/A/B0/(2.-D)*(HH**(2.-D) - 1.) + 0.5/AA;
 UU = 1./SQRT(2.*AA) /HH**D / SQRT(CF);
 BB = 2.*AA*HH**(D-1) * CF;
 DO OVER ROOT; H = 1. + A*B0/H0*R*SQRT(ROOT); END;
 DO OVER H; CFU= H0/A/B0/(2.-D)*(H**(2.-D) - 1.) + 0.5/AA; END;
     DO I = 1 TO 11;
 U =1./SQRT( 2.*AA) / H**D/SQRT(CFU);
     END;
 G1= -AI2*W/AI1*R/2.;
 G2= AI3*W/AI1/1.0/1.0*R/2.;
     DO I = 1 TO 11;
 SA = WT/H/U ;
 SB = WT*U/H ;
     END;
 SUM1 = SUM(OF SA1 - SA11);
 SUM2 = SUM(OF SB1 - SB11);
 C = EXP( G1*SUM1 + G2*SUM2 - LOG(HH*UU*BB) );
 C1 = C0*SQRT(1.-S*S)/EXP(S*S/2.)*C;
 CC1=(1. - S*S)/EXP(S*S);
 UD1=U0*CC1*UU;
 CD = W0*100.*C1*1.0E-6*(1. - UD1*UD1/UCR/UCR)*TIME;
 THICK = CD/DS;
 OUTPUT;END;END;
```

COMPUTER PROGRAM C2 (CONTINUED)

```
TITLE1 ;
TITLE2 ;
TITLE3 ;
TITLE4 ;
TITLE5 ;
TITLE6 .F=TRIPLEX .H=2 PLOT OF SEDIMENT THICKNESS;
TITLE7 .F=TRIPLEX .H=1       : IN CM;
TITLE8 .F=TRIPLEX .H=1 CASE 4: E = 0  AND  LINEAR H;
TITLE9 .F=TRIPLEX .H=1 BASE RESULTS,  2.0 YEARS DEPOSIT;
PROC G3D;
PLOT R*S=THICK;
//
```

PLOT OF SEDIMENT THICKNESS

: IN CM

CASE 4: E ≠ 0 AND LINEAR H

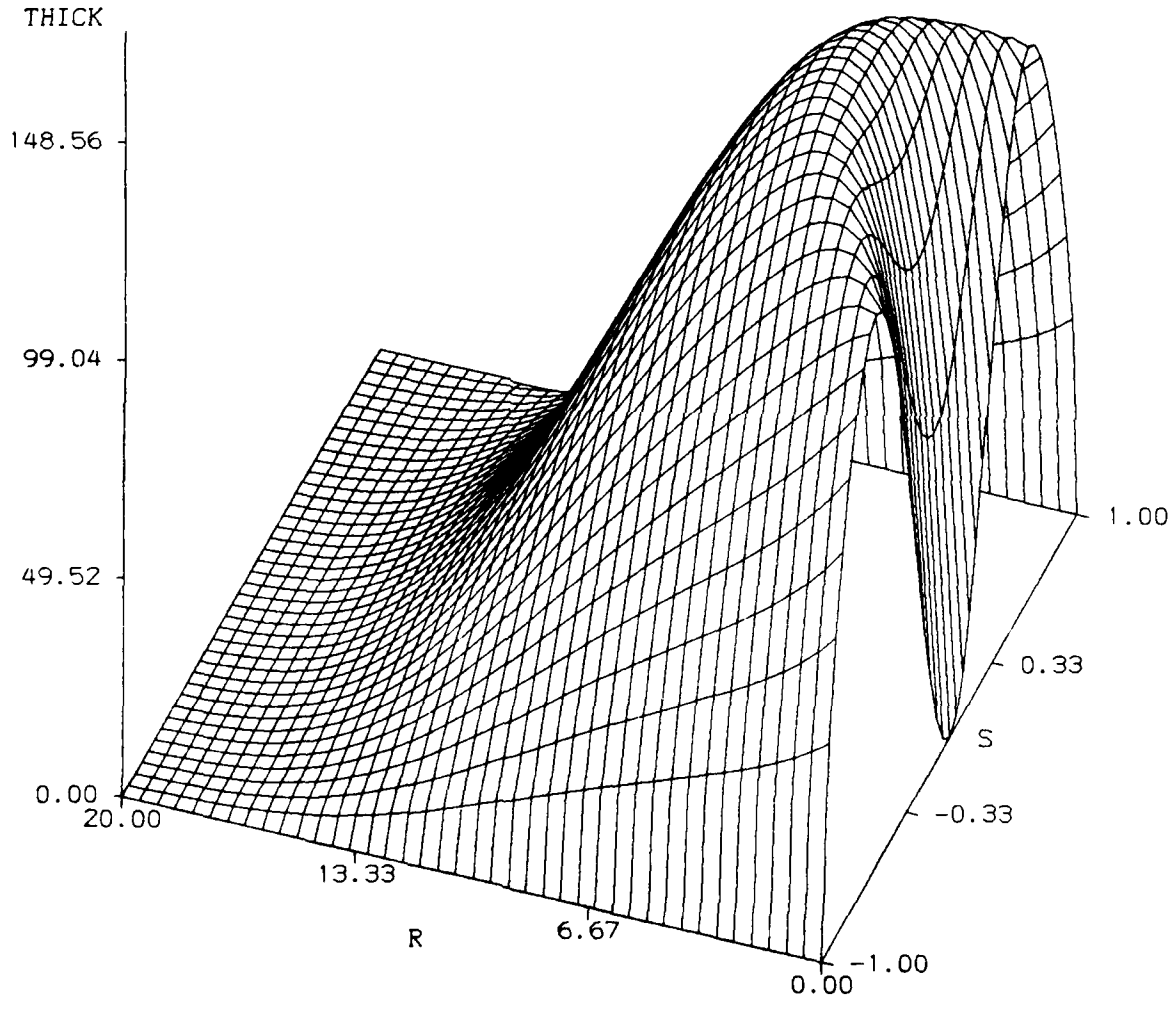

Figure C2. Plot of sediment thickness for Case 4

APPENDIX D: QUADRATURE INTEGRATION

1. Orthogonal collocation is an efficient method for solving differential equations (Villadsen and Michelson 1978). Based on this method, the profile of a dependent variable can be expressed in terms of the families of orthogonal polynomials and their derivatives at collocation points. In addition to its efficiency for solving differential equations the integration of the profile of dependent variables can be closely approximated by a quadrature formula which gives a semianalytical solution of integration.

Orthogonal Polynomial

2. The orthogonal polynomial may be of Jacobi, Legendre, or Chebycheff type of which the Jacobi polynomial is found to be the most efficient (Villadsen and Michelson 1978). The important features of orthogonal polynomials are illustrated in this appendix. The Jacobi family possesses the following orthogonal relationship:

$$\int_0^1 W(u)\, P_i^{(\alpha,\beta)}(u)\, P_j^{(\alpha,\beta)}(u)\, du = \begin{cases} 0, & i \neq j \\ C_i, & i = j \end{cases} \tag{D1}$$

where W(u) is the weight function for a Jacobi polynomial with the following expression:

$$W(u) = (1 - u)^{\alpha}\, u^{\beta} \tag{D2}$$

in which α and β are constants greater that -1. The polynomial $P_j(u)$ is automatically fixed when the weight function is given. $P_i^{(\alpha,\beta)}(u)$ and $P_j^{(\alpha,\beta)}(u)$ are the Jacobi polynomial with degree i and j respectively.

3. A Jacobi polynomial of degree n can be expressed by the following equation:

$$P^{(\alpha,\beta)}(u) = \sum_{i=0}^{n} (-1)^{n-i} a_i u_i \qquad \text{(D3)}$$

where the coefficient a_i can be expressed by the following recurrence formula:

$$a_i = \frac{n - i + 1}{i} \frac{n + i + \alpha + \beta}{i + \beta} r_{i-1} \qquad \text{(D4)}$$

with $a_0 = 1$, and $i = 1,2,\ldots\ldots, n$.
For $n = 3$ and $\alpha=\beta=0$, Equation D3 immediately gives

$$P_3^{(0,0)} = 20\,u^3 - 30\,u^2 + 12\,u - 1 \qquad \text{(D5)}$$

4. For convience of computer computation, Equations D3 and D4 may also be expressed by the following equations:

$$P_n^{(\alpha,\beta)} = [u - g_n(n,\alpha,\beta)]P_{n-1}^{(\alpha,\beta)} - h_n(n,\alpha,\beta)\, P_{n-2} \qquad \text{(D6)}$$

and

$$g_1 = \frac{\beta+1}{\alpha+\beta+2}, \quad g_n = \frac{1}{2}\left[1 - \frac{\alpha^2-\beta^2}{(2n+\alpha+\beta-1)^2 - 1}\right] \qquad \text{(D7)}$$

for $n>1$

$$h_1 = 0 \qquad \text{(D8)}$$

$$h_2 = \frac{(\alpha+1)\,(\beta+1)}{(\alpha+\beta+2)^2\,(\alpha+\beta+3)} \qquad \text{(D9)}$$

$$h_n = \frac{(n-1)\,(n+\alpha-1)\,(n+\beta-1)\,(n+\alpha+\beta-1)}{(2n+\alpha+\beta-1)\,(2n+\alpha+\beta-2)^2\,(2n+\alpha+\beta-3)}, \quad \text{for } n>2 \qquad \text{(D10)}$$

The recurrent evaluation of $P_n^{(\alpha,\beta)}$ (u) starts with n=1, $P_{-1}^{(\alpha,\beta)}$ (u) arbitrarily, and $P_o^{(\alpha,\beta)}$ (u)=1.

Quadrature Integration Formulae

5. In orthogonal collocation the integration can be conveniently and accurately performed by a numerical quadrature formula. Two types of quadrature formulas are described briefly in the following.

Gauss-Jacobi quadrature

6. The Gauss-Jacobi quadrature can integrate any polynomial Y(x) up to 2n-1 degree by the following equation:

$$\int_0^1 (1 - x)^{\alpha} x^{\beta} Y(x)\, dx = \sum_{i=1}^{n} W_i\, Y(x_i) \qquad \text{(D11)}$$

The integration can be obtained closely by summing the product of quadrature weight W_i and the function value $Y(x_i)$ evaluated at the collocation point x_i. In Equation D11 the value of W_i can be calculated by the following equation:

$$W_i = \frac{(2n + \alpha + \beta + 1)\, C_n^{(\alpha,\beta)}}{x_i\, (1 - x)\, (P_n^{(1)}\, (x_i)\,)^2} \qquad \text{(D12)}$$

where

$$C_n^{(\alpha,\beta)} = \int_0^1 P_n^2\, (x)\, (1 - x)^{\alpha} x^{\beta}\, dx \qquad \text{(D13)}$$

Radau quadrature formula

7. In Equation D11 the end points Y(0) and Y(1) are not required to be known. If either one of the end points is given, the quadrature integration can be obtained more accurately by using the Radau formula. In this case the interior quadrature points should be chosen as $P^{(\alpha+1,\beta)}$, if Y(x=1) is given, or $P^{(\alpha,\beta+1)}$, if Y(x=0) is given. The Radau formula

can integrate a polynomial of degree up to 2n exactly by the following equation:

$$\int_0^1 (1 - x)^{\alpha} x^{\beta} Y(x) = W_{n+1} Y(1) + \sum_{i=1}^{n} W_i Y_i \qquad (D14)$$

$$= W_{n+1} Y(0) + \sum_{i=1}^{n} W_i Y_i$$

The Radau quadrature weights in Equation D14 are calculated by the following equations:

Including $x_{n+1}=1$, but not $x_0=0$:

$$W_i = \frac{(2n + \alpha + \beta + 2)\, C_n^{(\alpha+1,\beta)}}{x_i \left(P_{n+1}^{(1)}(x_i)\right)^2} \qquad \begin{cases} 1, & i \neq n+1 \\ 1/(\alpha+1), & i = n+1 \end{cases} \qquad (D15)$$

Including $x_0=0$, but not $x_{n+1}=1$:

$$W_i = \frac{(2n + \alpha + \beta + 1)\, C_n^{(\alpha,\beta+1)}}{(1 - x_i) \left(P_{n+1}^{(1)}(x_i)\right)^2} \qquad \begin{cases} 1/(\beta+1), & i = 0 \\ 1, & i \neq 0 \end{cases} \qquad (D16)$$

Computer Programs D1 and D2

8. This computer program is for computing the roots of the Jacobi polynomial, the derivatives of each polynomial evaluated at the collocation points, and the quadrature weights. The program consists of two subroutines: Subroutines JCOBI computes the zeros of $P_n^{(\alpha,\beta)}$ and the first derivatives of the Jacobi polynomial; Subroutine RADAU determines the integration weights at collocation points.

9. The roots of the Jacobi polynomial and Radau quadrature weights for selected collocation points are listed in Table D1. An example of calculating the integration $\int_0^3 x^2\, dx$, using the roots and weights found from computer program D1, is illustrated in computer program D2.

COMPUTER PROGRAM D1

```
C**** THIS PROGRAM IS USED TO COMPUTE THE ROOTS AND
C     QUADRATURE WEIGHTS OF JACOBI POLYNOMIALS
C**** DIF1, DIF2, AND DIF3 ARE THE 1ST, 2ND, AND 3RD
C     DERIVATIVES OF JACOBI POLYNOMIALS AT COLLOCATION
C     POINTS, RESPECTIVELY
C**** ROOT(I) ARE ROOTS OF JACOBI POLYNOMIALS
C**** WT(I) ARE QUADRATURE WEIGHTS
C**** N IS NUMBER OF COLOCATION POINTS
C**** ALPHA AND BETA ARE THE TWO PARAMETERS OF
C     JACOBI POLYNOMIAL
C
      IMPLICIT REAL*8(A-H, O-Z)
      DIMENSION DIF1(11),DIF2(11),DIF3(11),ROOT(11),WT(11)
C
   1  FORMAT(2I5)
   3  FORMAT(1H1,' GEOMETRY:  0=PLANAR,1=CYLINDER,2=SPHERE',
     &  //,' NUMBER OF COLLOCATION POINTS =',I5,/,' GEOMETRY
     & FACTOR =',I5,///, '  COLLOCATION POINTS IN X**2 :',/)
   6  FORMAT(/,3(D16.8))
 200  READ(5,1,END=100) N,IS
C
C     N IS NUMBER OF COLLOCATION POINTS
C   FOR PLANE SHEET IS=0, FOR CYLINDER IS=1, FOR SPHERE IS=2
C
      S = IS
      WRITE (6,3) N, IS
      ALPHA = 1.0
      BETA = (S-1)/2
C
      CALL  JCOBI (11,N,0,1,ALPHA,BETA,DIF1,DIF2,DIF3,ROOT)
      NT = N + 1
      WRITE (6,6) (ROOT(I),I = 1,NT)
C
C.....FIND QUADRATURE WEIGHTS
      CALL RADAU (11,N,0,1,1,0.D0,BETA,ROOT,DIF1,WT)
C.....TO COMPUTE TRUE QUADRATURE WEIGHTS FOR SLAB GEOMETRY
C.....THE WEIGHTS WT(I) OBTAINED FROM SUBROUTINE RADAU NEED
C.....TO MULTIPLY BY  "2.0"
C
      DO 90 I = 1, NT
  90  WT(I) = WT(I)*2.0
      WRITE(6,55)
  55  FORMAT(/,3X,'  THE QUADRATURE WEIGHTS  WT(I)',/)
      WRITE(6,6) (WT(I), I=1,NT)
C
      GO TO 200
 100  STOP
      END
```

```
C*************************************************************
      SUBROUTINE JCOBI(ND,N,NO,N1,AL,BE,FA,FB,FC,ROOT)
C.....SUBROUTINE JCOBI IS USED TO COMPUTE THE ROOTS OF
C     JACOBI POLYNOMIALS
C.....ND IS DIMENSION OF VECTORS, N IS THE DEGREE OF
C     JACOBI POLYNOMIAL, NO DECIDES WHETHER X=0 IS INCLUDES
C     AS AN INTERPOLATION POINT.  NO MUST BE SET EQUAL TO
C     1 (INCLUDING X=0) OR 0 (EXCLUDING THIS POINT)
C.....N1 IS THE SAME AS FOR NO, BUT FOR THE POINT X=1
C.....FA,FB,FC ARE 1ST, 2ND, AND 3RD DERIVATIVES OF
C     JACOBI POLYNOMIAL AT THE NODES
C.....AL=ALPHA, BE=BETA, ROOT=ZEROS OF JACOBI POLYNOMIAL
C
      IMPLICIT REAL*8(A-H,O-Z)
      DIMENSION FA(ND),FB(ND),FC(ND),ROOT(ND)
C
C.....THE FIRST STEP IS TO CALCULATE GN & HN
C.....HERE FA(I)=GN, FB(I)=HN
C
      AB=AL+BE
      AD=BE-AL
      AP=BE*AL
C
C.....INITIAL VALUE
C.....FA(1) IS G1, FB(1) IS H(1)
C
      FA(1)=(AD/(AB+2.)+1.)/2.
      FB(1)=0.
      IF (N .LT. 2) GO TO 15
C
C.....THEN CONPUTE FA(2), FB(2), FA(3), FB(3),.... ETC.
C.....FA(I)=GN, FB(I)=HN
C
      DO 10 I = 2,N
      Z1 =I - 1
      Z = AB + 2.*Z1
C
C.... FA(I) IS GN,  FB(I) IS HN
C
      FA(I)=(AB*AD/Z/(Z+2.)+1.)/2.
      IF(I .NE. 2) GO TO 11
      FB(I)=(AB + AP + Z1)/Z/Z/(Z+1.)
      GO TO 10
  11  Z=Z*Z
      Y=Z1*( AB + Z1)
      Y=Y*(AP+Y)
      FB(I)=Y/Z/(Z-1.)
  10  CONTINUE
```

```
C
C.....THE SECOND STEP
C.....ROOT DETERMINATION BY NEWTON METRHOD WITH SUPPRESION
C.....OF PREVIOUSLY DETERMINED ROOTS
C
 15   X=0.
      DO 20 I=1,N
 25   XD=0.
      XN=1.
      XD1=0.
      XN1=0.
      DO 30 J=1,N
C
C.....FA(J)=GN, FB(J)=HN
C.....XP IS JACOBI POLYNOMIAL, AND XP1 IS THE FIRST
C     DERIVATIVE OF JACOBI POLYNOMIAL
C
      XP=(FA(J)-X)*XN-FB(J)*XD
      XP1=(FA(J)-X)*XN1-FB(J)*XD1-XN
      XD=XN
      XD1=XN1
C
C.....XN AND XN1 ACCUMULATE THE FOREGOING RESULTS
C
      XN=XP
 30   XN1=XP1
      ZC=1.
      Z=XN/XN1
      IF(I .EQ. 1 ) GO TO 21
      DO 22 J = 2, I
C
C.....EXCLUDE PREVIOUS DETERMINED ROOT: ROOT(J-1)
C
 22   ZC=ZC-Z/(X-ROOT(J-1))
C
 21   Z=Z/ZC
C
C.....FIND NEW X
C
      X=X-Z
      IF ( DABS(Z) .GT. 1.D-09 ) GO TO 25
      ROOT(I)=X
C
C.....NEW STARTING POINT FOR NEXT ROOT
C
      X=X + .0001
 20   CONTINUE
C
C.....ADD EVENTUAL INTERPOLATION POINTS AT X=0 OR X=1
C
```

```
      NT=N+NO+N1
      IF(NO .EQ. 0) GO TO 35
      DO 31 I=1,N
      J = N + 1 - I
   31 ROOT(J+1)=ROOT(J)
      ROOT(1)=0.
   35 IF(N1 .EQ. 1) ROOT(NT) = 1.
C
C.....NOW EVALUATE DERIVATIVES OF POLYNOMIAL
C.... FA, FB, FC ARE 1ST, 2ND, AND 3RD DERIVATIVES
C
      DO 40 I=1,NT
      X=ROOT(I)
      FA(I)=1.
      FB(I)=0.
      FC(I)=0.
      DO 40 J=1,NT
      IF (J .EQ. I) GO TO 40
      Y=X - ROOT(J)
      FC(I) = FC(I) * Y + 3. * FB(I)
      FB(I) = Y * FB(I) + 2. * FA(I)
      FA(I) = Y * FA(I)
   40 CONTINUE
      RETURN
      END
```

COMPUTER PROGRAM D1 (CONTINUED)

```
C*************************************************************
      SUBROUTINE RADAU(ND,N,NO,N1,ID,AL,BE,ROD,FA,V)
C
C.....SUBROUTINE RADAU IS USED TO EVALUATE RADAU OR LOBATTO
C     QUADRATURE WEIGHTS OF JACOBI POLYNOMIAL
C.....FA(I) COME FROM JCOBI, V(I) ARE QUADRATURE WEIGHTS
C.....ND, N, AND NO ARE THE SAME AS FOR SUBROUTINE JCOBI
C.....ID=1 GIVES RADAU QUADRATURE WITH X=1
C.....ID=2 GIVES RADAU QUADRATURE WITH X=0
C.....ID=3 GIVES LOBATTO QUADRATURE WITH BOTH POINTS
C
      IMPLICIT REAL*8(A-H,O-Z)
      DIMENSION ROD(ND),FA(ND),V(ND)
      S=0.
      NT=N+NO+N1
      DO 40 I=1,NT
      X=ROD(I)
      IF (ID-2) 10,20,30
C
C     ID = 1 GIVES RADAU QUADRATURE WITH X = 1
C     ID = 2 GIVES RADAU QUDRATURE WITH X = 0
C     ID=3 GIVES LOBATTO QUADRATURE WITH BOTH ENDPOINTS
 10   AX=X
      IF (NO) 11,11,40
 11   AX=1./AX
      GO TO 40
 20   AX=1.-X
      IF (N1) 21,21,40
 21   AX=1./AX
      GO TO 40
 30   AX=1.
 40   V(I)=AX/FA(I)**2
      IF (ID-2) 41,42,41
 41   V(NT)=V(NT)/(1.+AL)
 42   IF (ID-2) 43,44,44
 44   V(1)=V(1)/(1.+BE)
 43   DO 50 I=1,NT
C
C.....S=V(1) + V(2) + .......
C
 50   S=S+V(I)
      DO 60 I=1,NT
C
C  V(I) ARE NORMALIZED SO THAT THE SUM OF V(I) EQUALS TO ONE
C*** NOTE THE QUADRATURE WEIGHTS COMPUTED FROM RADAU ARE NOT
C    TRUE WEIGHTS
C
 60   V(I)=V(I)/S
      RETURN
      END
```

COMPUTER PROGRAM D2

```
C
C  CALCULATING THE INTEGRATION OF X**2 BY USING RADAU
C  QUADRATURE
C
C  INTEGRATION INTERVAL: FROM 0 TO 3
C
      IMPLICIT REAL*8(A-H,O-Z)
      DIMENSION ROOT(11),WT(11),XX(11)
      DATA ROOT/0.00533697, 0.04735263, 0.12782106,
     &          0.23991861, 0.37413950, 0.51910186,
     &          0.66251286, 0.79221088, 0.89719596,
     &          0.96855602, 1.00000000/
      DATA WT/0.29169804, 0.28548098, 0.27317938,
     &        0.25505539, 0.23149529, 0.20300115,
     &        0.17018012, 0.13373121, 0.09442893,
     &        0.05309150, 0.00865801/
C
      SUM = 0.D0
      X = 3.D0
C
      DO 10 I = 1, 11
      XX(I) = X * DSQRT(ROOT(I))
   10 CONTINUE
C
      DO 20 I = 1, 11
      SUM = SUM + WT(I) * XX(I) * XX(I)
   20 CONTINUE
C
      SUM = 3./2.* SUM
C
      WRITE(6,1) SUM
    1 FORMAT(/15X,' INTEGRAL_0^3 X**2 DX = ', F10.6)
      STOP
      END
```

==========

***** SOLUTION: $\int_0^3 X^2\,DX = 9.000000$ ********

Table D1. The Roots and Quadrature Weights of Jacobi Polynomial for 10-points Collocation

Geometry: Slab

Collocation Points in u:

0.00533697	0.04735263	0.12782106
0.23991861	0.37413950	0.51910186
0.66251286	0.79221088	0.89719596
0.96855602	1.00000000	

Quadrature Weights:

0.29169804	0.28548098	0.27317938
0.25505539	0.23149529	0.20300115
0.17018012	0.13373121	0.09442893
0.05309150	0.00865801	

APPENDIX E: INTEGRATION OF SEDIMENT VOLUME

1. In this study, Simpson's rule is used for the calculation of the sediment volume deposited. Detailed formulation is discussed by Scheid (1968). Computation procedure and computer programs are briefly described in the following.

2. The volume integration of a two-variable sediment thickness function f(x,y) can be expressed as

$$\int_0^{Rb_0} \int_0^{b(x)} f(x,y)dydx = \int_0^{Rb_0} G(x)dx \qquad \text{(E1)}$$

where Rb_0 is the dimensional sediment length in the x-direction, expressed as the x_1-direction; and b(x) is the width of sediment in the y-direction, expressed as the x_2-direction.

By setting $y_0 = 0$

and $$y_j - y_{j-1} = h_1(x) = \frac{b(x)}{n}$$

where h_1 is the discrete distance in y-direction and n is the number of discretizations,

$$G(x) = \int_0^{b(x)} f(x,y)dy$$

$$= \frac{b(x)}{3} [\, f(x,y_0) + 4f(x,y_1) + 2f(x,y_2) + \ldots\ldots \qquad \text{(E2)}$$

$$+ 4f(x,y_{n-1}) + f(x,y_n)]$$

Again, setting $x_0 = 0$

and $$x_i - x_{i-1} = h_2 = \frac{Rb_0}{m}$$

where h_2 is the discrete distance in x-direction and m is the number of discretizations,

$$\int_0^{Rb_0} G(x)dx = \frac{h_2}{3} [G(x_0) + 4G(x_1) + 2G(x_2) + ... + 4G(x_{m-1}) + G(x_m)] \quad \text{(E3)}$$

Therefore

$$\int_0^{Rb_0} \int_0^{b(x)} f(x,y)dydx = \frac{h_2}{3} \frac{h_1(x_0)}{3} [f(x_0,y_0) + 4f(x_0,y_1) + 2f(x_0,y_2) + ... + f(x_0,y_n)]$$

$$+ \frac{4h_1(x_1)}{3} [f(x_1,y_0) + 4f(x_1,y_1) + 2f(x_1,y_2) + ... + f(x_1,y_n)]$$

$$+ \frac{2h_1(x_2)}{3} [f(x_2,y_0) + 4f(x_2,y_1) + 2f(x_2,y_2) + ... + f(x_2,y_n)]$$

$$+ .....$$

$$+ \frac{h_1(x_m)}{3} [f(x_m,y_0) + 4f(x_m,y_1) + 2f(x_m,y_2) + ... + f(x_m,y_n)] \quad \text{(E4)}$$

The integration of the foregoing equation is illustrated in Figure E1. The numbers in Figure E1 represent the coefficients of $f(x_i,y_j)$ in Equation E4.

Computer Program E1

3. This program is for plotting a two-dimensional sediment thickness for a given set of parameters. Using the equations derived in PART V, the SAS/GRAPH is executed for displaying the plot. The longitudinal

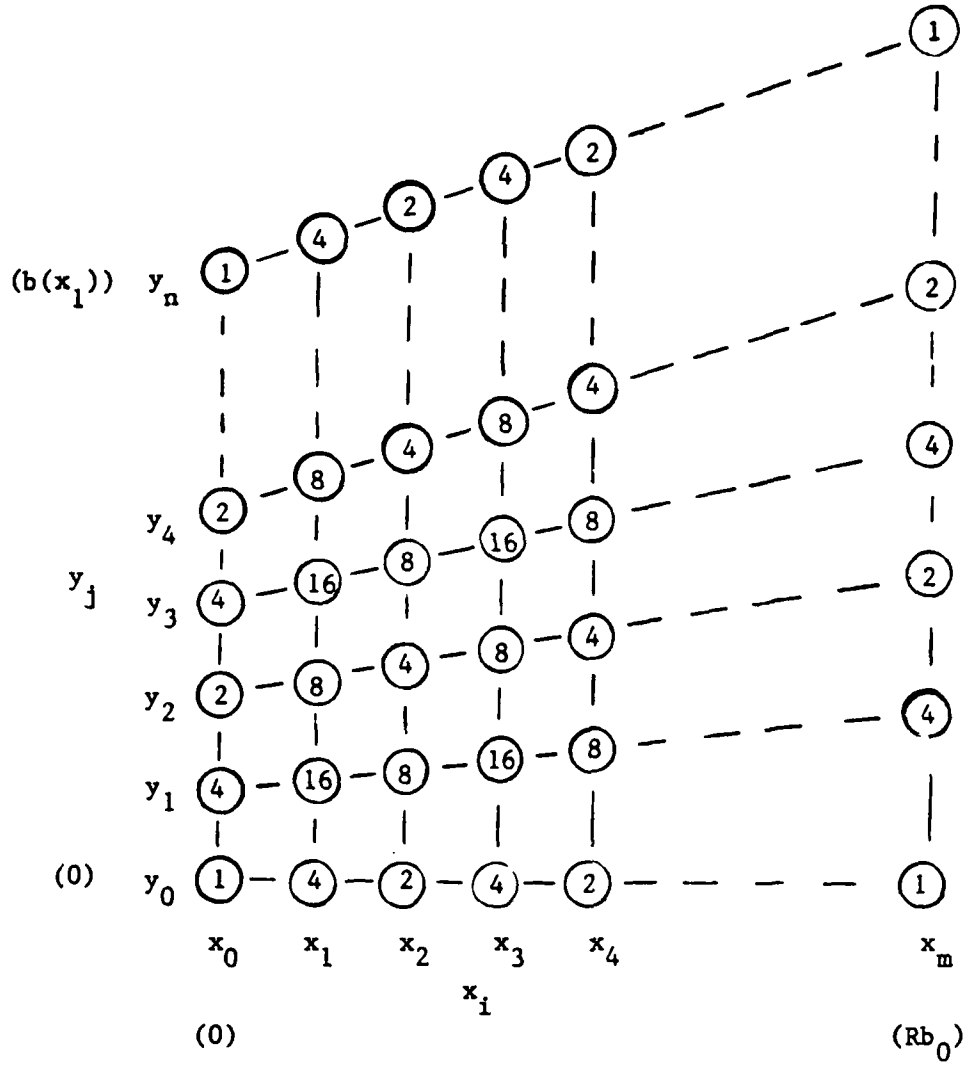

Figure E1. Integration coefficients of Simpson's rule

COMPUTER PROGRAM E1

```
DATA ONE;
U0=1.0; W0=0.05E-3;F=0.001; B0=500.; C0=300.; E=0.075;
H0=2.0; AI1=0.948; AI2=1.397; AI3=0.76;
TIME=2.*365.*86400.; DS=0.4;
   ROOT1=0.00533697; ROOT2=0.04735263; ROOT3=0.12782106;
   ROOT4=0.23991861; ROOT5=0.37413950; ROOT6=0.51910186;
   ROOT7=0.66251286; ROOT8=0.79221088; ROOT9=0.89719596;
   ROOT10=0.96855602; ROOT11=1.00000000;
   WT1=0.29169804; WT2=0.28548098; WT3=0.27317938;
   WT4=0.25505539; WT5=0.23149529; WT6=0.20300115;
   WT7=0.17018012; WT8=0.13373121; WT9=0.09442893;
   WT10=0.05309150; WT11=0.00865801;
   A=0.0001;
S1 = 0.0; S2=0.2; S3=0.4; S4=0.5; S5=0.6; S6=0.8;
UCR = U0;
W = B0*W0/U0/H0;
AA = 1.794*E;
FF = F*B0/H0;
D = F/A;
    DO R = 0.0 TO  20.0 BY  1.0;
H = 1. + A*B0/H0*R;
CF =  H0/A/B0/(2.-D)*( H**(2.-D) - 1.) + 0.5/AA;
U = 1./SQRT(2.*AA) / H**D / SQRT(CF);
B= 2.*AA*H**(D-1) * CF;
HU1 = 1. + A*B0/H0*R*SQRT(ROOT1);
HU2 = 1. + A*B0/H0*R*SQRT(ROOT2);
HU3 = 1. + A*B0/H0*R*SQRT(ROOT3);
HU4 = 1. + A*B0/H0*R*SQRT(ROOT4);
HU5 = 1. + A*B0/H0*R*SQRT(ROOT5);
HU6 = 1. + A*B0/H0*R*SQRT(ROOT6);
HU7 = 1. + A*B0/H0*R*SQRT(ROOT7);
HU8 = 1. + A*B0/H0*R*SQRT(ROOT8);
HU9 = 1. + A*B0/H0*R*SQRT(ROOT9);
HU10 = 1. + A*B0/H0*R*SQRT(ROOT10);
HU11 = 1. + A*B0/H0*R*SQRT(ROOT11);
CFU1 =  H0/A/B0/(2.-D)*( HU1**(2.-D) - 1.) + 0.5/AA;
CFU2 =  H0/A/B0/(2.-D)*( HU2**(2.-D) - 1.) + 0.5/AA;
CFU3 =  H0/A/B0/(2.-D)*( HU3**(2.-D) - 1.) + 0.5/AA;
CFU4 =  H0/A/B0/(2.-D)*( HU4**(2.-D) - 1.) + 0.5/AA;
CFU5 =  H0/A/B0/(2.-D)*( HU5**(2.-D) - 1.) + 0.5/AA;
CFU6 =  H0/A/B0/(2.-D)*( HU6**(2.-D) - 1.) + 0.5/AA;
CFU7 =  H0/A/B0/(2.-D)*( HU7**(2.-D) - 1.) + 0.5/AA;
CFU8 =  H0/A/B0/(2.-D)*( HU8**(2.-D) - 1.) + 0.5/AA;
CFU9 =  H0/A/B0/(2.-D)*( HU9**(2.-D) - 1.) + 0.5/AA;
CFU10 =  H0/A/B0/(2.-D)*( HU10**(2.-D) - 1.) + 0.5/AA;
CFU11 =  H0/A/B0/(2.-D)*( HU11**(2.-D) - 1.) + 0.5/AA;
UU1=1./SQRT( 2.*AA) / HU1**D/SQRT(CFU1);
UU2=1./SQRT( 2.*AA) / HU2**D/SQRT(CFU2);
UU3=1./SQRT( 2.*AA) / HU3**D/SQRT(CFU3);
```

```
UU4=1./SQRT( 2.*AA) / HU4**D/SQRT(CFU4);
UU5=1./SQRT( 2.*AA) / HU5**D/SQRT(CFU5);
UU6=1./SQRT( 2.*AA) / HU6**D/SQRT(CFU6);
UU7=1./SQRT( 2.*AA) / HU7**D/SQRT(CFU7);
UU8=1./SQRT( 2.*AA) / HU8**D/SQRT(CFU8);
UU9=1./SQRT( 2.*AA) / HU9**D/SQRT(CFU9);
UU10=1./SQRT( 2.*AA) / HU10**D/SQRT(CFU10);
UU11=1./SQRT( 2.*AA) / HU11**D/SQRT(CFU11);
G1= -AI2*W/AI1*R/2.;
G2= AI3*W/AI1/UCR/UCR*R/2.;
SUM1 = WT1/HU1/UU1 + WT2/HU2/UU2 + WT3/HU3/UU3
     + WT4/HU4/UU4 + WT5/HU5/UU5 + WT6/HU6/UU6
     + WT7/HU7/UU7 + WT8/HU8/UU8 + WT9/HU9/UU9
     + WT10/HU10/UU10 + WT11/HU11/UU11;
SUM2 = WT1*UU1/HU1 + WT2*UU2/HU2 + WT3*UU3/HU3
     + WT4*UU4/HU4 + WT5*UU5/HU5 + WT6*UU6/HU6
     + WT7*UU7/HU7 + WT8*UU8/HU8 + WT9*UU9/HU9
     + WT10*UU10/HU10 + WT11*UU11/HU11;
C = EXP( G1*SUM1 + G2*SUM2 - LOG(H*U*B) );
CA1 = C0*SQRT(1.-S1*S1)/EXP(S1*S1/2.)*C;
CA2 = C0*SQRT(1.-S2*S2)/EXP(S2*S2/2.)*C;
CA3 = C0*SQRT(1.-S3*S3)/EXP(S3*S3/2.)*C;
CA4 = C0*SQRT(1.-S4*S4)/EXP(S4*S4/2.)*C;
CA5 = C0*SQRT(1.-S5*S5)/EXP(S5*S5/2.)*C;
CA6 = C0*SQRT(1.-S6*S6)/EXP(S6*S6/2.)*C;
CCA1=(1. - S1*S1)/EXP(S1*S1);
CCA2=(1. - S2*S2)/EXP(S2*S2);
CCA3=(1. - S3*S3)/EXP(S3*S3);
CCA4=(1. - S4*S4)/EXP(S4*S4);
CCA5=(1. - S5*S5)/EXP(S5*S5);
CCA6=(1. - S6*S6)/EXP(S6*S6);
UA1=U0*CCA1*U;
UA2=U0*CCA2*U;
UA3=U0*CCA3*U;
UA4=U0*CCA4*U;
UA5=U0*CCA5*U;
UA6=U0*CCA6*U;
CD1 = W0*100.*CA1*1.0E-6*(1. - UA1*UA1/UCR/UCR)*TIME;
CD2 = W0*100.*CA2*1.0E-6*(1. - UA2*UA2/UCR/UCR)*TIME;
CD3 = W0*100.*CA3*1.0E-6*(1. - UA3*UA3/UCR/UCR)*TIME;
CD4 = W0*100.*CA4*1.0E-6*(1. - UA4*UA4/UCR/UCR)*TIME;
CD5 = W0*100.*CA5*1.0E-6*(1. - UA5*UA5/UCR/UCR)*TIME;
CD6 = W0*100.*CA6*1.0E-6*(1. - UA6*UA6/UCR/UCR)*TIME;
TH1 = CD1/DS;
TH2 = CD2/DS;
TH3 = CD3/DS;
TH4 = CD4/DS;
TH5 = CD5/DS;
TH6 = CD6/DS;
```

```
   OUTPUT;END;
TITLE1 .F=TRIPLEX .H=2 PLOT OF SEDIMENT THICKNESS;
TITLE2 .F=TRIPLEX .H=1 :IN CM, TWO YEARS OF DEPOSITION;
TITLE3 .F=TRIPLEX .H=1 CASE 4: B0=500., U0=1.0, W0=0.05;
TITLE4 .F=TRIPLEX .H=1 H0=2.0, F=0.001;
TITLE5 .F=TRIPLEX .H=1 S = 0.0: DIAMOND,    S = 0.2: STAR;
TITLE6 .F=TRIPLEX .H=1 S = 0.4: PLUS,       S = 0.5: SQUARE;
TITLE7 .F=TRIPLEX .H=1 S = 0.6: TRIANGLE,   S = 0.8: HASH;
PROC GPLOT;
PLOT TH1*R TH2*R TH3*R TH4*R TH5*R TH6*R / OVERLAY;
SYMBOL1 I=SPLINE V=DIAMOND;
SYMBOL2 I=SPLINE V=STAR;
SYMBOL3 I=SPLINE V=PLUS;
SYMBOL4 I=SPLINE V=SQUARE;
SYMBOL5 I=SPLINE V=TRIANGLE;
SYMBOL6 I=SPLINE V=HASH;
```

distance RV is taken corresponding to the maximum sediment extent from the plot (for the sake of computation, RV is used as corresponding to 0.5 cm sediment thickness).

4. For Case 4, linearly varying depth with entrainment, the following nominal values are given:

b_0 = 500 m w_0 = 0.05 mm/sec

u_0 = 1.0 m/sec h_0 = 2.0 m

f = 0.001 a = 0.0001

c_0 = 300 ppm e = 0.075

ρ_s = 400 kg/m^3

The roots and quadrature weights of collocation for integration, taken from Appendix D as inputs, are shown in Table E1.

5. The resulting plot of sediment thickness of this example is shown in Figure E2; the longitudinal distance RV is 19.7. The plots for other bifurcation levels can be generated in a like manner by supplying the appropriate values for b_0.

Computer Program E2

6. Using the longitudinal distance RV from the plot of Computer Program E1 and other given parameters as inputs, this FORTRAN computer program evaluates total volume of sediments VOL by Simpson's rule for the integration. The variable names in the computer program, written as similarly as possible to the expressions shown in PART V, are not explained in detail here.

7. For Case 4, the RV's and b_0's are given as following:

RV = 19.7, 51.9, 130.0, 229.0, and 387.5

b_0 = 500., 166.7, 55.6, 27.8, and 13.9

The calculated volume of sediments are shown in Table E2.

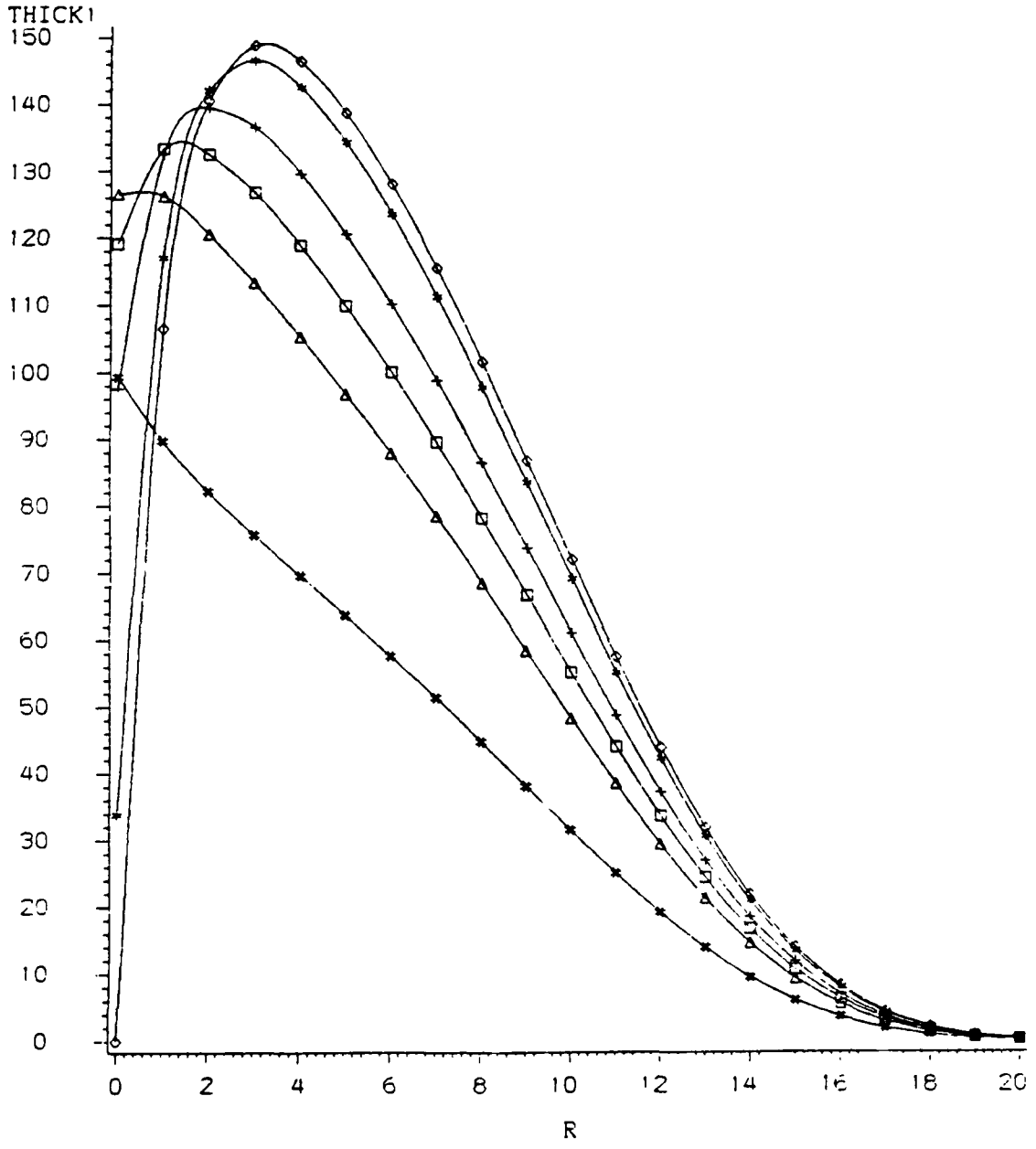

Figure E2. Plot of sediment thickness for various lateral distances

COMPUTER PROGRAM E2

```
C
C       EVALUATE TOTAL SEDIMENT FOR GIVEN B0
C       CASE 4,  REAL DIMENSION
C
      IMPLICIT REAL*8(A-H, O-Z)
C
      DATA DS/0.4D0/, U0/1.00D0/,H0/2.0D0/,C0/300.D0/
C
      TIME = 2.0
  100 READ(5,51,END=999) RV, B0
   51 FORMAT(2F10.4)
C
      CALL INTEG(RV,B0,TIME,VOL)
C
C
      WRITE(6,1) RV,B0,VOL
    1 FORMAT(1H1,///' RV =',F10.4,/,' B0 =',F9.4,'  (M)',/,
     &         ' VOLUME OF SEDIMENT VOL (M**3) =',D16.6)
C
      GO TO 100
  999 STOP
      END
C=======================================================
      SUBROUTINE INTEG(R0,B0,TIME,VOL)
      IMPLICIT REAL*8(A-H, O-Z)
      DIMENSION H1(11),THICK(11,11),A(11),B(11),C(11)
C
C       Y IS X2 COORDINATE, X IS X1 COORDINATE
C
      RB0 = R0*B0
C
      E = 0.075
      F = 0.001
      H0 = 2.0
      AA = 1.794*E
      FF = F*B0/H0
      SA = 0.1D-3
      D = F/SA
      M = 5
      N = 5
C
      DO 20 J = 1, 11
      X1 = (J - 1)/10. * RB0
      H2 = RB0 /M/2.
C
C       B1=S*B(X1),  NOTE : S=1.0
C       FIND JET WIDTH AT VARIOUS X1
C
      R = X1/B0
      HH = 1. + SA*B0/H0*R
```

```
      CF = H0/SA/B0/(2.-D) * (HH**(2.-D)-1.) + 0.5/AA
      B1 = B0 * 2. * AA * HH**(D-1.) * CF
      H1(J) = B1 /N /2.
C
      DO 10 I = 1, 11
      X2 = (I - 1)/10. * B1
C
C       CONPUTE SEDIMENT THICKNESS AT (X1,X2)
C
      CALL BED(B0,TIME,X1,X2,B1,THK)
      THICK(I,J) = THK
   10 CONTINUE
   20 CONTINUE
C
C       THUS ALL VALUES OF THICK(I,J) HAVE BEEN OBTAINED
C
C       START CALCULATING SEDIMENT VOLUME
C
C       FIND  END POINT ON THE R COORDINATE FOR SIMPSON'S
C       RULE
C
      DO 30 I = 1, 11
   30 A(I) = THICK(I,1)
      H = H1(1)
      CALL SIMPS(N,H,A,SUM)
      SUMT1 = H2/3. * SUM
C
      DO 40 I = 1, 11
   40 B(I) = THICK(I,11)
      H = H1(11)
      CALL SIMPS(N,H,B,SUM)
      SUMT2 = H2/3. * SUM
C
C       COMPUTE ALL VALUES BETWEEN TWO END POINTS
C
      SUMT3 = 0.0
      IFLAG = 1
      DO 50 J = 2, 10
      H = H1(J)
      DO 60 I = 1, 11
      C(I) = THICK(I,J)
C
   60 CONTINUE
      CALL SIMPS(N,H,C,SUM)
      IF(IFLAG .EQ. 1) GO TO 111
      IF(IFLAG .EQ. 2) GO TO 222
  111 SUM = H2/3. *4. * SUM
      SUMT3 = SUMT3 + SUM
      IFLAG = 2
      GO TO 50
```

COMPUTER PROGRAM E2 (CONTINUED)

```
 222  SUM = H2/3. * 2. * SUM
      SUMT3 = SUMT3 + SUM
      IFLAG = 1
  50  CONTINUE
C
      SUMTT = SUMT1 + SUMT2 + SUMT3
C
C       VOL IS VOLUME OF SEDIMENT IN  (M**3)
C
      VOL = SUMTT
      RETURN
      END
C=======================================================
      SUBROUTINE SIMPS(N,H1,FUNC,SUMM)
      IMPLICIT REAL*8(A-H, O-Z)
      DIMENSION FUNC(11)
C
C       USE SIMPSON'S RULE FOR INTEGRATION
C       SUMEND IS SUM OF ALL FUNC(I) FOR EVEN I
C       SUMMID IS SUM OF ALL FUNC(I) FOR ODD I
C       H1 IS STEP SIZE
C       FUNC IS INTEGRAND
C
C       INITIALIZE PARAMETERS
C
      SUMEND = 0.0
      SUMMID = 0.0
C
C       EVALUATE SUMEND AND SUMMID
C
      DO 1 K = 1, N
      K1 = 2*K - 1
      K2 = 2*K
      SUMEND = SUMEND + FUNC(K1)
   1  SUMMID = SUMMID + FUNC(K2)
      IT = 2*N + 1
      SUMM = (2.0*(SUMEND-FUNC(1)) + 4.0*SUMMID + FUNC(1)
     & + FUNC(IT)) * H1/3.0
      RETURN
      END
C=======================================================
      SUBROUTINE  BED(B0,TIME,X1,X2,BX1,THICK)
      IMPLICIT REAL*8(A-H, O-Z)
      DIMENSION ROOT(11),WT(11)
C
      DATA H0/2.0D0/,A/0.0001D0/,AI1/0.948D0/,AI2/1.397D0/,
     &   AI3/0.76D0/, DS/0.4D0/, E/0.075D0/, U0/1.0D0/,
     &   F/0.001D0/, W0/0.05D-3/,C0/300.D0/, UCR/1.0D0/
C
      DATA ROOT /0.005337D0, 0.047353D0, 0.127821D0,
```

```
     &           0.239919D0, 0.374139D0, 0.519102D0,
     &           0.662513D0, 0.792211D0, 0.897196D0,
     &           0.968556D0, 1.000000D0 /
C
      DATA WT / 0.291698D0, 0.285481D0, 0.273180D0,
     &          0.255056D0, 0.231495D0, 0.203001D0,
     &          0.170180D0, 0.133731D0, 0.094429D0,
     &          0.053091D0, 0.008658D0 /
      CUCR = UCR/U0
      W = B0*W0/U0/H0
      D = F/A
      AA = 1.794*E
      FF = F*B0/H0
C
      R = X1/B0
      S = X2/BX1
      HH = 1. + A*B0/H0*R
C
      G1 = -AI2*W/AI1*R/2.
      G2 = AI3*W/AI1/CUCR/CUCR*R/2.
C
      AG1 = H0/A/B0/(2.-D) * (HH**(2.-D)-1.) + 0.5/AA
C
      U = 1./DSQRT(2.*AA)/ HH**D /DSQRT(AG1)
C
      B = 2.*AA*HH**(D-1) * AG1
C
      SUM1 = 0.0
      SUM2 = 0.0
C
      DO 10 I = 1, 11
      HU = 1. + A*B0/H0*R*DSQRT(ROOT(I))
      CFU = H0/A/B0/(2.-D) * (HU**(2.-D)-1.) + 0.5/AA
      UU = 1./DSQRT(2.*AA)/ HU**D /DSQRT(CFU)
      SUM1 = SUM1 + WT(I)/HU/UU
      SUM2 = SUM2 + WT(I)/HU*UU
 10   CONTINUE
C
      C = DEXP( G1*SUM1 + G2*SUM2 - DLOG(HH*U*B))
      C1 = C0*DSQRT(1.-S*S)/DEXP(S*S/2.)*C
      CC1 = (1. - S*S)/DEXP(S*S)
      U1 = U0*CC1*U
C
C       THICK IS THICKNESS OF SEDIMENT IN METER
C
      THICK = W0*C1*1.0D-6*(1.-U1*U1/UCR/UCR)
     &        *TIME*365*86400./DS
      RETURN
      END
```

COMPUTER PROGRAM E2 (CONCLUDED)

```
//GO.SYSIN DD *
  19.7       500.0
  51.9       166.7
 130.0        55.6
 229.0        27.8
 387.5        13.9
//
```

Computer Program E3

8. Using 50 percent of the total volume of sediments calculated from Computer Program E2 and other given parameters as inputs, this computer program searches for the longitudinal distance RA of the deposited sediments by the bisection method.

9. For Case 4, after two years of deposition, the total sediments volume VOL is 59.58×10^6 m^3 for the 1st generation. The normalized longitudinal distance RA, for a given volume of total sediments, is found to be 9.36 after 11 iterations. A sample output of this case is shown in Table E3.

Computer Program E4

10. This computer program is used for searching the time-step required to fill the known volume (which is 50 percent of the total volume) of sediments to an average thickness. Using the longitudinal distance RV of the total volume (calculated from Computer Program E2) and RA of the 50 percent total volume (calculated from Computer Program E3) as inputs, the time-step is obtained by the method of bisection method. Also the dimensional distance of x_1 (length), x_2 (width), total area AREA, and total volume VOL of the deposited sediments are calculated.

11. For Case 4, first generation,

RV = 19.7

RA = 9.36

A listing of output for this case is shown in Table E4.

```
C       SEARCH FOR R OF DEPOSITION CORRESPONDING TO 50%
C       OF TOTAL VOLUME
C
C       CASE 4,  REAL DIMENSION
C
C       USING BISECTION METHOD FOR SEARCH
C
      IMPLICIT REAL*8(A-H, O-Z)
C
      DATA DS/0.4D0/, U0/1.0D0/, H0/2.0D0/, C0/300.D0/
C
C       XN AND XP ARE THE SEARCH RANGE OF R
C       VOL1 IS THE TOTAL VOLUME
C       RV IS LONGITUDINAL DISTANCE OF TOTAL VOLUME
C
  100 READ(5,51,END=999) XN, XP, B0, RV, VOL1
   51 FORMAT(4F10.4,D20.4)
C
      WRITE(6,31)  B0, RV, VOL1
   31 FORMAT(//,'  B0 = ',F10.4,'  (M)'/,'  RV =',F10.4,/,
     &        '  INITIAL VOLUME VOL1 = ',D16.6,'  (M**3)')
C
      ITER = 0
   12 XM = (XN + XP)/2.
      ITER = ITER + 1
      IF( DABS(XP-XN) .LT. 0.01 ) GO TO 10
C
C       DIF IF THE DIFERENCE BETWEEN EXPECTED AND
C       COMPUTED VOLUMES
C
      TIME = 2.0
      VOL2 = VOL1 * 0.5
      R = XM
      CALL INTEG(B0,R,TIME,VOL)
C
      DIF =  VOL - VOL2
C
      WRITE(6,1) ITER, DIF, VOL, XM
    1 FORMAT(/,'  NO. OF ITERATION =',I5,/,
     &'  ERROR OF VOLUME (M**3) =',D16.6,/,
     &'  VOLUME OF SEDIMENT (M**3) =',D16.6,/,
     &'  RA =',F12.4,/)
      IF(DIF) 11, 10, 13
   11 XN = XM
      GO TO 12
   13 XP = XM
      GO TO 12
   10 WRITE(6,21)  XM
   21 FORMAT(/,'  ******* RA =', F12.5,/)
```

```
      GO TO 100
  999 STOP
      END
C=====================================================
      SUBROUTINE INTEG(BO,RO,TIME,VOL)
      IMPLICIT REAL*8(A-H, O-Z)
      DIMENSION H1(11),THICK(11,11),A(11),B(11),C(11)
C
C       Y IS X2 COORDINATE, X IS X1 COORDINATE
C
      RBO = RO*BO
C
      E = 0.075
      F = 0.001
      HO = 2.0
      AA = 1.794*E
      FF = F*BO/HO
      SA = 0.1D-3
      D = F/SA
      M = 5
      N = 5
C
      DO 20 J = 1, 11
      X1 = (J - 1)/10. * RBO
      H2 = RBO /M/2.
C
C       B1=S*B(X1),  NOTE : S=1.0
C       FIND JET WIDTH AT VARIOUS X1
C
      R = X1/BO
      HH = 1. + SA*BO/HO*R
      CF = HO/SA/BO/(2.-D)*(HH**(2.-D)-1.) + 0.5/AA
      B1 = BO*2.*AA*HH**(D-1.)*CF
      H1(J) = B1 /N /2.
C
      DO 10 I = 1, 11
      X2 = (I - 1)/10. * B1
C
C       CONPUTE SEDIMENT THICKNESS AT (X1,X2)
C
      CALL BED(BO,TIME,X1,X2,B1,THK)
      THICK(I,J) = THK
   10 CONTINUE
   20 CONTINUE
C
C       THUS ALL VALUES OF THICK(I,J) HAVE BEEN OBTAINED
C
C       START CALCULATING TOTAL VOLUME
C
C       FIND  END POINT ON THE R COORDINATE FOR SIMPSON'S
C       RULE
```

COMPUTER PROGRAM E3 (CONTINUED)

```
C
      DO 30 I = 1, 11
   30 A(I) = THICK(I,1)
      H = H1(1)
      CALL SIMPS(N,H,A,SUM)
      SUMT1 = H2/3. * SUM
C
      DO 40 I = 1, 11
   40 B(I) = THICK(I,11)
      H = H1(11)
      CALL SIMPS(N,H,B,SUM)
      SUMT2 = H2/3. * SUM
C
C       COMPUTE ALL VALUES BETWEEN TWO END POINTS
C
      SUMT3 = 0.0
      IFLAG = 1
      DO 50 J = 2, 10
      H = H1(J)
      DO 60 I = 1, 11
      C(I) = THICK(I,J)
C
   60 CONTINUE
      CALL SIMPS(N,H,C,SUM)
      IF(IFLAG .EQ. 1) GO TO 111
      IF(IFLAG .EQ. 2) GO TO 222
  111 SUM = H2/3. *4. * SUM
      SUMT3 = SUMT3 + SUM
      IFLAG = 2
      GO TO 50
  222 SUM = H2/3. * 2. * SUM
      SUMT3 = SUMT3 + SUM
      IFLAG = 1
   50 CONTINUE
C
      SUMTT = SUMT1 + SUMT2 + SUMT3
C       VOL IS VOLUME OF SEDIMENT IN  (M**3)
      VOL = SUMTT
      RETURN
      END
C=======================================================
      SUBROUTINE SIMPS(N,H1,FUNC,SUMM)
      IMPLICIT REAL*8(A-H, O-Z)
      DIMENSION FUNC(11)
C
C       USE SIMPSON'S RULE FOR INTEGRATION
C       SUMEND IS SUM OF ALL FUNC(I) FOR EVEN I
C       SUMMID IS SUM OF ALL FUNC(I) FOR ODD I
C       H1 IS STEP SIZE
C       FUNC IS INTEGRAND
```

```
C
C       INITIALIZE PARAMETERS
C
      SUMEND = 0.0
      SUMMID = 0.0
C
C       EVALUATE SUMEND AND SUMMID
C
      DO 1 K = 1, N
      K1 = 2*K - 1
      K2 = 2*K
      SUMEND = SUMEND + FUNC(K1)
    1 SUMMID = SUMMID + FUNC(K2)
      IT = 2*N + 1
      SUMM = (2.0*(SUMEND-FUNC(1)) + 4.0*SUMMID + FUNC(1)
     & + FUNC(IT)) * H1/3.0
      RETURN
      END
C=============================================================
      SUBROUTINE  BED(B0,TIME,X1,X2,BX1,THICK)
      IMPLICIT REAL*8(A-H, O-Z)
      DIMENSION ROOT(11),WT(11)
C
      DATA H0/2.0D0/,A/0.0001D0/,AI1/0.948D0/,AI2/1.397D0/,
     &   AI3/0.76D0/, DS/0.4D0/, E/0.075D0/, U0/1.0D0/,
     &   F/0.001D0/, W0/0.05D-3/,C0/300.D0/, UCR/1.0D0/
C
      DATA ROOT /0.005337D0, 0.047353D0, 0.127821D0,
     &           0.239319D0, 0.374139D0, 0.519102D0,
     &           0.662513D0, 0.792211D0, 0.897196D0,
     &           0.968556D0, 1.000000D0 /
C
      DATA WT / 0.291698D0, 0.285481D0, 0.273180D0,
     &          0.255056D0, 0.231495D0, 0.203001D0,
     &          0.170180D0, 0.133731D0, 0.094429D0,
     &          0.053091D0, 0.008658D0 /
      CUCR = UCR/U0
      W = B0*W0/U0/H0
      D = F/A
      AA = 1.794*E
      FF = F*B0/H0
C
      R = X1/B0
      S = X2/BX1
      HH = 1. + A*B0/H0*R
C
      G1= -AI2*W/AI1*R/2.
      G2 = AI3*W/AI1/UCR/UCR*R/2.
C
      AG1 = H0/A/B0/(2.-D)*(HH**(2.-D)-1.) + 0.5/AA
```

AD-A164 931 THE ATCHAFALAYA RIVER DELTA REPORT 7 ANALYTICAL ANALYSIS OF THE DEVELOPME (U) LOUISIANA STATE UNIV BATON ROUGE COASTAL ECOLOGY LAB F C WANG SEP 85 3/3

UNCLASSIFIED WES/TR/HL-82-15 DAC339-81-C-0004 F/G 8/8 NL

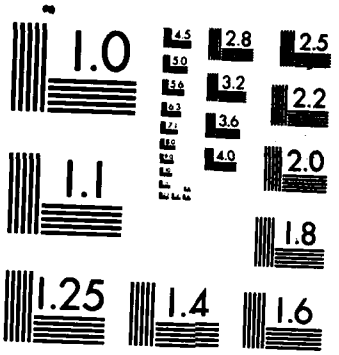

COMPUTER PROGRAM E3 (CONCLUDED)

```
C
      U= 1./DSQRT(2.*AA)/HH**D/DSQRT(AG1)
C
      B = 2.*AA*HH**(D-1)*AG1
C
      SUM1 = 0.0
      SUM2 = 0.0
C
      DO 10 I = 1, 11
      HU = 1. + A*B0/H0*R*DSQRT(ROOT(I))
      CFU = H0/A/B0/(2.-D)*(HU**(2.-D)-1.) + 0.5/AA
      UU = 1./DSQRT(2.*AA)/HU**D/DSQRT(CFU)
      SUM1 = SUM1 + WT(I)/HU/UU
      SUM2 = SUM2 + WT(I)/HU*UU
 10   CONTINUE
C
      C = DEXP(G1*SUM1 + G2*SUM2 - DLOG(HH*U*B))
      C1 = C0*DSQRT(1.-S*S)/DEXP(S*S/2.)*C
      CC1 = (1. - S*S)/DEXP(S*S)
      U1 = U0*CC1*U
C
C       THICK IS THICKNESS OF SEDIMENT IN METERS
C
      THICK = W0*C1*1.0D-6*(1.-U1*U1/UCR/UCR)
     &        *TIME*365.*86400./DS
      RETURN
      END
C ==========================================================
//GO.SYSIN DD *
       5.0       10.0      500.0       19.7            0.5958D08
//
```

COMPUTER PROGRAM E4

```
C       SEARCH FOR TIME OF DEPOSITION FOR GIVEN RV (OF VOLUME)
C       AND RA  (OF AREA), AND AVERAGE THICKNESS OF DEPOSITION
C       CASE 4,  REAL DIMENSION
C
C       USING BI-SECTIONAL METHOD FOR SEARCH
C
      IMPLICIT REAL*8(A-H, O-Z)
C
C       XN AND XP ARE THE SEARCH RANGE OF SEDIMENTATION TIME
C       RV IS R FOR VOLUME, RA IS R FOR AREA
C
  100 READ(5,51,END=999)RV,RA,XN,XP,B0
   51 FORMAT(5F10.2)
C
      WRITE(6,31)  B0, RV, RA
   31 FORMAT(1H1,///,'  B0 = ',F10.4,'  (M)',/,
     &       '  RV = ',F10.4,/,'  RA = ',F10.4)
C
      ITER = 0
   12 XM = (XN + XP)/2.
      ITER = ITER + 1
      IF( DABS(XP-XN) .LT. 0.01D0 ) GO TO 10
C
C       DIF IF THE DIFERENCE BETWEEN EXPECTED AND
C       COMPUTED AVERAGE SEDIMENT THICKNESS
C
      TIME = XM
      CALL INTEG(B0,RV,TIME,VOL)
C
C       UNIT OF AREA = M**2
C
      CALL INTEG2(B0,RA,AREA,X2)
      A = 0.1D-3
      H0 = 2.0D0
      DIF =  VOL/AREA - (H0 + 0.5 * A * RA * B0)
C
      WRITE(6,1) ITER, DIF, VOL, AREA, XM
    1 FORMAT(/,'  NO. OF ITERATION =',I5,/,
     &'  ERROR OF BED THICKNESS (M) =',D16.6,/,
     &'  VOLUME OF SEDIMENT (M**3) =',D16.6,/,
     &'  AREA OF SEDIMENT (M**2) =',D16.6,/,
     &'  TIME (YEARS) =',F12.4)
      IF(DIF) 11, 10, 13
   11 XN = XM
      GO TO 12
   13 XP = XM
      GO TO 12
   10 X1 = RA*B0
      WRITE(6,21)  X1, X2, B0, XM
```

COMPUTER PROGRAM E4 (CONTINUED)

```
   21  FORMAT(/,'  X1 = ',F10.4,/,'  X2 = ',F10.4,/,
      &          '  B0 = ',F10.4,/,
      & '  ******* TIME (YEARS) =', F12.5)
       GO TO 100
  999  STOP
       END
C=================================================
       SUBROUTINE INTEG(B0,R0,TIME,VOL)
       IMPLICIT REAL*8(A-H, O-Z)
       DIMENSION H1(11),THICK(11,11),A(11),B(11),C(11)
C
C        Y IS X2 COORDINATE, X IS X1 COORDINATE
C
       RB0 = R0*B0
C
       E = 0.075
       F = 0.001
       H0 = 2.0
       AA = 1.794*E
       FF = F*B0/H0
       SA = 0.1D-3
       D=F/SA
       M = 5
       N = 5
C
       DO 20 J = 1, 11
       X1 = (J - 1)/10. * RB0
       H2 = RB0 /M/2.
C
C        B1=S*B(X1),  NOTE : S=1.0
C        FIND JET WIDTH AT VARIOUS X1
C
       R = X1/B0
       HH = 1. + SA*B0/H0*R
       CF = H0/SA/B0/(2.-D)*(HH**(2.-D)-1.)+0.5/AA
       B1=B0*2.*AA*HH**(D-1.)*CF
       H1(J) = B1 /N /2.
C
       DO 10 I = 1, 11
       X2 = (I - 1)/10. * B1
C
C        CONPUTE SEDIMENT THICKNESS AT (X1,X2)
       CALL BED(B0,TIME,X1,X2,B1,THK)
       THICK(I,J) = THK
   10  CONTINUE
   20  CONTINUE
C
C        THUS ALL VALUES OF THICK(I,J) HAVE BEEN OBTAINED
C
C        START CALCULATING TOTAL VOLUME
```

COMPUTER PROGRAM E4 (CONTINUED)

```
C
C       FIND  END POINT ON THE R COORDINATE FOR SIMPSON'S
C       RULE
C
      DO 30 I = 1, 11
   30 A(I) = THICK(I,1)
      H = H1(1)
      CALL SIMPS(N,H,A,SUM)
      SUMT1 = H2/3. * SUM
C
      DO 40 I = 1, 11
   40 B(I) = THICK(I,11)
      H = H1(11)
      CALL SIMPS(N,H,B,SUM)
      SUMT2 = H2/3. * SUM
C
C       COMPUTE ALL VALUES BETWEEN TWO END POINTS
C
      SUMT3 = 0.0
      IFLAG = 1
      DO 50 J = 2, 10
      H = H1(J)
      DO 60 I = 1, 11
      C(I) = THICK(I,J)
   60 CONTINUE
      CALL SIMPS(N,H,C,SUM)
      IF(IFLAG .EQ. 1) GO TO 111
      IF(IFLAG .EQ. 2) GO TO 222
  111 SUM = H2/3. *4. * SUM
      SUMT3 = SUMT3 + SUM
      IFLAG = 2
      GO TO 50
  222 SUM = H2/3. * 2. * SUM
      SUMT3 = SUMT3 + SUM
      IFLAG = 1
   50 CONTINUE
C
      SUMTT = SUMT1 + SUMT2 + SUMT3
C
C       VOL IS VOLUME OF SEDIMENT IN  (M**3)
C
      VOL = SUMTT
      RETURN
      END
C=============================================================
      SUBROUTINE INTEG2(B0,R0,AREA,X2)
      IMPLICIT REAL*8(A-H, O-Z)
C
      A = 0.1D-3
      F = 0.001D0
```

COMPUTER PROGRAM E4 (CONTINUED)

```
      D = F/A
      S = 1.0
      E = 0.075
      F = 0.001
      H0 = 2.0
      AA = 1.794*E
      FF = F*B0/H0
C
C       UNIT OF AREA = M**2
C
      CK1 = H0**2/(2.*(A*B0)**2*(2.-D))
      CK2 = H0/(D*A*B0) * (0.5/AA - H0/(A*B0)/(2.-D))
      HH = 1. + A * B0/H0 * R0
      CF = H0/A/B0/(2.-D) * (HH ** (2.-D) - 1.) + 0.5/AA
      X2 = B0 * 2.* AA * HH**(D-1.) * CF
      AREA = (2.*AA*B0**2) * (CK1*(1. + A*B0/H0*R0)**2
     &    + CK2 * (1. + A*B0/H0*R0)**D - CK1 - CK2)
      RETURN
      END
C =====================================================
      SUBROUTINE SIMPS(N,H1,FUNC,SUMM)
      IMPLICIT REAL*8(A-H, O-Z)
      DIMENSION FUNC(11)
C
C       USE SIMPSON'S RULE FOR INTEGRATION
C       SUMEND IS SUM OF ALL FUNC(I) FOR EVEN I
C       SUMMID IS SUM OF ALL FUNC(I) FOR ODD I
C       H1 IS STEP SIZE
C       FUNC IS INTEGRAND
C
C       INITIALIZE PARAMETERS
C
      SUMEND = 0.0
      SUMMID = 0.0
C
C       EVALUATE SUMEND AND SUMMID
C
      DO 1 K = 1, N
      K1 = 2*K - 1
      K2 = 2*K
      SUMEND = SUMEND + FUNC(K1)
    1 SUMMID = SUMMID + FUNC(K2)
      IT = 2*N + 1
      SUMM = (2.0*(SUMEND-FUNC(1)) + 4.0*SUMMID + FUNC(1)
     & + FUNC(IT)) * H1/3.0
      RETURN
      END
C=====================================================
```

COMPUTER PROGRAM E4 (CONTINUED)

```
      SUBROUTINE  BED(B0,TIME,X1,X2,BX1,THICK)
      IMPLICIT REAL*8(A-H, O-Z)
      DIMENSION ROOT(11),WT(11)
C
      DATA H0/2.0D0/,A/0.0001D0/,AI1/0.948D0/,AI2/1.397D0/,
     &   AI3/0.76D0/, DS/0.4D0/, E/0.075D0/, U0/1.0D0/,
     &   F/0.001D0/, W0/0.05D-3/,C0/300.D0/, UCR/1.0D0/
C
      DATA ROOT /0.005337D0, 0.047353D0, 0.127821D0,
     &           0.239919D0, 0.374139D0, 0.519102D0,
     &           0.662513D0, 0.792211D0, 0.897196D0,
     &           0.968556D0, 1.000000D0 /
C
      DATA WT / 0.291698D0, 0.285481D0, 0.273180D0,
     &          0.255056D0, 0.231495D0, 0.203001D0,
     &          0.170180D0, 0.133731D0, 0.094429D0,
     &          0.053091D0, 0.008658D0 /
      CUCR = UCR/U0
      W = B0*W0/U0/H0
      D = F/A
      AA = 1.794*E
      FF = F*B0/H0
C
      R = X1/B0
      S = X2/BX1
      HH = 1. + A*B0/H0*R
C
      G1= -AI2*W/AI1*R/2.
      G2= AI3*W/AI1/CUCR/CUCR*R/2.
C
      AG1 = H0/A/B0/(2.-D)*(HH**(2.-D)-1.) + 0.5/AA
C
      U = 1./DSQRT(2.*AA)/HH**D/DSQRT(AG1)
C
      B= 2.*AA*HH**(D-1)*AG1
C
      SUM1 = 0.0
      SUM2 = 0.0
C
      DO 10 I = 1, 11
      HU = 1. + A*B0/H0*R*DSQRT(ROOT(I))
      CFU = H0/A/B0/(2.-D)*(HU**(2.-D)-1.) + 0.5/AA
      UU = 1./DSQRT(2.*AA)/HU**D/DSQRT(CFU)
      SUM1 = SUM1 + WT(I)/HU/UU
      SUM2 = SUM2 + WT(I)/HU*UU
 10   CONTINUE
C
      C = DEXP( G1*SUM1 + G2*SUM2 - DLOG(HH*U*B))
      C1 = C0*DSQRT(1.-S*S)/DEXP(S*S/2.)*C
      CC1 = (1. - S*S)/DEXP(S*S)
      U1 = U0*CC1*U
```

COMPUTER PROGRAM E4 (CONCLUDED)

```
C
C       THICK IS THICKNESS OF SEDIMENT IN METERS
C
       THICK   W0*C1*1.0D-6*(1.-U1/UCR/UCR)
      &        *TIME*365.*86400./DS
       RETURN
       END
C=============================================================
//GO.SYSIN DD *
       19.7      9.36       0.0       8.0     500.0
//
```

Table E1

Roots and Quadrature Weights of Collocation for Integration

Collocation point	Roots	Weights
1	0.00533697	0.29169804
2	0.04735263	0.28548098
3	0.12782106	0.27317938
4	0.23991861	0.25505539
5	0.37413950	0.23149529
6	0.51910186	0.20300115
7	0.66251286	0.17018012
8	0.79221088	0.13373121
9	0.89719596	0.09442893
10	0.96855602	0.05309150
11	1.00000000	0.00865801

Table E2

Computed Output for Total Sediment Volume

RV	BO	Volume of Sediment (m**3)
19.7000	500.0000	0.222537D+08
51.9000	166.7000	0.740607D+07
130.0000	55.6000	0.246097D+07
229.0000	27.8000	0.122709D+07
387.5000	13.9000	0.609021D+06

Table E3

Bisection Search for the Longitudinal Distance of a Given Total Sediment Volume

No. of Iteration	Error of Volume (m**3)	Volume of Sediment (m**3)	RA
1	-0.695266D+06	0.104316D+08	9.0000
2	0.746710D+07	0.185939D+08	13.5000
3	0.370580D+07	0.148326D+08	11.2500
4	0.152459D+07	0.126514D+08	10.1250
5	0.411904D+06	0.115387D+08	9.5625
6	-0.143270D+06	0.109836D+08	9.2813
7	0.134029D+06	0.112609D+08	9.4219
8	-0.470647D+04	0.111221D+08	9.3516
9	0.646416D+05	0.111915D+08	9.3867
10	0.299624D+05	0.111568D+08	9.3691
11	0.126266D+05	0.111395D+08	9.3604

Final value of RA = 9.35596

Table E4

Time Required for Accumulating a Known Volume of Total Sediment and Its Areal Extent

Iteration	Bed Thickness Error (m)	Sediment Volume (m**3)	Sediment Area (m**2)	Time (Years)
1	0.270754D+00	0.333805D+08	0.133274D+08	3.0000
2	-0.981573D+00	0.166903D+08	0.133274D+08	1.5000
3	-0.355409D+00	0.250354D+08	0.133274D+08	2.2500
4	-0.423279D-01	0.292080D+08	0.133274D+08	2.6250
5	0.144213D+00	0.312942D+08	0.133274D+08	2.8125
6	0.359425D-01	0.302511D+08	0.133274D+08	2.7188
7	-0.319273D-02	0.297295D+08	0.133274D+08	2.6719
8	0.163749D-01	0.299903D+08	0.133274D+08	2.6953
9	0.659107D-02	0.298599D+08	0.133274D+08	2.6836
10	0.169917D-02	0.297947D+08	0.133274D+08	2.6777

Final Time (Years) = 2.67480

END

FILMED

3 -86

DTIC